Progress in Light-Matter Interplay in 2D Materials from the Near-Infrared to Terahertz Lightwaves towards Monolithic Optoelectronic Devices

Jian-Bin Xu (许建斌)[1, 2]

[1]Department of Electronic Engineering & Materials Science and Technology Research Center The Chinese University of Hong Kong, Shatin, NT, Hong Kong SAR, China（香港中文大学）

[2]Institute of Advanced Materials Science and Engineering, Shenzhen Institutes of Advanced Technology, Chinese Academy of Sciences, Photonics, China (中科院先进技术研究院)

jbxu@ee.cuhk.edu.hk

http:www.ee.cuhk.edu.hk/~jbxu; https://english.siat.ac.cn/about/il/

Chair of Materials Science and Nanotechnology, Technische Universität Dresden — TU Dresden, Dresden, Germany, May 30, 2025

Acknowledgement

Group Members

Dr. Z. F. Chen

Dr. Jingwen Ma

Dr. L. Tong

Dr. F. H. Shen

Dr. L. Ye

Dr. X. Wan

Dr. K. Chen

Dr. L. Tao

Collaborators

Prof. H. K. Tsang	CUHK
Prof. Emma Pickwell-MacPherson	CUHK
Prof. X. K. Sun	CUHK
Prof. W. G. Xie	Jinan Univ
Prof. H. J. Chen	Zhong S. Univ
Prof. J. Wei	Renmin Univ
Prof. R. Sun	SAIT, CAS

Alumni/Former Collaborators

Prof. X. M. Wang	Nanjing Univ	Dr. K. Xu	HIT, Shenzhen	Dr. W. G. Xie	Jinan Univ
Dr. Z. Z. Cheng	Tokyo University	Dr. X. Tian	Shenzhen Univ	Prof. M. S. Xu	Zhejiang U

Research Grants Council of Hong Kong 香港 研究資助局

UGC 大學教育資助委員會 University Grants Committee

NSFC National Natural Science Foundation of China

香港中文大學 THE CHINESE UNIVERSITY OF HONG KONG

Guangdong Provincial Government

Shenzhen Municipal Government

100th Anniversary of Quantum & FET

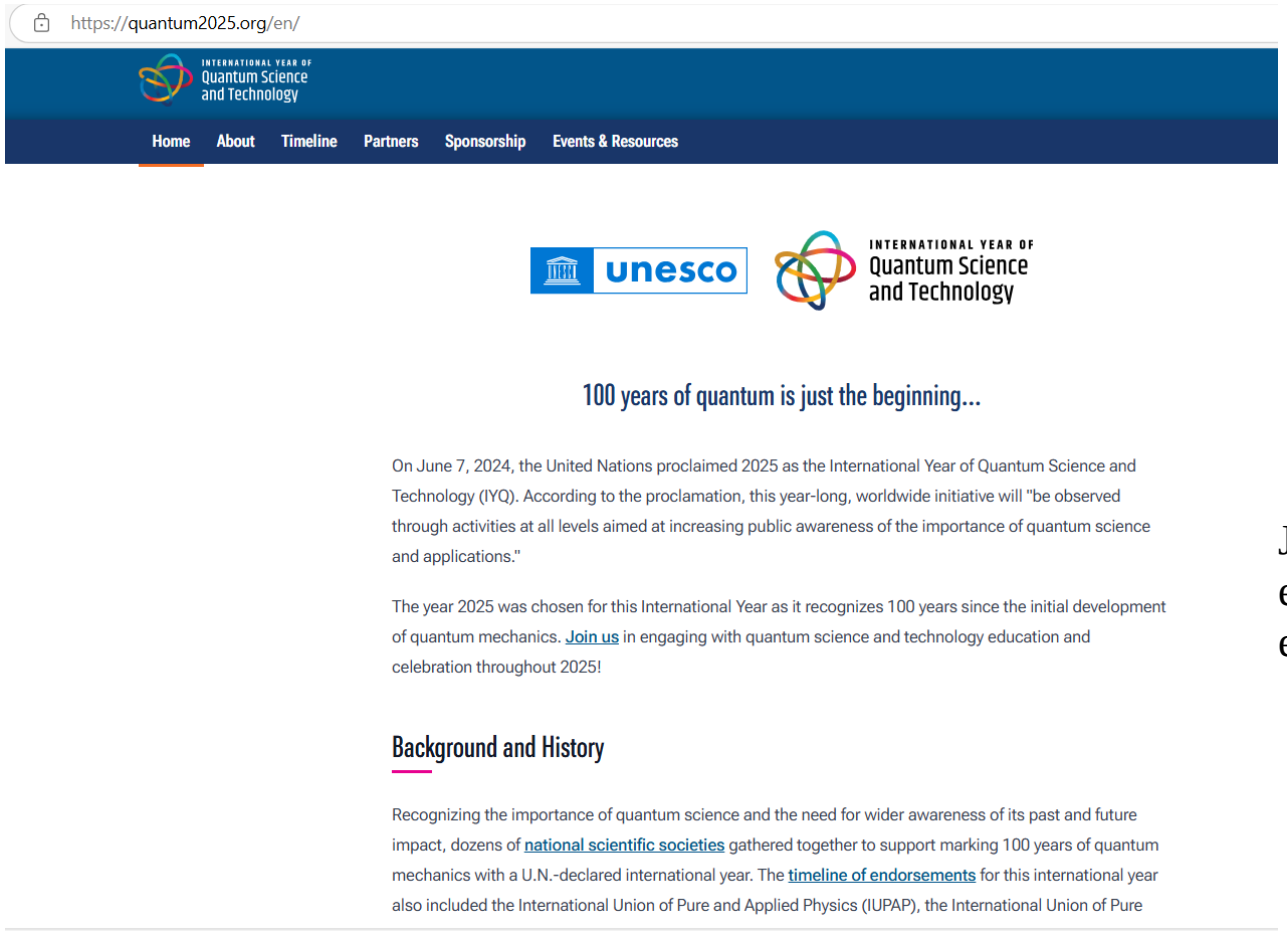

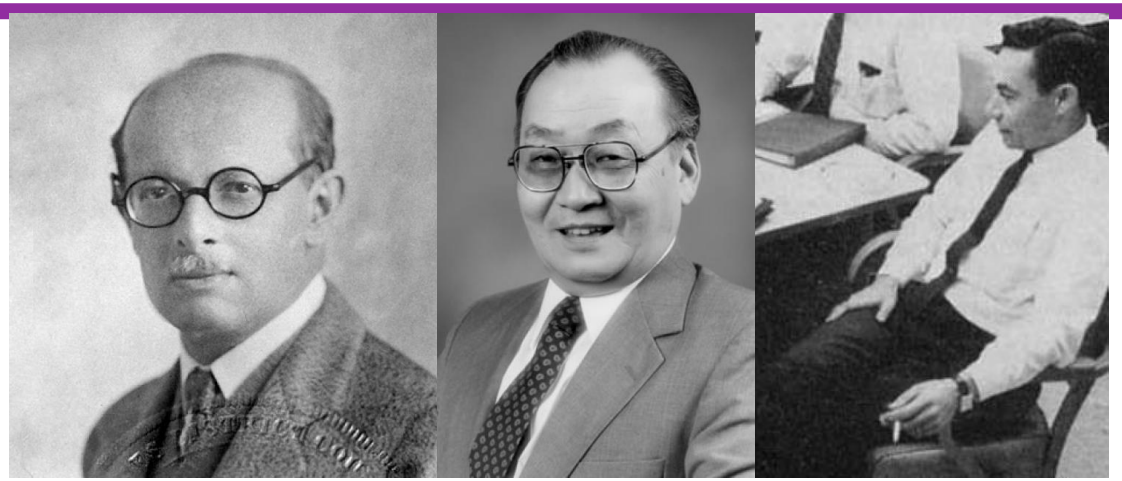

Julius Edgar Lilienfeld was an Austro-Hungarian-American physicist and electrical engineer, who has been credited with the first patent on the field effect transistor (FET) (1925).

Mohamed Atalla and Dawon Kahng（姜大元) proposed a silicon MOS transistor in 1959[25] and successfully demonstrated a working MOS device with their Bell Labs team in 1960.

https://en.wikipedia.org/wiki/Field-effect_transistor

Group Photo Dec. 2018 & Oct. 2023

Map of the Mainland

china-holiday.com

Hong Kong-Shen Zhen, GBA

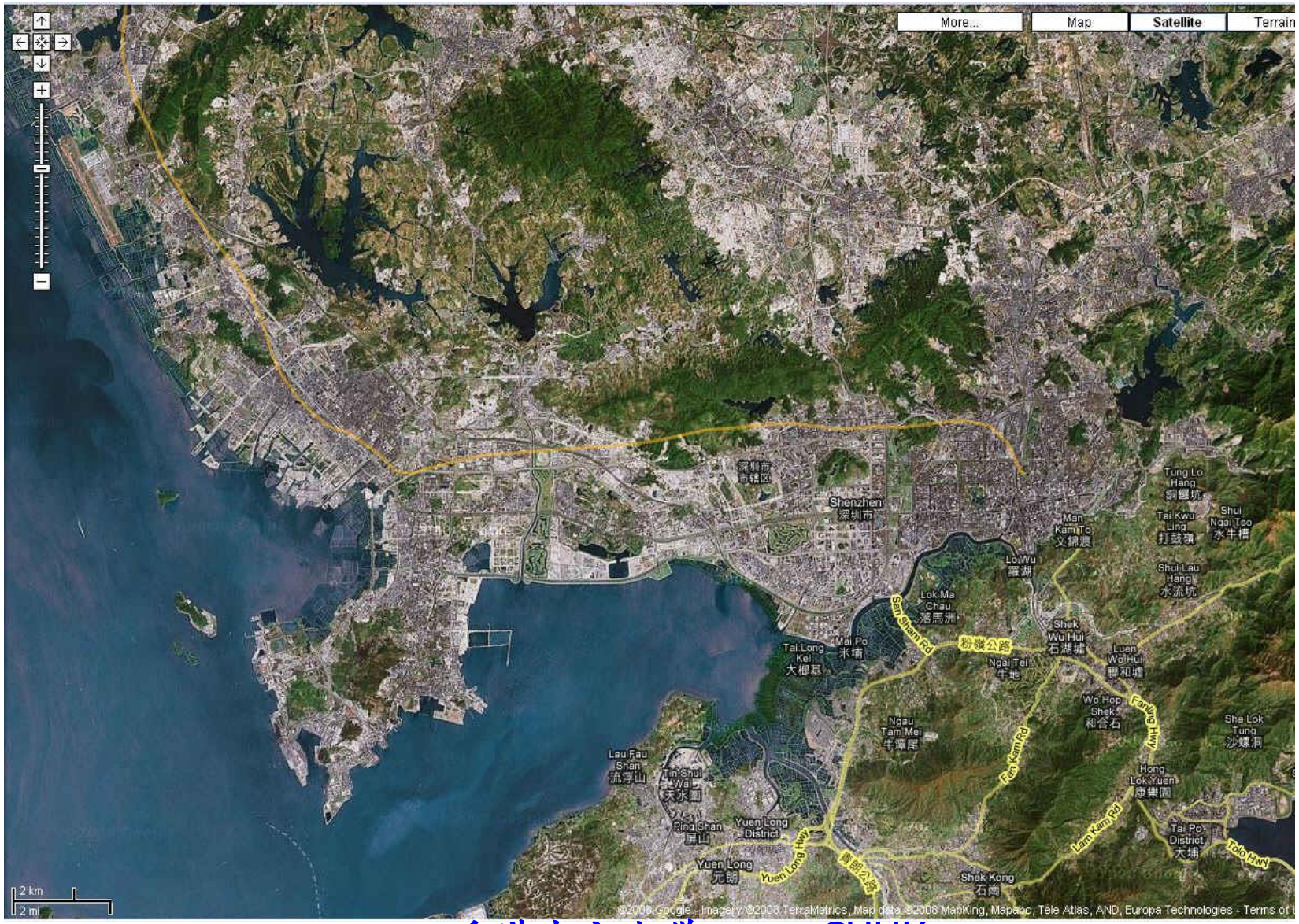

Hong Kong-Shen Zhen, GBA

Hong Kong


TUGO CHENG Photography
fb: tugochengphotography | ig: tcycheng

Bird-View of Chinese University of Hong Kong

- Establishment: 1963
- Campus: 1.37 km^2
- 8 faculties
- 53 major programs
- 1,400 + faculty members
- 22,000 + students, c.a. 40% PGS

Courtesy by Prof. Philip W. Y. Chiu, Faculty of Medicine, CUHK, Feb 2025

Research Activities in CUHK

Thin Film Technology

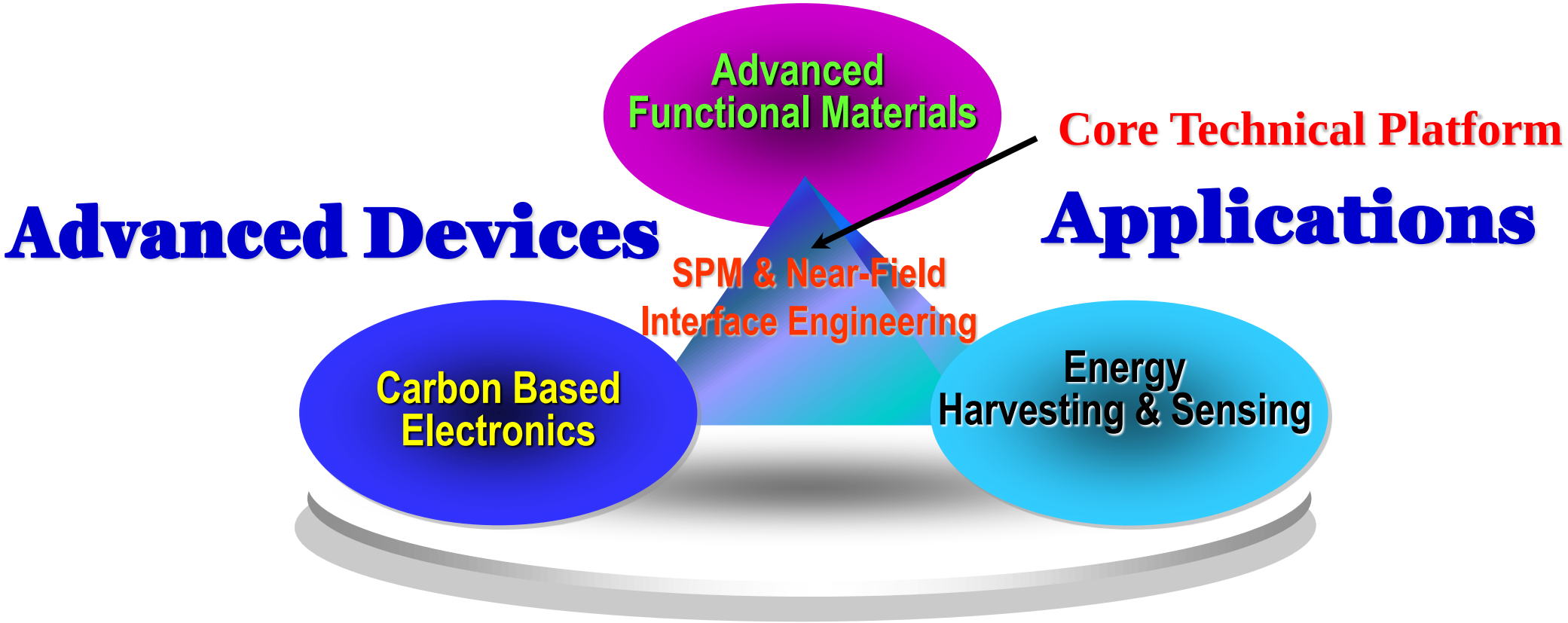

Research Links & NNI

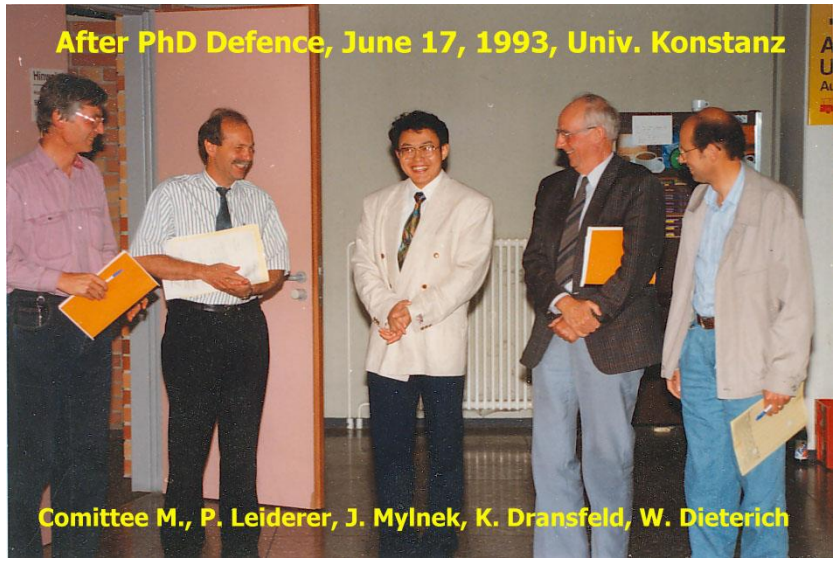

Doctor Exam, Jürgen Mlynek (Chair), now Chairman of the Strategic Advisory Board of the European Quantum Technology Flagship Initiative Universität Konstanz (June 1993)

University of Konstanz (an Elite University), Germany (1988-1993, under supervision of Prof. Dr. Klaus Dransfeld)

Nanoscience and Nanotechnology: STM/AFM; C_{60}; Nano-phase Materials, QDs (Louis E. Brus), superlattices, clusters, nanowires, atomic fabrication, quantum tech, etc.

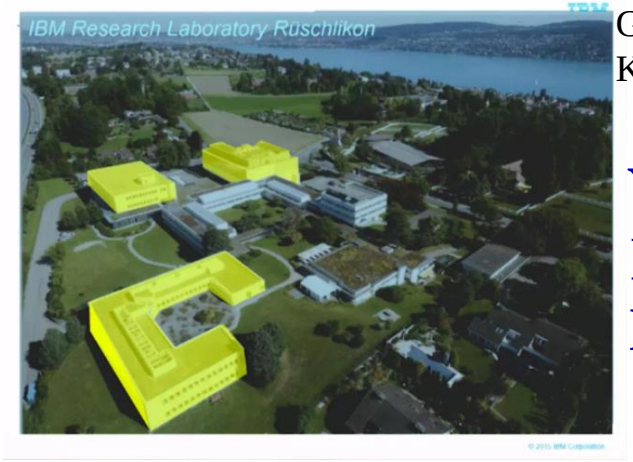

IBM Zurich Research Lab, Switzerland

Yellow Buildings: The Binning and Rohrer Nanotechnology Center, 17 May, 2011, operated by ETH and IBM

https://www.youtube.com/watch?v=dtSt04tYT9E

Research Links & NNI

NATIONAL NANOTECHNOLOGY INITIATIVE:

Leading to the Next Industrial Revolution

A Report by the Interagency Working Group on Nanoscience, Engineering and Technology

Committee on Technology
National Science and Technology Council

February 2000
Washington, D.C.

https://en.wikipedia.org/wiki/National_Nanotechnology_Initiative
https://www.nano.gov/ https://www.nano.gov/timeline
https://clintonwhitehouse4.archives.gov/media/pdf/nni.pdf

Nanoscience and Nanotechnology: STM/AFM (Nobel Prize 1988, Kavli Prize 2016); C_{60};(Nobel Prize 1996) Nano-phase Materials, QDs (Louis E. Brus, Nobel Prize 2023), superlattices, clusters, nanowires, etc.

The National Nanotechnology Steering and Coordination Committee was established in 2000, and the National Center for Nanoscience and Technology was established in 2003.

Allotropes of Carbon

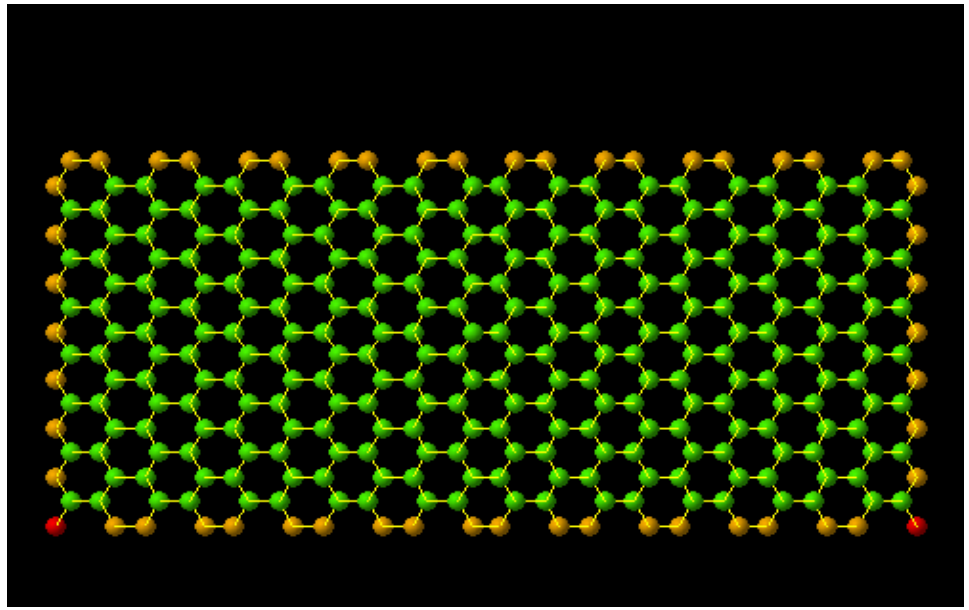

http://en.wikipedia.org/wiki/Graphite

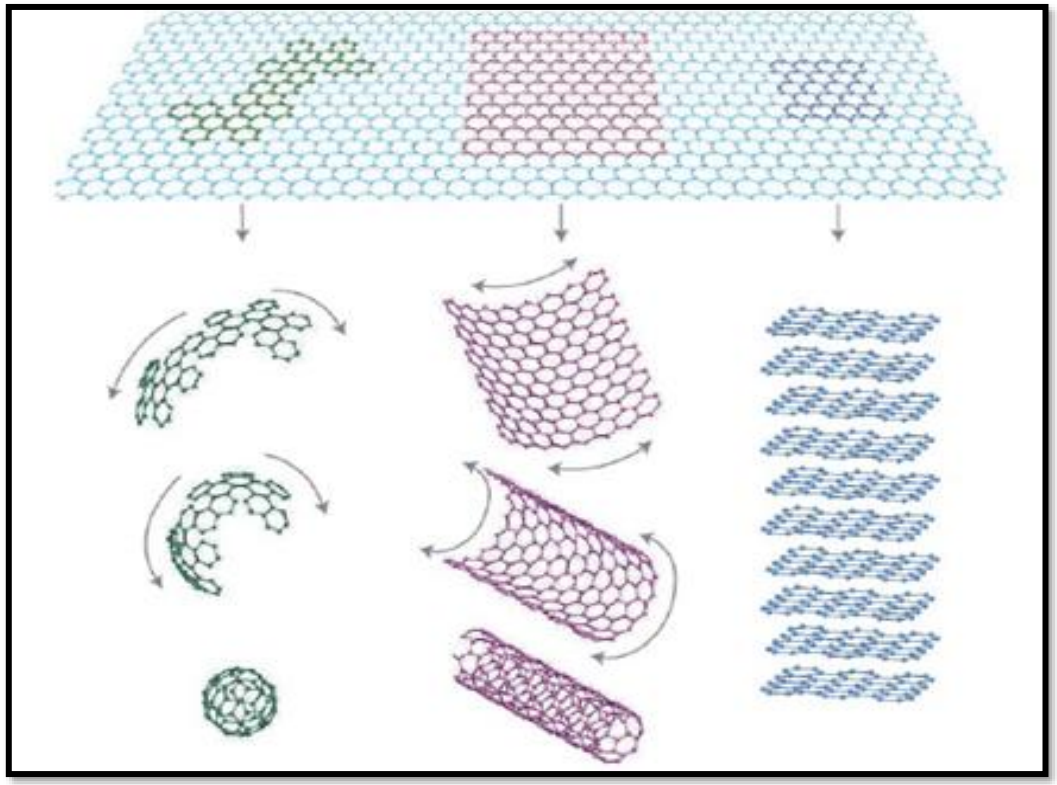

Fullerene (Bucky ball*) Nanotube Graphene

0D 1D 2D

***Nobel Prize in Chemistry 1996**

***Nobel Prize in Physics 2010**

Outline

- **Introduction and Background**
- **Graphene-Silicon Hybrid Detectors based on Photodiode Mode**
- **Graphene-Silicon Hybrid Detectors based on Photoconductor Mode**
- **Graphene based THz Modulator**
- **Conclusions**

Research Activities in CUHK

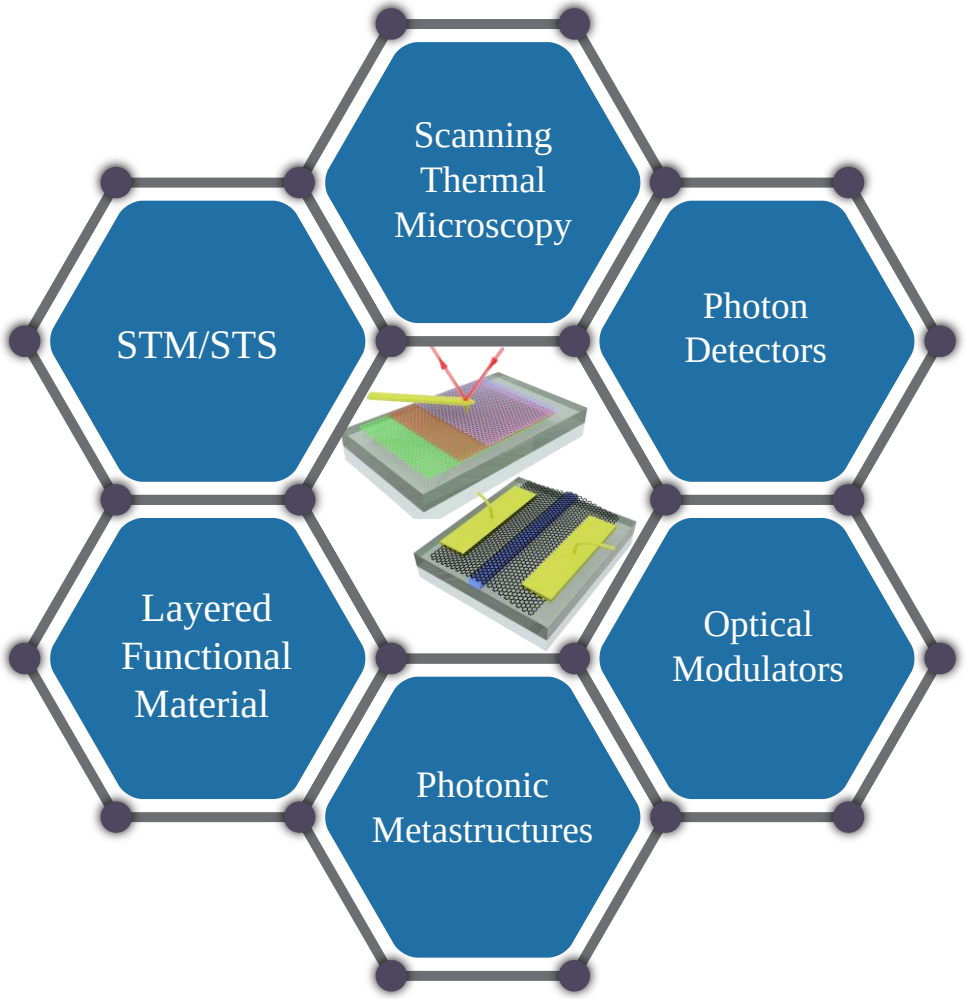

- Ultrathin Films of Electro-/Photo-Active Materials
- Nanometric Characterization
- Interface Engineering
- Nanoscaled Electron Devices
- 2D and Flexible Devices

What are 2D Materials?

2D layered materials typically have strong covalent or ionic bonds in plane and weaker van der Waals bonds between planes

<table>
<tr><td>Graphene family</td><td>Graphene</td><td colspan="2">hBN
'white graphene'</td><td>BCN</td><td>Fluorographene</td><td>Graphene oxide</td></tr>
<tr><td rowspan="2">2D chalcogenIdes</td><td colspan="2" rowspan="2">MoS_2, WS_2, $MoSe_2$, WSe_2</td><td colspan="2" rowspan="2">Semiconducting dichalcogenides:
$MoTe_2$, WTe_2,
ZrS_2, $ZrSe_2$ and so on</td><td colspan="2">Metallic dichalcogenides:
$NbSe_2$, NbS_2, TaS_2, TiS_2, $NiSe_2$ and so on</td></tr>
<tr><td colspan="2">Layered semiconductors:
GaSe, GaTe, InSe, Bi_2Se_3 and so on</td></tr>
<tr><td rowspan="2">2D oxides</td><td>Micas,
BSCCO</td><td colspan="2">MoO_3, WO_3</td><td rowspan="2" colspan="2">Perovskite-type:
$LaNb_2O_7$, $(Ca,Sr)_2Nb_3O_{10}$,
$Bi_4Ti_3O_{12}$, $Ca_2Ta_2TiO_{10}$ and so on</td><td>Hydroxides:
$Ni(OH)_2$, $Eu(OH)_2$ and so on</td></tr>
<tr><td>Layered
Cu oxides</td><td colspan="2">TiO_2, MnO_2, V_2O_5,
TaO_3, RuO_2 and so on</td><td>Others</td></tr>
</table>

- **Why?**
  - **Useful unique properties, e.g., high mobility, high thermal conductivity, broadband optical absorption, high optical nonlinearity.**
  - **Planar geometry compatible for integration with silicon photonics**

K. S. Novoselov, A. H. C. Neto, Science 353, aac9439 (2016)

M. S. Xu, et al, Chemical Review 113, 3766 (2013)

A. K. Geim, I. V. Grigorieva, Nature 499, 419 (2013)

2D Layered Materials

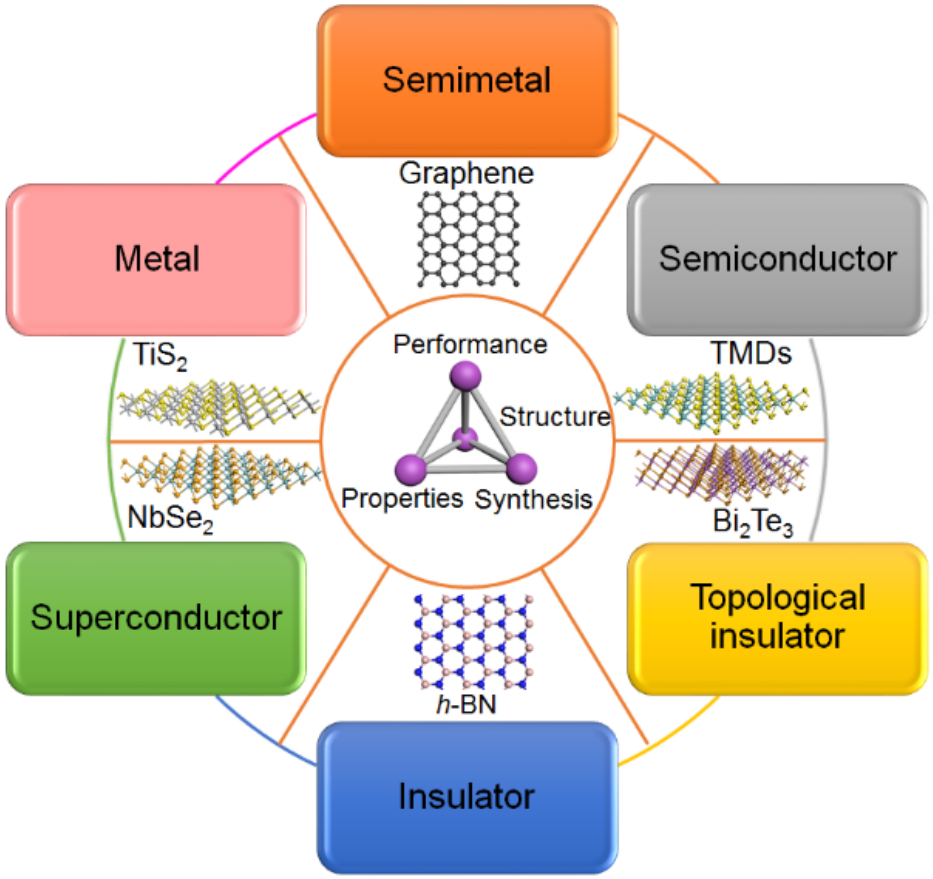

Classification of 2D Materials

1. Semimetals/Metals
2. Semiconductors
3. Insulators
4. Topological Insulators
5. Superconductors

X. M. Li, L. Tao, Z. F. Chen, J. B. XU, et al., *Applied Physics Reviews*, June 2017

2D Layered Materials

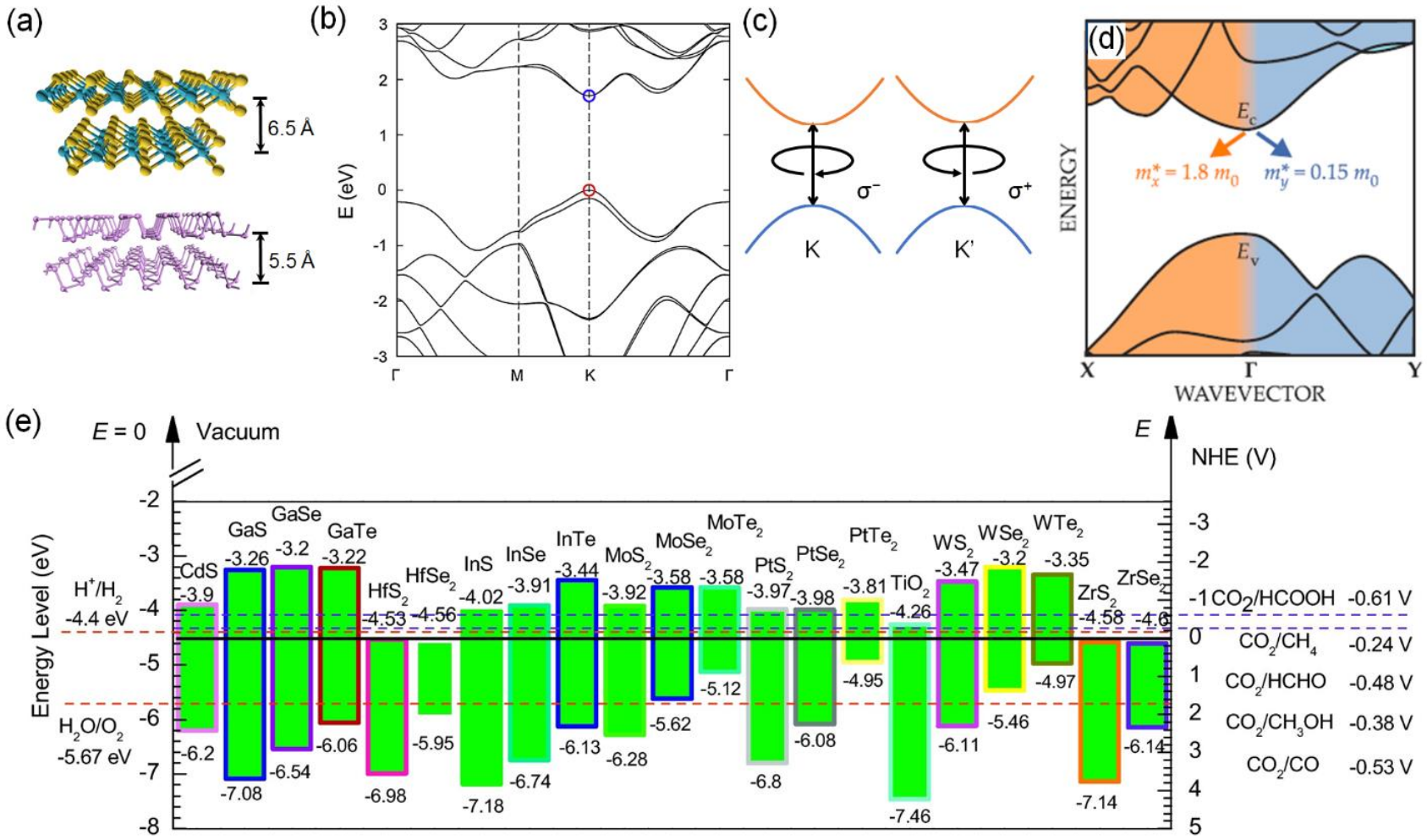

X. M. Li, L. Tao, Z. F. Chen, J. B. XU, et al., *Applied Physics Reviews*, June 2017

2D Layered Materials

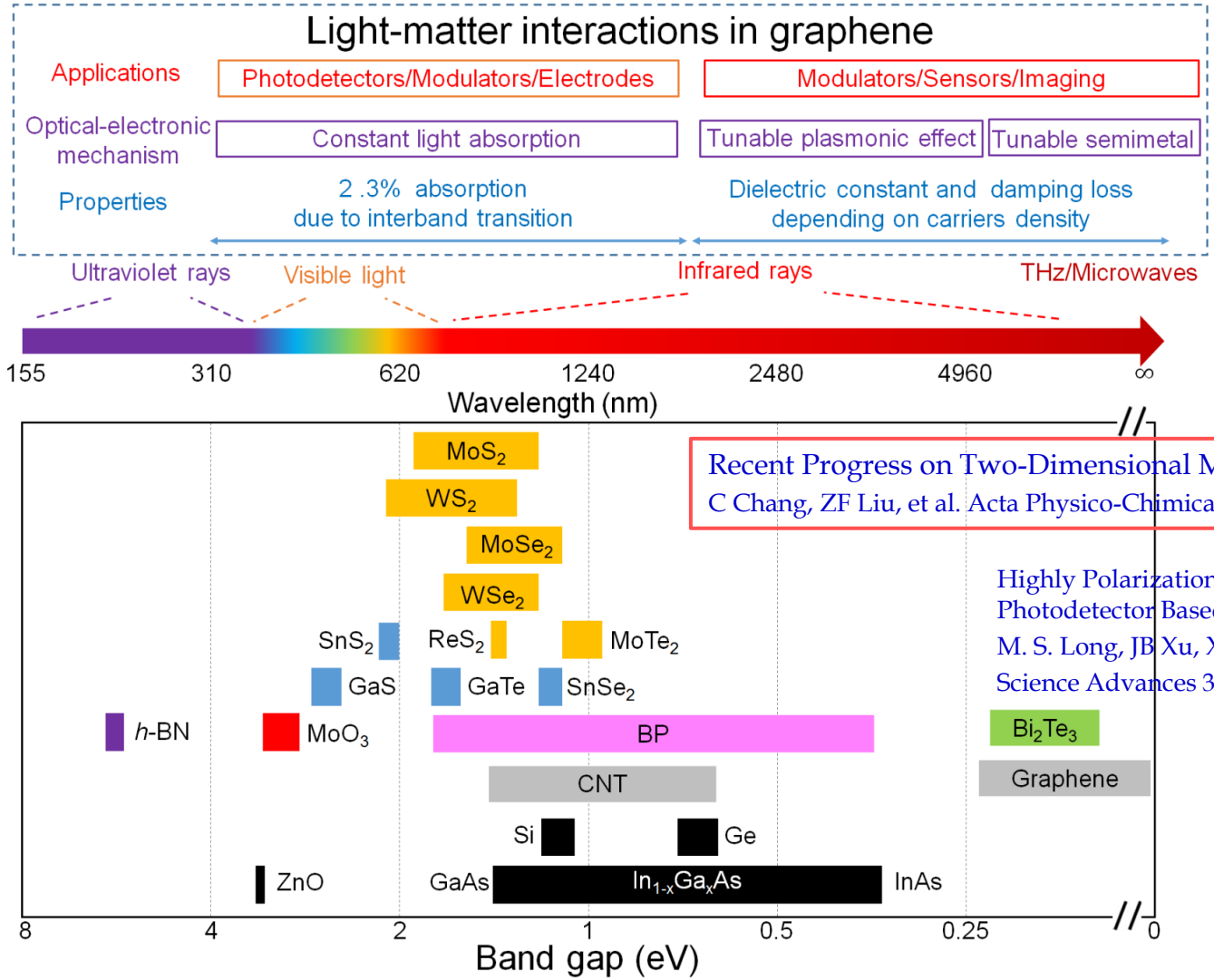

Highly Polarization Sensitive Infrared Photodetector Based on Black Phosphorus-on-WSe_2 Photogate Vertical Heterostructure
L Ye, P Wang, WJ Luo, L Gonf, Fan, Lei, T Liu, L Tong, JF Zang, JB Xu
Nano Energy 37, 53-60 (2017)

High-Performance Broadband Floating-Base Bipolar Phototransistor Based on WSe_2/BP/MoS_2 Heterostructure,
H Li, L Ye, JB Xu
ACS Photonics 4 (4), 823–829 (2017)

Near-Infrared Photodetector Based on MoS_2/Black Phosphorus Heterojunction
L Ye, H Li, ZF Chen, JB Xu
ACS PHOTONICS 3 (4), 692-699 (2016)

Recent Progress on Two-Dimensional Materials
C Chang, ZF Liu, et al. Acta Physico-Chimica Sinica 37 (12), Oct 13 2021

Highly Polarization Sensitive Mid-Infrared Photodetector Based on PAs
M. S. Long, JB Xu, X. M. Wang, F. Miao
Science Advances 3, (2017)

X. M. Li, L. Tao, Z. F. Chen, J. B. XU, et al., *Applied Physics Reviews*, June 2017

Various Interactions

"The Interface is the Device." by Herbert Kroemer, Nobel Laureate 2000

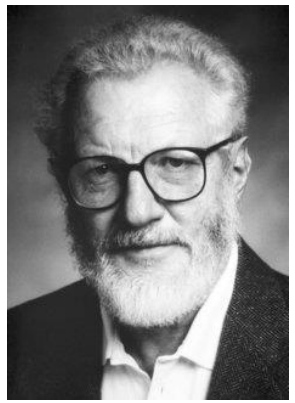

Aug. 1928 - Mar. 2024

Interactions of 2D Materials at Interfaces/Surfaces

1. van der Waals force
2. π-π interactions
3. Electrostatic interactions
4. Chemical bonds
5. Electromagnetic interactions, plasmonics

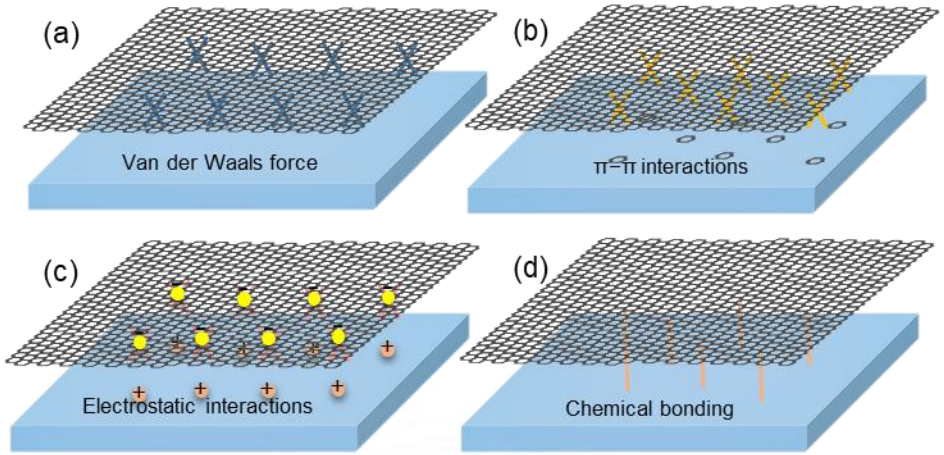

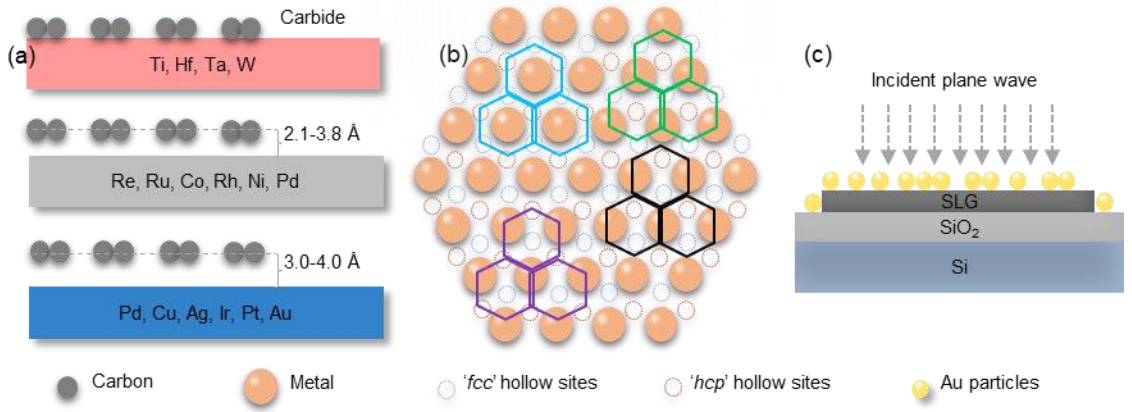

G. K. Zhao, X. M. Li, L. Tao, M. R. Huang, J. B. Xu, R. Ruoff, H. W. Zhu, et al., *Chemical Society Reviews*, July 2017
DOI: 10.1039/c7cs00256d

Enhancement Schemes for 2D

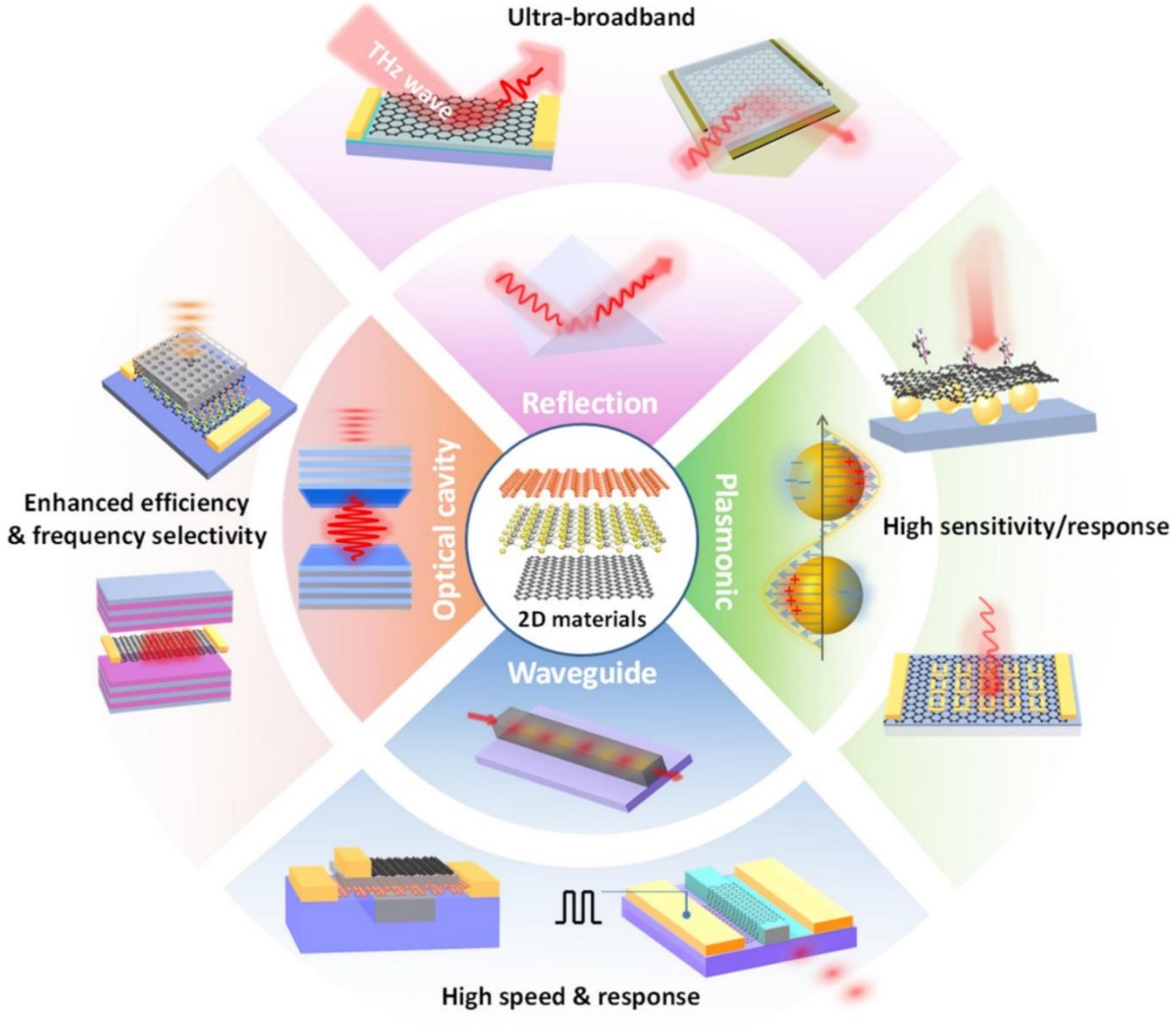

Li Tao, Zefeng Chen, Zhiyong Li, Jiaqi Wang, Xin Xu, Jian-Bin Xu, InfoMat 3(1), 36-60, 2020
https://doi.org/10.1002/inf2.12148

Polaritons in van der Waals (vdW) Materials

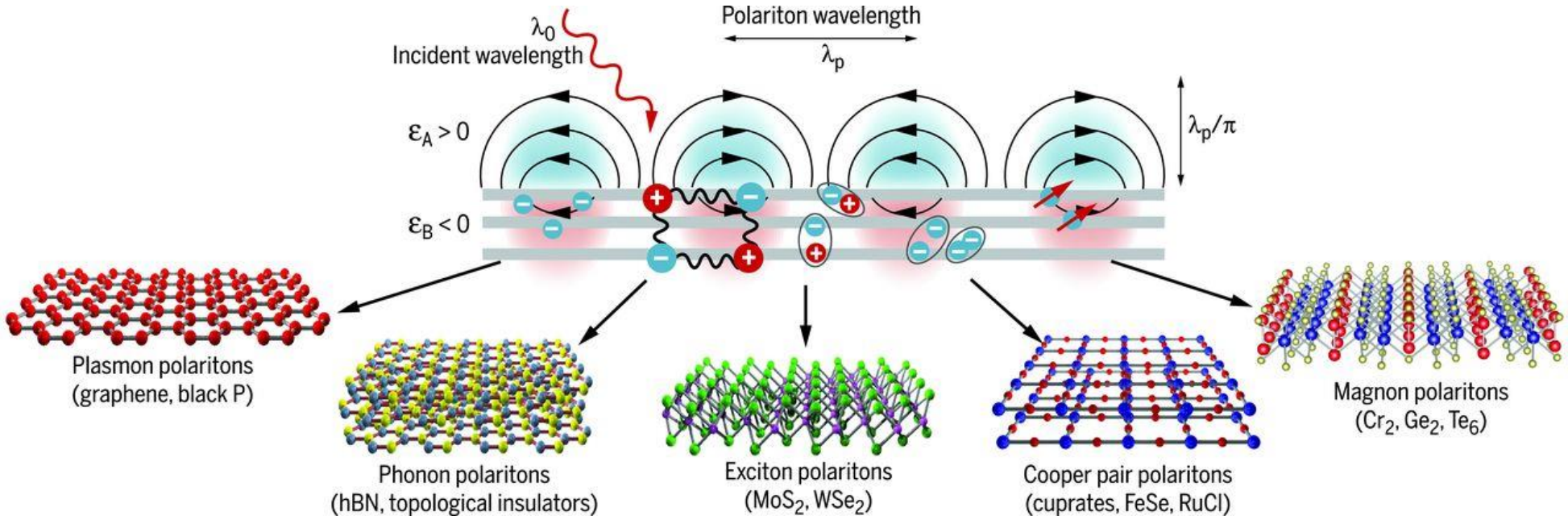

D. N. Basov, M. M. Fogler, F. J. Garcia de Abajo

Science **354** (6309), Article No. aag1992, DOI 10.1126/science.aag1992, 2016-10-14

Brief of Exciton-Polaritons in TMDs

Investigating interactions between excitonic and photonic modes is one of the central issues in the research of 2D optoelectronic materials.

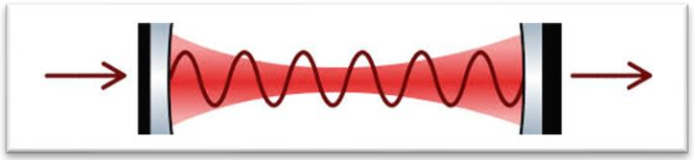

Photonic mode

+

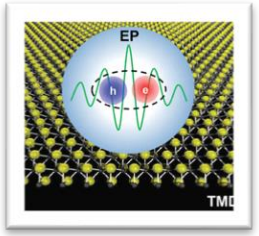

Exciton mode

In the weak-coupling regime, photonic resonances can enhance the excitonic emission of TMDs to facilitate 2D-material light sources, especially nanolasers.

Development of 2D TMDs nanolasers

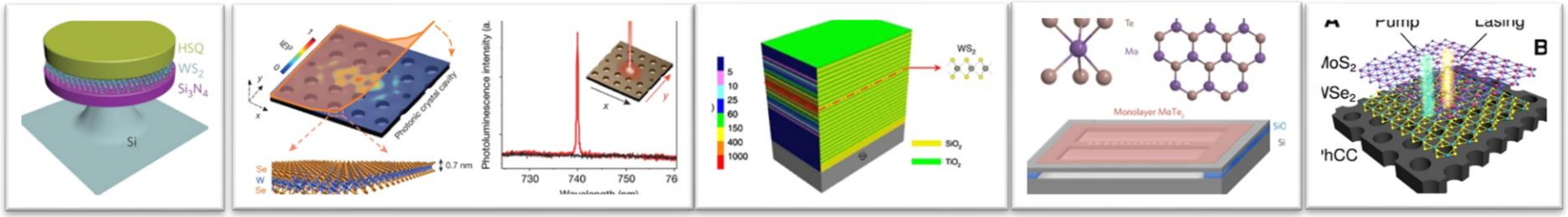

Nat. Photon. 9, 733–737 (2015) | *Nature* 520, 69–72 (2015) | *Nat Commun* 8, 543 (2017) | Nat. Nanotech. 12, 987–992 (2017) | Sci. Adv., 7, 30, (2021)

low temperature, pulsed-pump 2D nanolasers

room temperature, continuous-wave 2D nanolasers

Interlayer-exciton nanolasers

2015 — 2017 — 2021 — Time

Brief of Exciton-Polaritons in TMDs

Further enhancing exciton-photon coupling into strong-coupling regime can leads to half-photon half-exciton polaritonic states. Such hybrid states inherit unique properties from both photons and excitons.

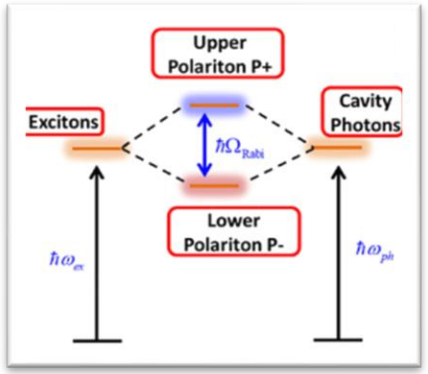

Various polaritonic phenomena inherit from excitonic physics

Valley-dependent polaritons

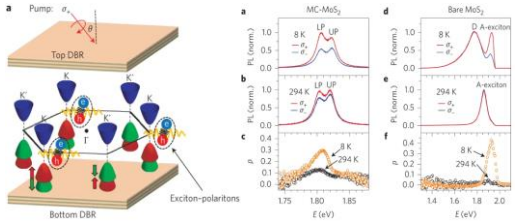

Nature Photon 11, 431–435 (2017)

Polaritonic condensates

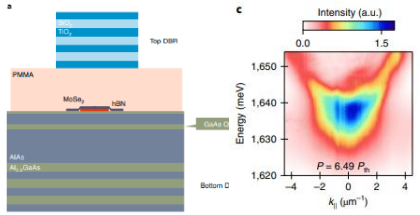

Nat. Nanotechnol. 17, 396–402 (2022)

Nonlinear polaritonic interactions

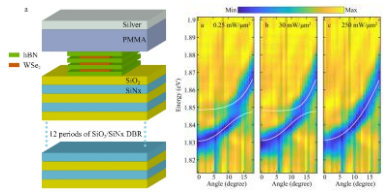

Nat Commun. 12, 2269 (2021)

Various photonic configurations to realize polaritons

Plasmonic cavities

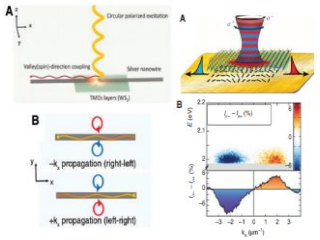

Science 359, 443–7 (2018)

ACS Photon. 5, 4, 1281–1287 (2018)

Dielectric Fabry–Pérot cavities

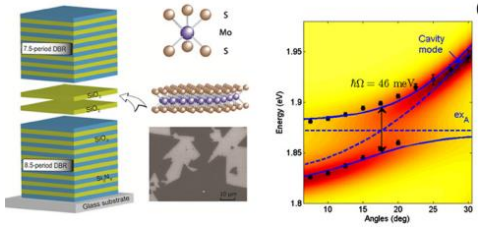

Nat. Photon. 9, 30–34 (2015)

Photonic crystal cavities

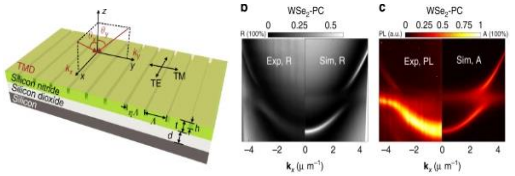

Nat. Commun. 9, 713 (2018)

F. H. Shen, Z. F. Chen, JBX, et al., Nat. Comm., https://doi.org/10.1038/s41467-022-33088-0 (2022)

FH Shen, ZF Chen, ZF; JBX, et al., ACS Photonics, 8 (12) , 3583-3590 (Dec 15 2021)

MoS_2 Electronics/Photonics

Second harmonic generation [1]

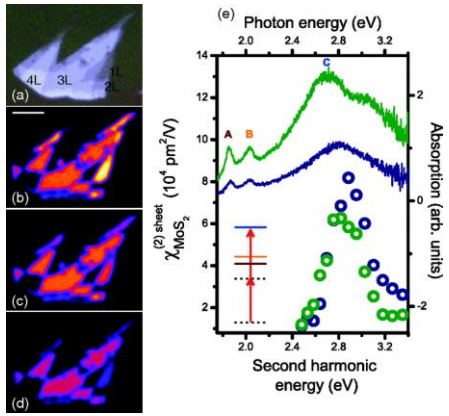

Photoluminescence in MoS_2 [2]

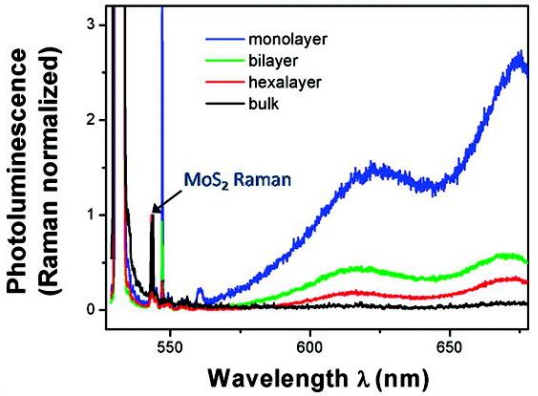

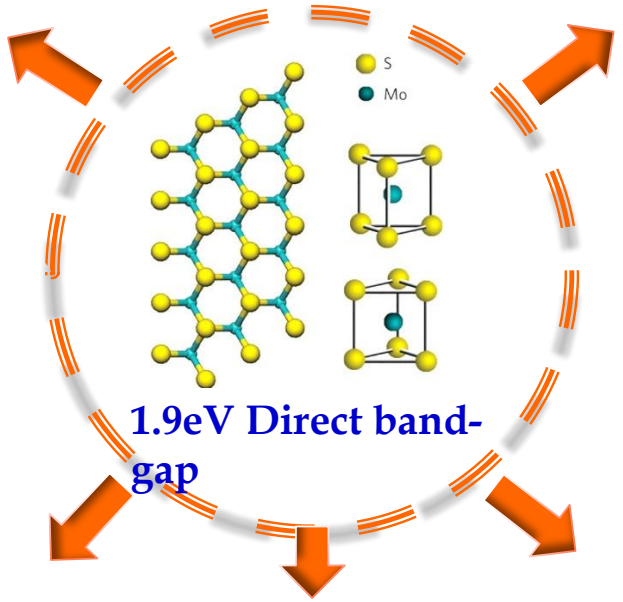

Ultrafast saturable absorber [3]

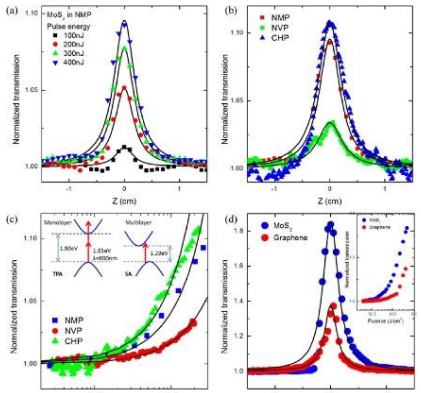

Single-Layer MoS_2 Phototransistors [4]

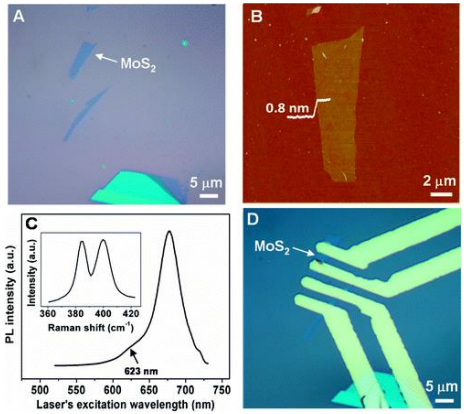

Photodetectors based on graphene-MoS_2 heterostructures [5]

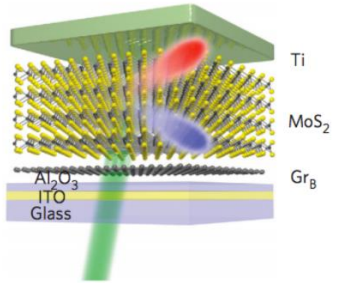

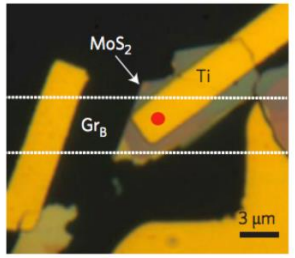

[1] L. M. Malard, et al, Physical Review B, p. 201401 (2013).
[2] A. Splendiani, et al, Nano letters, p. 1271 (2010).
[3] K. Wang, et al, ACS Nano, p. 9260 (2013).
[4] Z. Yin, et al, ACS Nano, p. 74 (2011).
[5] W. J. Yu, et al, Nat. Nanotechnol, p. 952, (2013).

PC Shen, LJ Li, J. Kong, et al., Nature 593, 211 (2021)

L Liu, TT Li, XR Wang, et al., Nature 605, 69 (2022)
WS Li, XR Wang, et al., Nature 613, 274- (2023)
WQ Meng, XR Wang, et al., Nature Nano 16, 1231 (2021); TT Li, XR Wang, et al, 16, 1201 (2021)

Review & Development

- Review by K. S. Novoselov, *et al*. Nature 490, 192–200 (2012)
- 24 m £ by UK, 1 B€ (flagship) by EU

REVIEW

doi:10.1038/nature11458

A roadmap for graphene

K. S. Novoselov[1], V. I. Fal'ko[2], L. Colombo[3], P. R. Gellert[4], M. G. Schwab[5] & K. Kim[6]

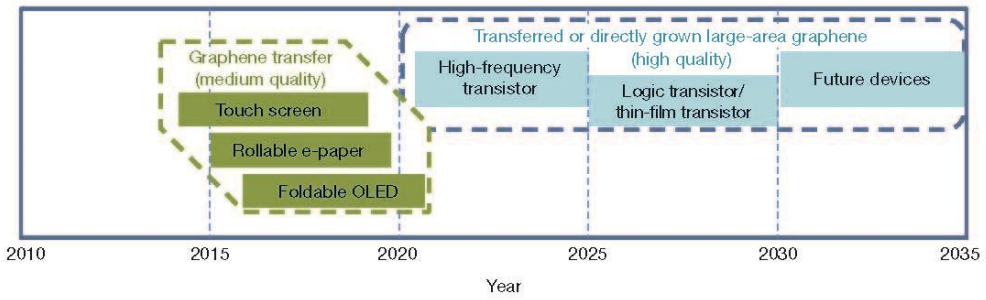

Figure 2 | Graphene-based display and electronic devices. Display applications are shown in green; electronic applications are shown in blue. Possible application timeline, based on projections of products requiring advanced materials such as graphene. The figure gives an indication of when a functional device prototype could be expected based on device roadmaps and the development schedules of industry leaders.

MoS_2/BP Heterojunction

Near-infrared photodetector based on MoS_2/black phosphorus heterojunction

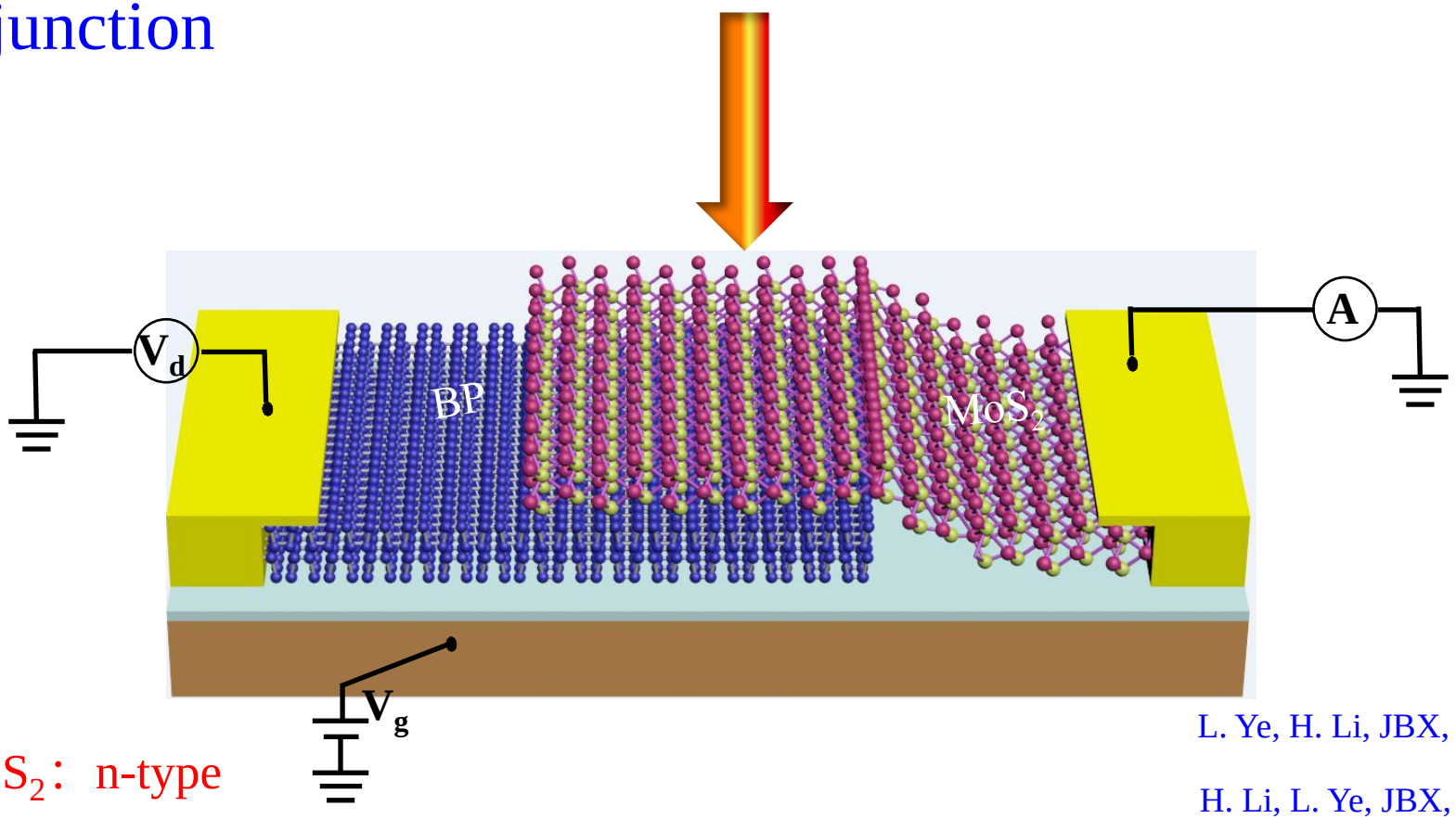

BP：p-type; MoS_2：n-type

BP- MoS_2：p-n junction; Gate-tunable

Visible-infrared

L. Ye, H. Li, JBX, ACS Photonics, 2016

H. Li, L. Ye, JBX, ACS Photonics, 2017

L. Ye, H. Li, JBX, et al., Nano Energy 37, 53-60, 2017

MS Long, A Gao, P Wang, H Xia, C Ott, JBX, F. Miao, Science Advances 3 (6), e1700589 (2017)

Photodection at 532 nm

L. Ye, H. Li, JBX, ACS Photonics, 2016

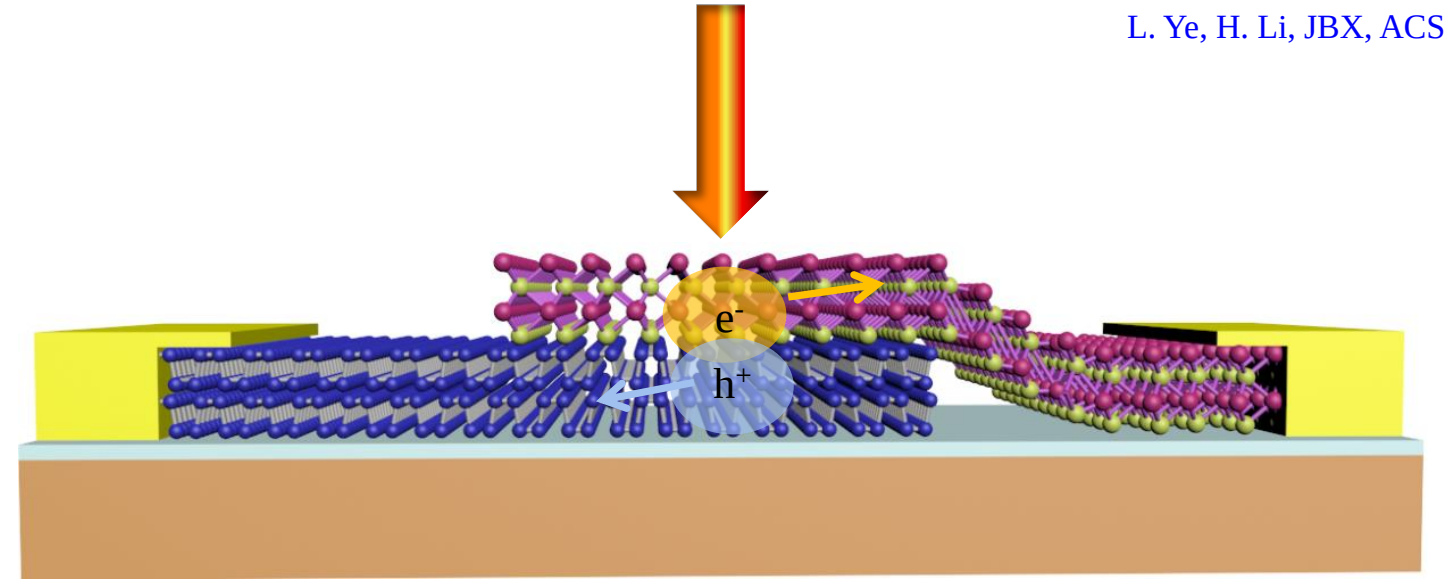

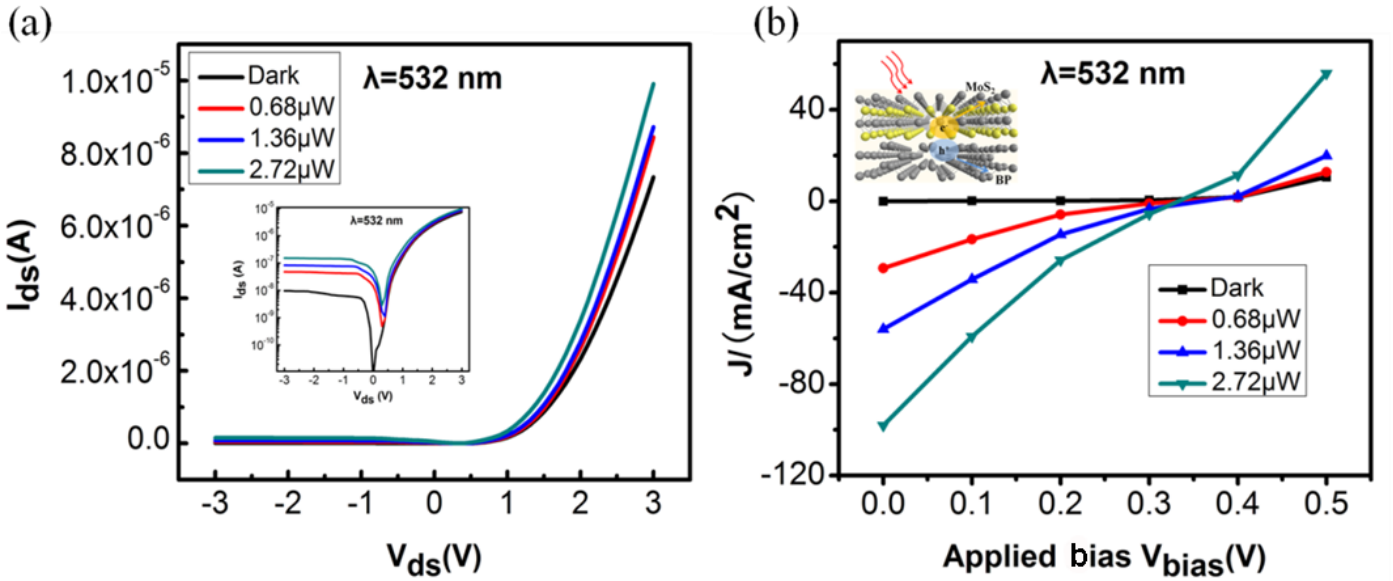

Outline

- Introduction and Background
- **Graphene-Silicon Hybrid Detectors based on Photodiode Mode**
- Graphene-Silicon Hybrid Detectors based on Photoconductor Mode
- Graphene based THz Modulator
- Conclusions

Mid-IR Photonics

1. Spectroscopy

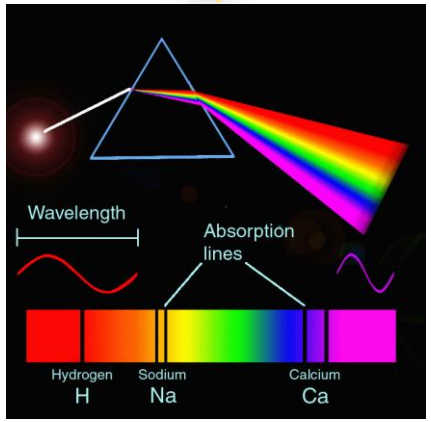

http://michaeljacksun123.blogspot.hk

2. "Fingerprint" Sensing

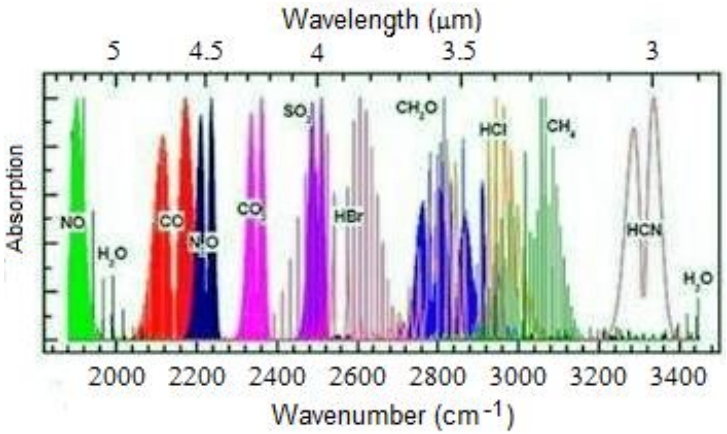

http://materion.com

3. Light Generation

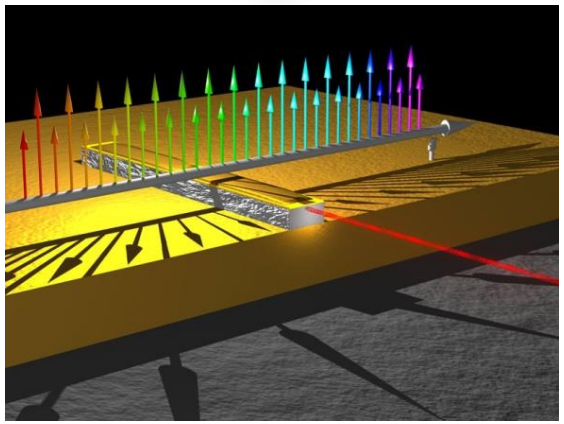

www.ethlife.ethz.ch

Applications

- Environmental Monitoring
- Health Diagnosis
- Alcohol Testing
- ……

Si Photonics & Gr Photonics

Silicon Photonics

Low Loss

No two photon absorption induced free carriers absorption [1]
Sidewall roughness loss reduced [2]

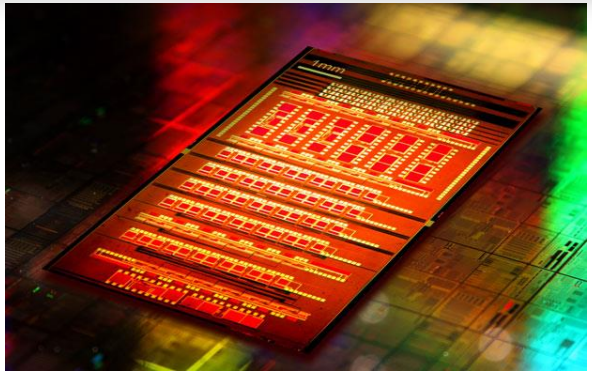

http://news.cnet.com

High Nonlinearity

Three magnitudes larger nonlinearity than standard single mode fiber [3]

Graphene Photonics

2D Material

(Compatible with Photonics Integrated Circuit) [4]

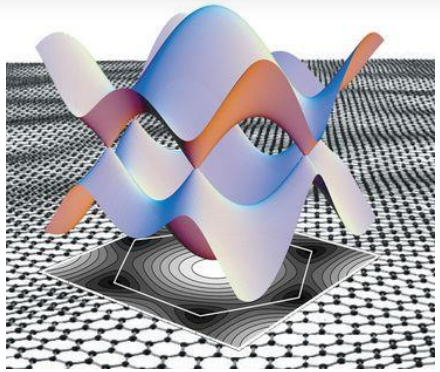

http://www.graphene.ac.rs/graphene.html

Zero Energy Band Gap

(Wide Spectral Range) [5]

[1] R. Soref, et al., J. Opt. A:,8, p. 840 (2006).
[2] X. Liu, et al., OE 19, p. 7778 (2011).
[3] Z.Cheng, et al., IEEE Photon. J. 4, p. 1510 (Oct. 2012).
[4] H. Li, et al., APL 101, p. 111110 (2012).
[5] A. H. C. Neto, et al., Rev. of Mod. Phy. 81, p. 109 (2009).

Optical Properties of Graphene

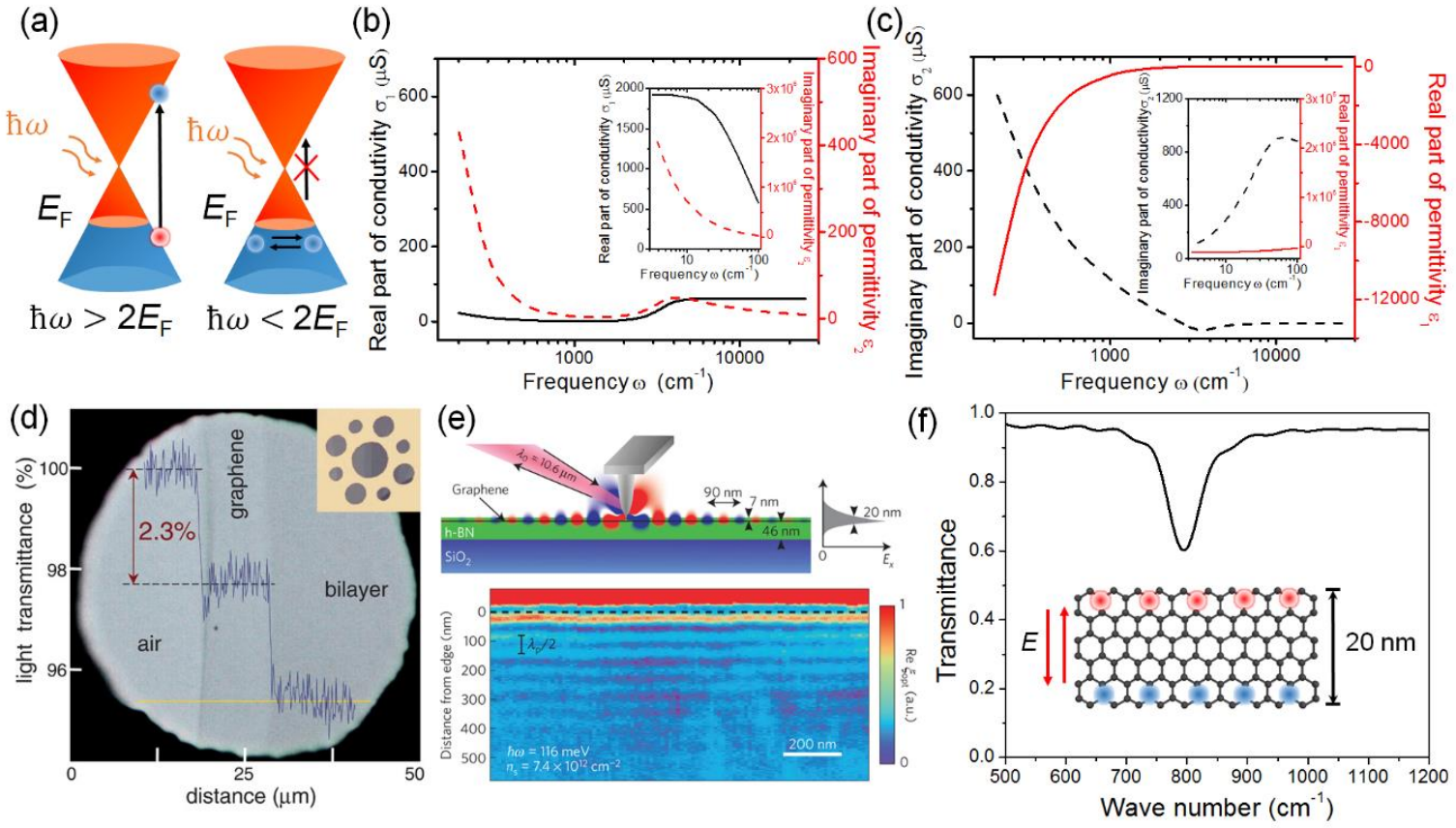

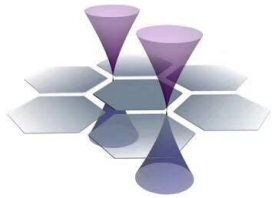

X. M. Li, L. Tao, Z. F. Chen, J. B. XU, et al., *Applied Physics Reviews*, June 2017

Gr Hybrid Structure for Integrated & Flexible Optoelectronics

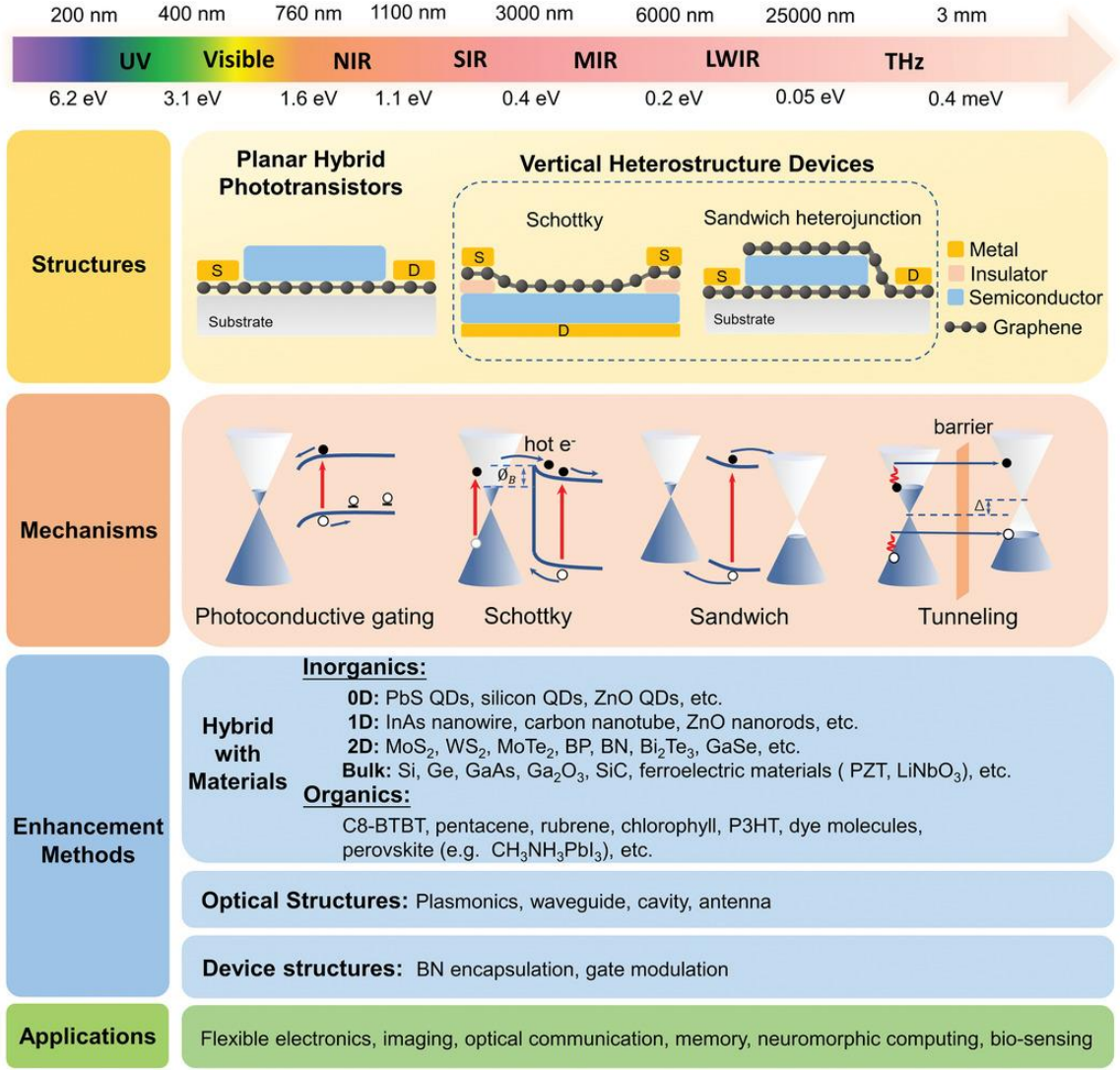

L. Gao, X.R. Wang, Y. Xu, et al., Advanced Materials, First published: 08 July 2019, DOI: (10.1002/adma.201902039)

Possible Mechanisms for Photo-Activities

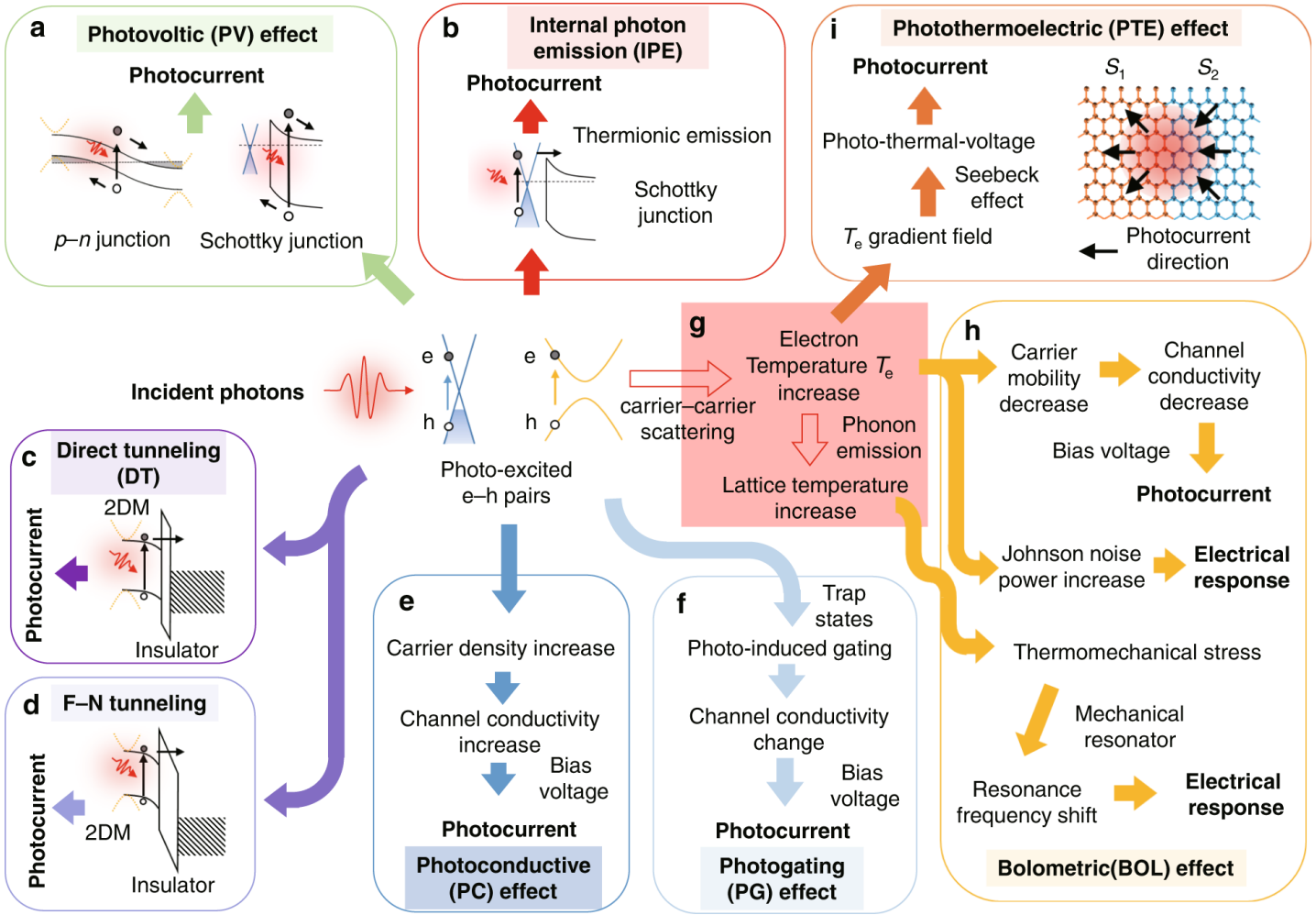

[1] C. Y. Liu, D. X., Dai, et al, Light: Science and Applications, 10(1), 123 (2021)

Background

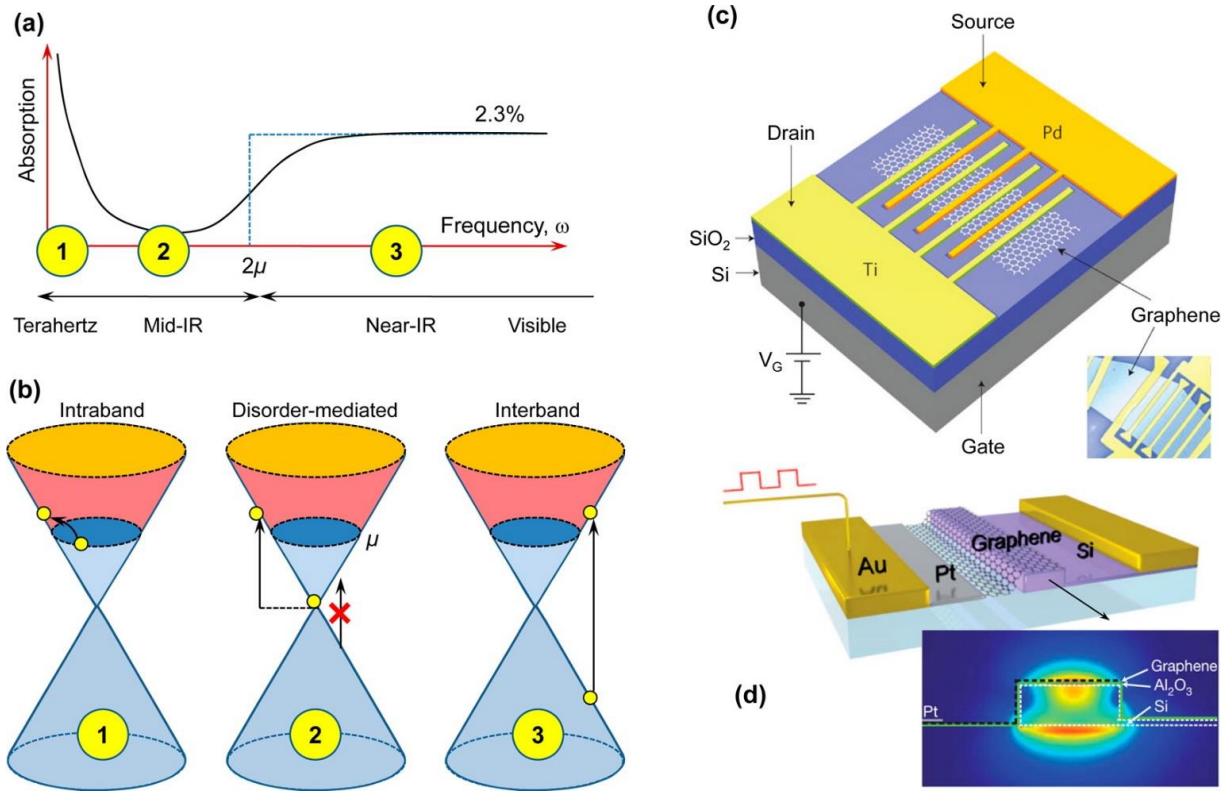

Tony Low; Phaedon Avouris; *ACS Nano* 2014, 8, 1086-1101.
DOI: 10.1021/nn406627u

M. Liu, X. Zhang, et al., Nature 474 (7349), 64-67 (2011)

(a) Illustration of a typical absorption spectrum of doped graphene.(29-32) It has characteristic features such as a Drude peak at terahertz frequencies, minimal absorption in the mid-infrared frequencies due to Pauli blocking and a transition to the universal 2.3% absorption beyond the far-infrared. (b) Illustration of the various optical transition processes. At small ω less than the thermal energy, transitions occur *via* intraband processes. At finite ω < 2 μ, disorder plays an important role in imparting the momentum for the optical transition. A transition occurs around ω ≈ 2 μ, where direct interband processes lead to a universal 2.3% absorption. (c) Schematic of a metal–graphene–metal photodetector with asymmetric metal contacts, which was operated at 10 Gbits/s data rate with 1.55 μm light excitation as described in ref 34. (d) Schematic of a graphene-based waveguide-integrated optical modulator reported in ref 35. Inset shows a finite element simulation of the waveguide's optical mode, designed so as to maximize the field at the interface between the waveguide and the graphene for maximal absorption efficiency.

Various Configurations of Devices

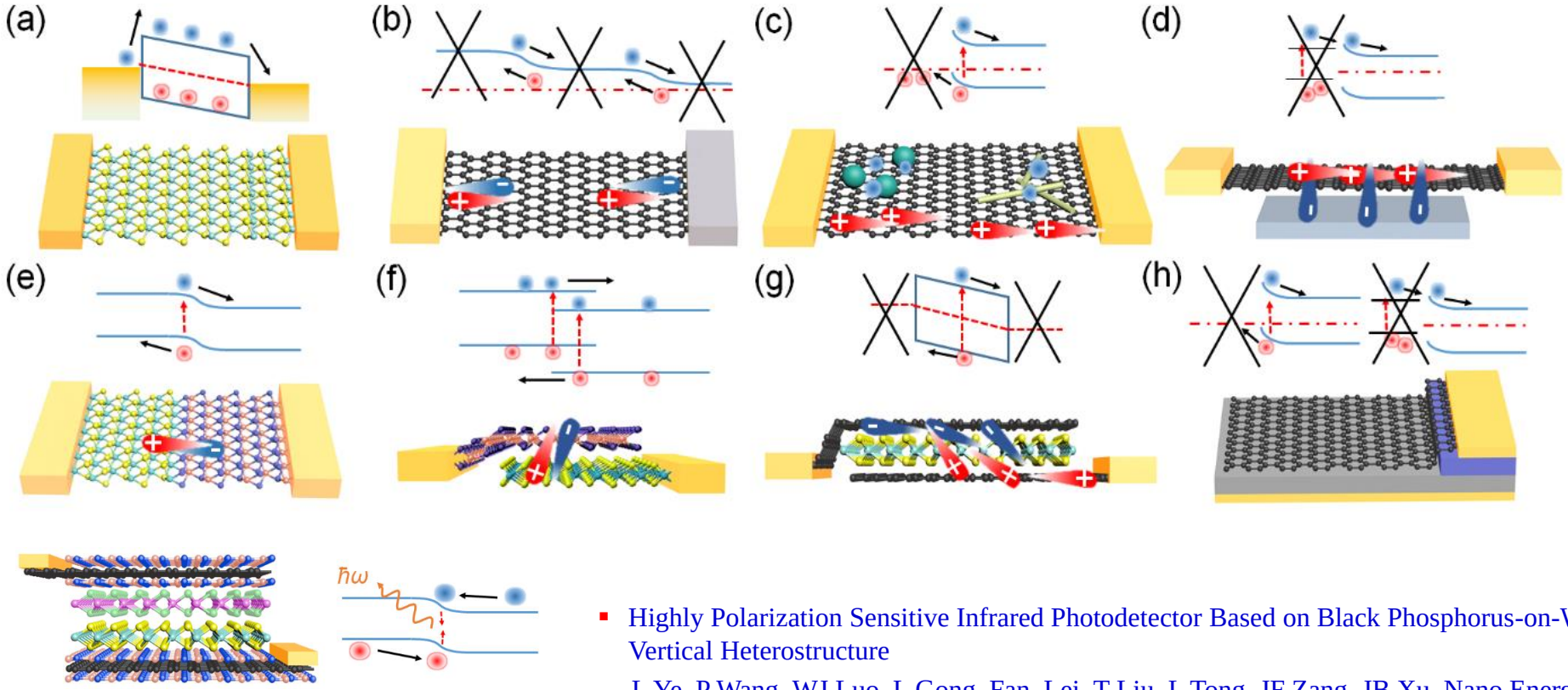

X. M. Li, L. Tao, Z. F. Chen, J. B. XU, et al., *Applied Physics Reviews*, June 2017

- Highly Polarization Sensitive Infrared Photodetector Based on Black Phosphorus-on-WSe_2 Photogate Vertical Heterostructure
  L Ye, P Wang, WJ Luo, L Gong, Fan, Lei, T Liu, L Tong, JF Zang, JB Xu, Nano Energy 37, 53-60 (2017)
- High-Performance Broadband Floating-Base Bipolar Phototransistor Based on WSe_2/BP/MoS_2 Heterostructure,
  H Li, L Ye, JB Xu, ACS Photonics 4 (4), 823–829 (2017)
- Near-Infrared Photodetector Based on MoS_2/Black Phosphorus Heterojunction
  L Ye, H Li, ZF Chen, JB Xu, ACS Photonics 3 (4), 692-699 (2016)

Optical Properties of Graphene

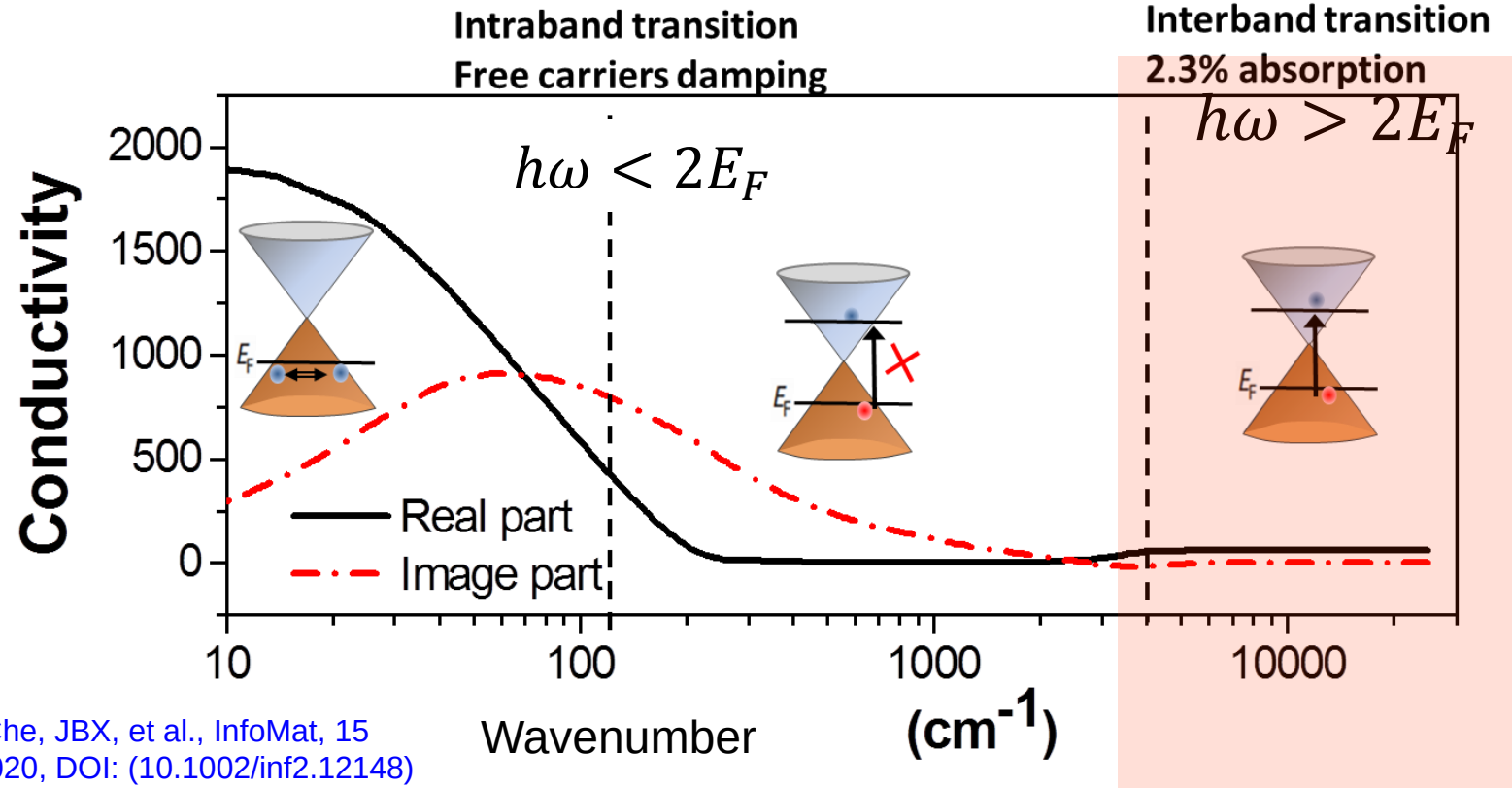

L. Tao, Z. F. Che, JBX, et al., InfoMat, 15 September 2020, DOI: (10.1002/inf2.12148)

Spectrum: Tera Hertz — Far / Mid infrared — Near infrared/Visible

Application: THz device — surface plasmonic — photodetector

Mechanism: Tunable conductivity — Interband Light absorption

Comparison of PC and PD

Advantage and disadvantage for PC photodetector

❖ Advantage:

1. high mobility leads to high gain in phototransisitor/photoconductor
2. zero- band gap leads to broadband response from visible light to infrared light
3. stable monolayer leads to flexible device

❖ Disadvantage:

1. zero- band gap lead to low light on/off ration (high dark current)
2. monolayer to low light absorption (2.3%) and reduce the photoresponse

➢ **Using hybrid structure (heterostructure) to overcome the disadvantage,**

Including:

1) graphene/semiconductor photodiode (use semiconductor as absorption material)
2) graphene hybrid photoconductor (use semiconductor as absorption material and graphene as conduction channel)

Photodiode Mode

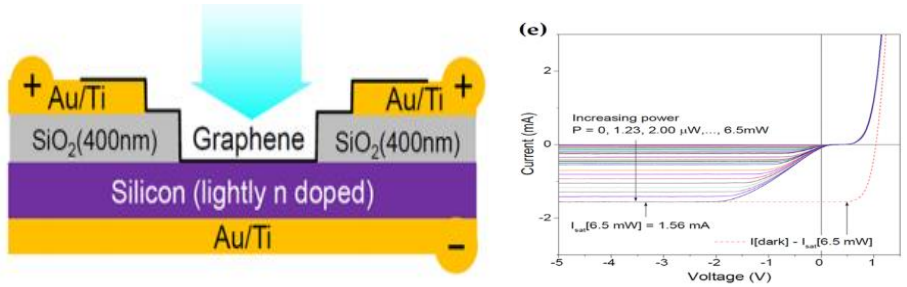

Xiaohong An *et al.* Nano Lett. 2013, 13, 909−916

1) graphene-semiconductor heterosjuncution

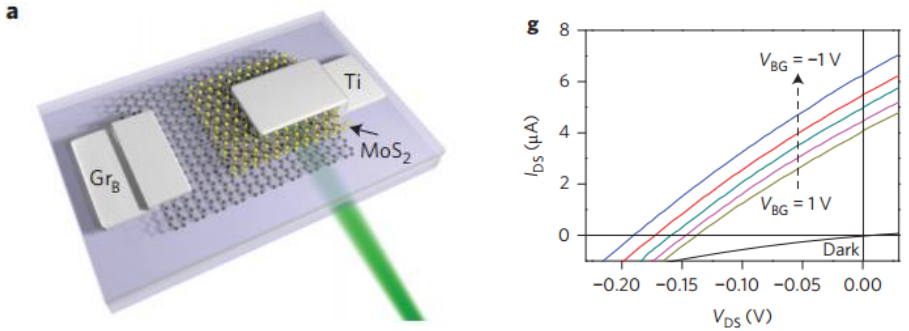

Xiangfeng Duan *et al.* Nature Nanotechnology 8, 952–958 (2013)

2) Graphene/ MoS_2 heterojunction

1. **Light absorption depends on the other material, such as silicon or MoS_2**
2. **photo-induced carriers are separated by the built-in field**
3. **low responsivity ~ < 1A/W**
4. **high light on/off ration**

Photodoide Mode do not present the advantage of graphene such as high mobility and broadband light absorption

Photoconductor/Photo-Transistor Mode

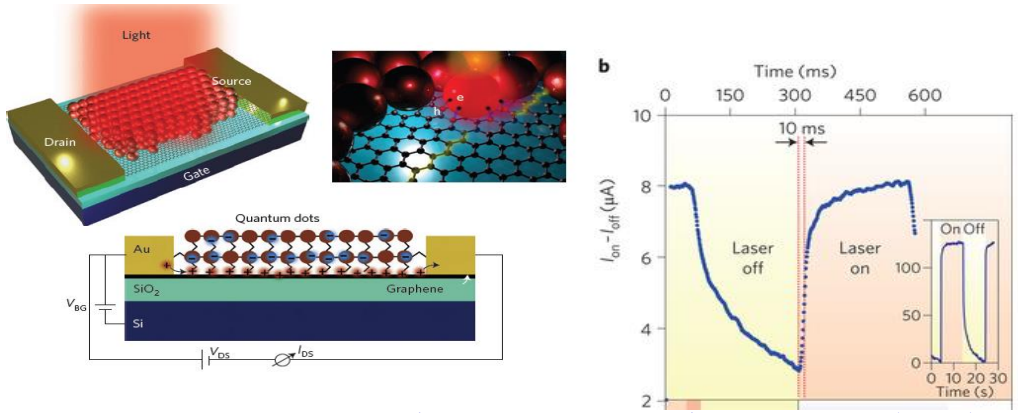

Koppens et al Nature Nanotech. 7, 363–368 (2012)

1) hybrid graphene phototransistor

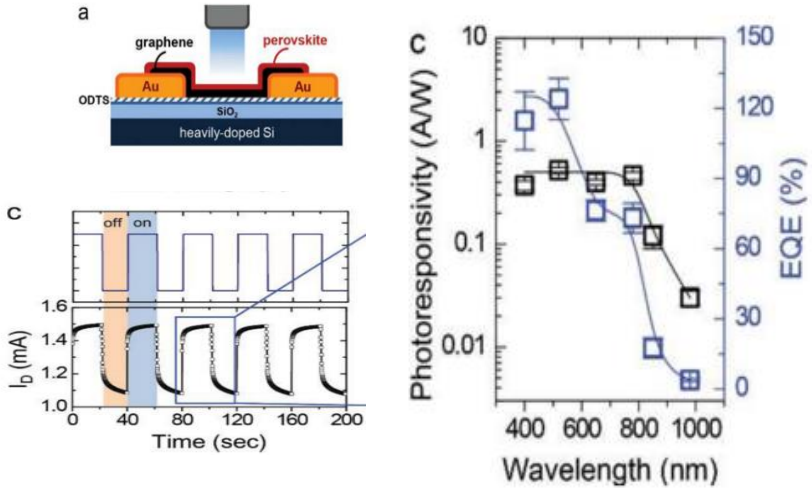

Youngbin Lee Adv. Mater. 2015, 27, 41–46

2) Perovskit/ graphene phototransistor

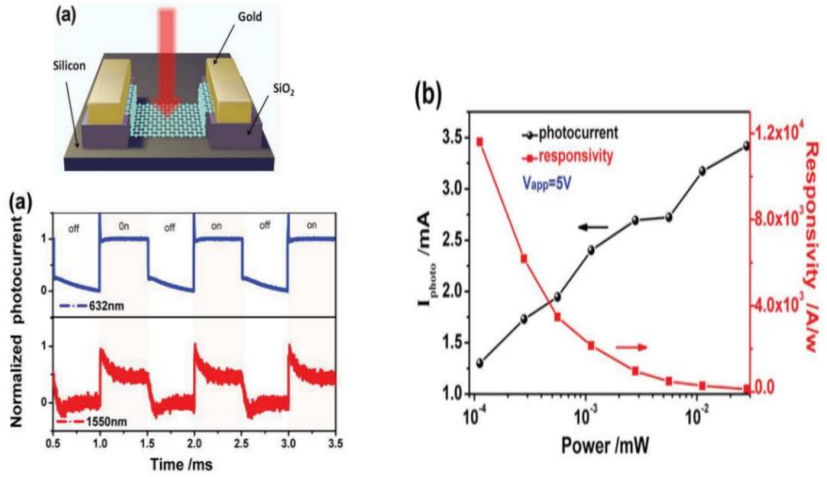

Chen Zefeng Adv. Optical Mater. 2015, 3, 1207–1214

3) graphene/silicon photoconductor

Enhancement Schemes

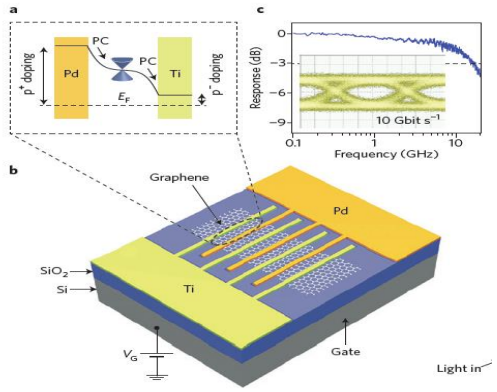

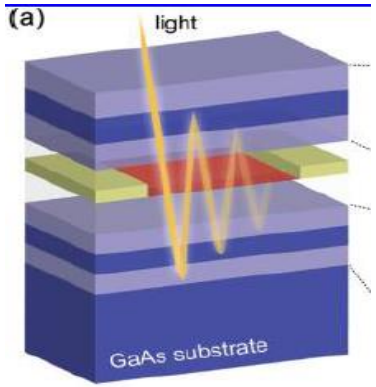

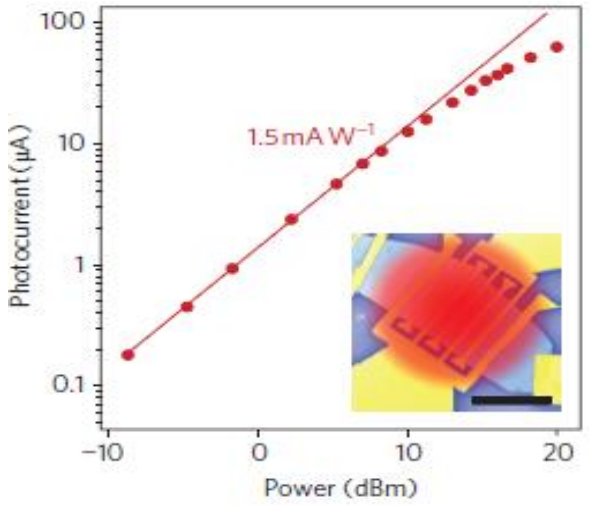

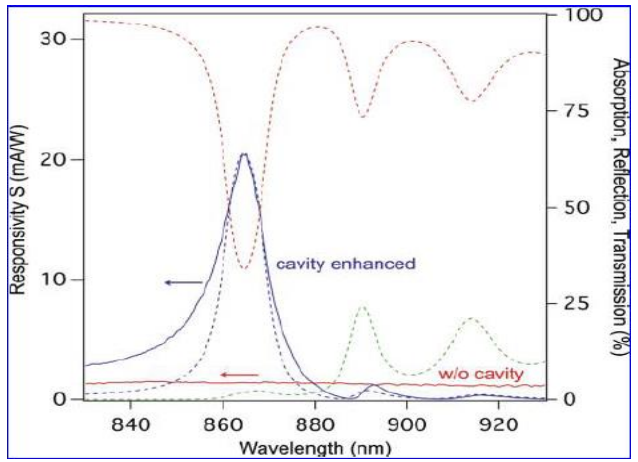

- graphene–metal junctions.
- ultral fast but low responsivity.

Nature Photon. 4, 297–301 (2010).

- light absorbtion enhancement by
- optical cavity.Enhancement effect only for certain wavelength

Nano Lett. 12, 2773–2777 (2012).

Waveguide Enhancement Scheme

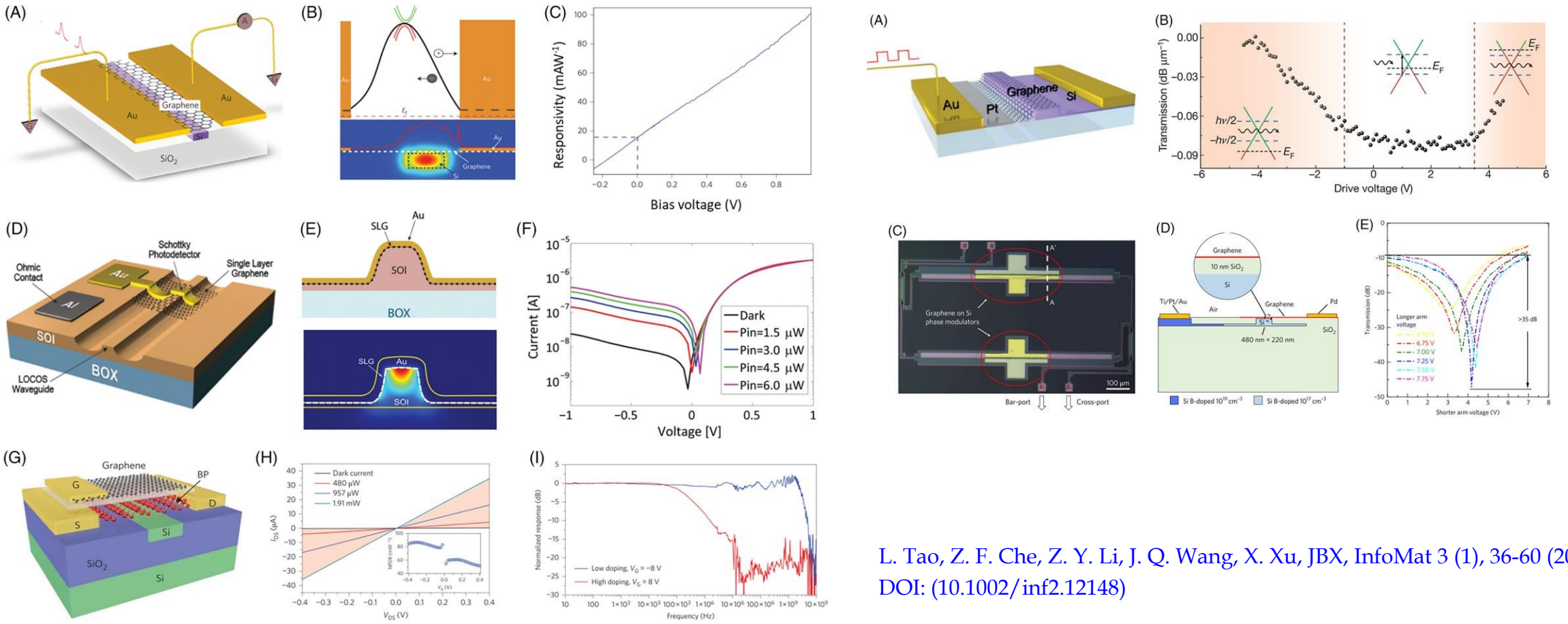

L. Tao, Z. F. Che, Z. Y. Li, J. Q. Wang, X. Xu, JBX, InfoMat 3 (1), 36-60 (2020), DOI: (10.1002/inf2.12148)

SOS & SOI

- Silicon-on-Insulator (**SOI**)[1] and Silicon-on-Sapphire (**SOS**)[2-4] have been proposed for mid-IR applications.

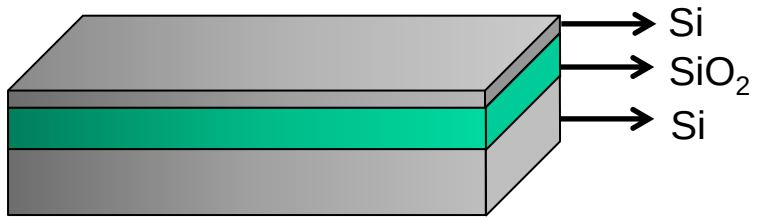

SOI Wafer

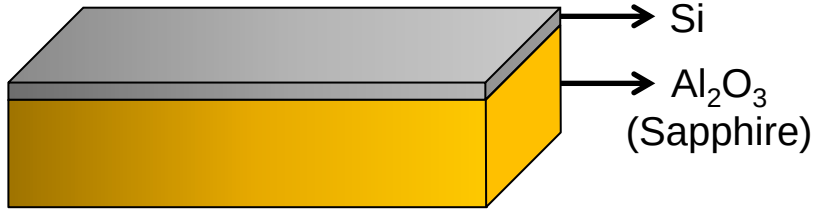

SOS Wafer

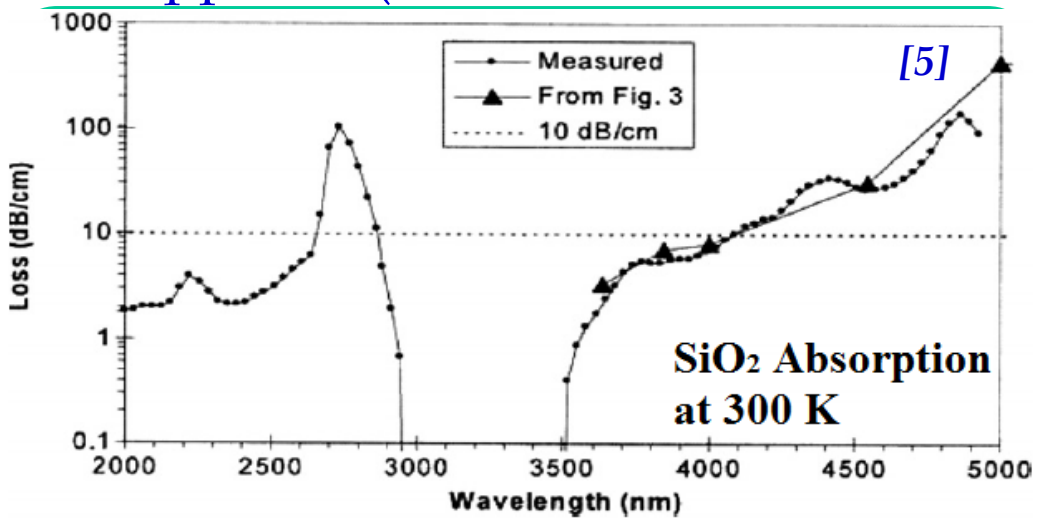

- ✓ Substrate is very lossy beyond 5.0 μm [5]
- ✓ More defect

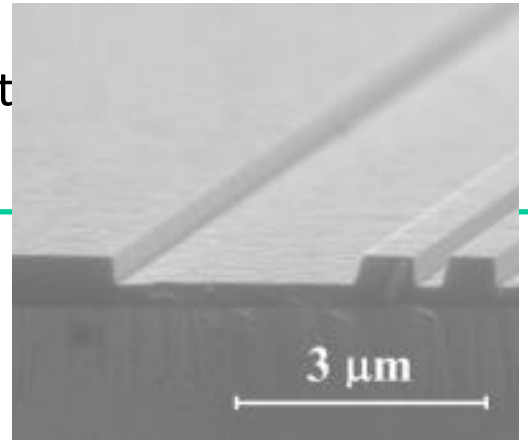

SOS waveguide surface

[1] B. Jalali, et al., IEEE JSTQE 12, p. 1618 (2006).
[2] N. K. Hon, et al., APL 94, p. 091116 (2009).
[3] A. Spott, et al., APL 97, p. 213501 (2009).
[4] Z. Cheng, et al. IEEE Photon. J. 4, p. 104 (Jan. 2012).
[5] R. Soref, et al., J. Opt. A: Pure Appl. Opt. 8, p. 840 (2006).

Suspended Membrane

Suspended Membrane Waveguides (SMWs). [1-2]

R A Soref *et al*

[3]

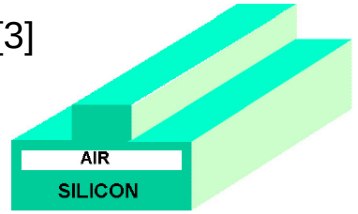

Figure 7. Proposed low-loss 'suspended' LWIR rib-channel waveguide consisting of a silicon membrane clad below and above by air. This waveguide is constructed from a rib-etched SOI wafer that is undercut (oxide etched away) locally beneath the rib area.

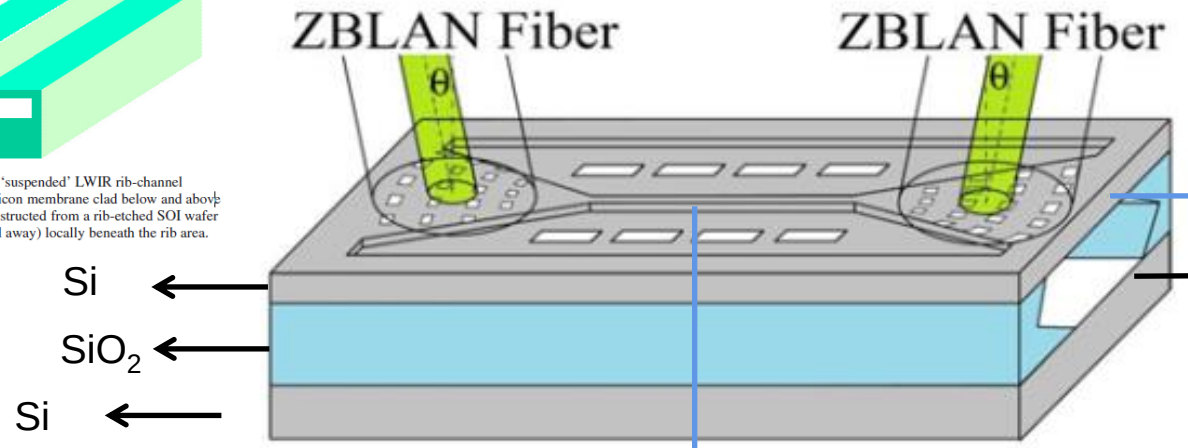

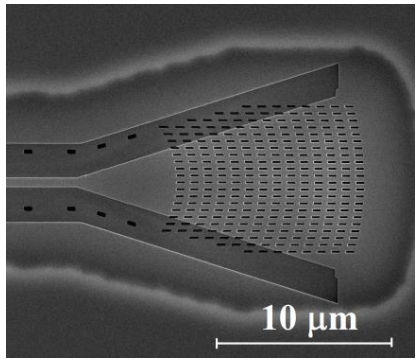

BOX under device is locally removed by wet etching.

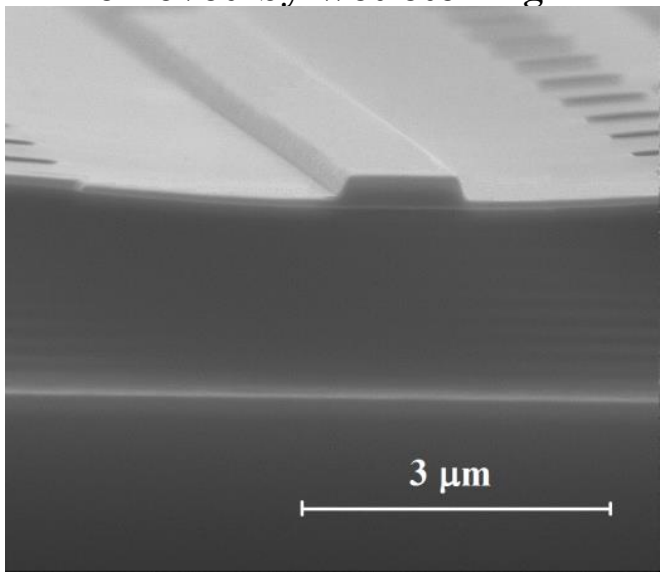

Advantages of *SMW*

1. High quality SOI start wafer
2. Using the high-yield silicon fabrication process
3. Accurate & repeatable dimension control
4. Less limitation on device size and wavelength

[1] Z. Cheng, et al., Opt. Lett.37, p. 1217 (April 2012).
[2] Z. Cheng, et al., GFP. San Diego, USA, (Sep. 2012).
[3] R. Soref, et al., J. Opt. A:,8, p. 840 (2006).

Graphene on Si Suspended Membrane

- Integrated graphene on silicon suspended membrane devices.

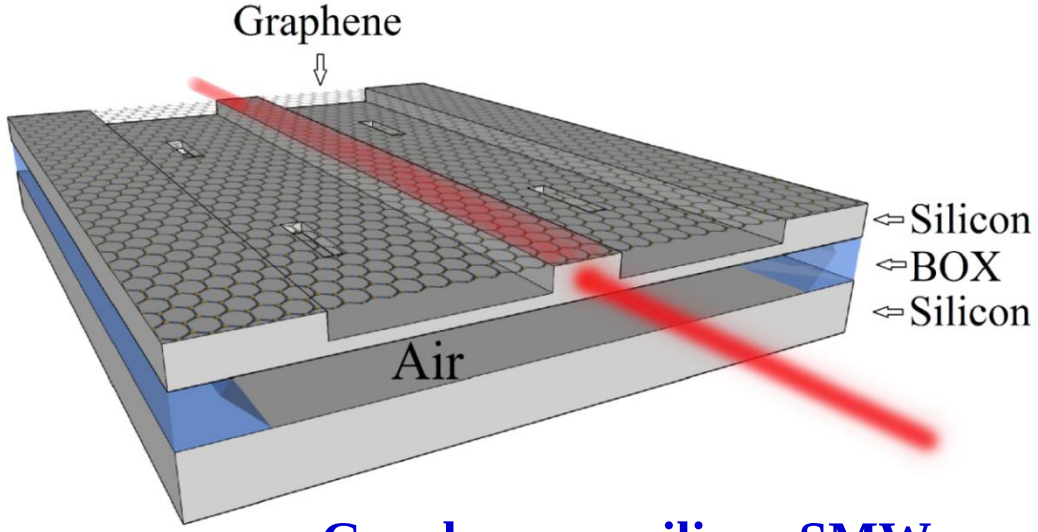

PROS.

→ **Ultra-wide bandwidth devices (from 1.1 μm to 8.0 μm)** [1]

→ **In-plane absorption increase the interaction** [2]

Graphene-on-silicon SMW

→ **Polarization dependence** [3]

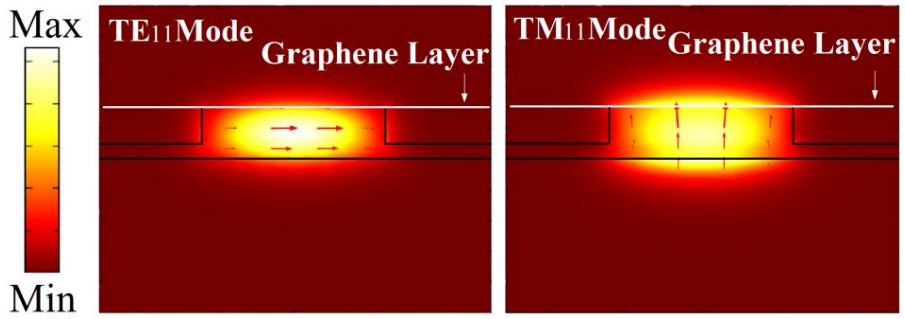

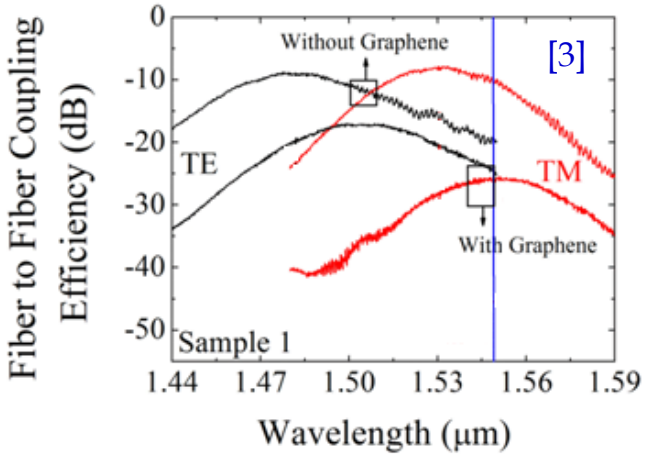

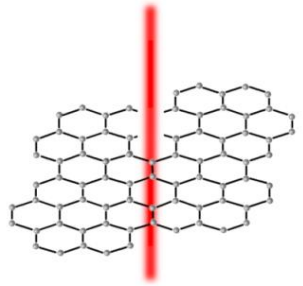

2.3% absorption

[1] R. Soref, et al., J. Opt. A: Pure Appl. Opt. 8, p. 840 (2006)

[2] H. Li, et al., APL 101, p. 111110 (2012).

[3] Z. Cheng, et al., IEEE IPC, Bellevue Washington, USA, (Sep. 2013)

Focused Subwavelength Grating

- Novel grating coupler for mid-IR silicon photonics. [1]

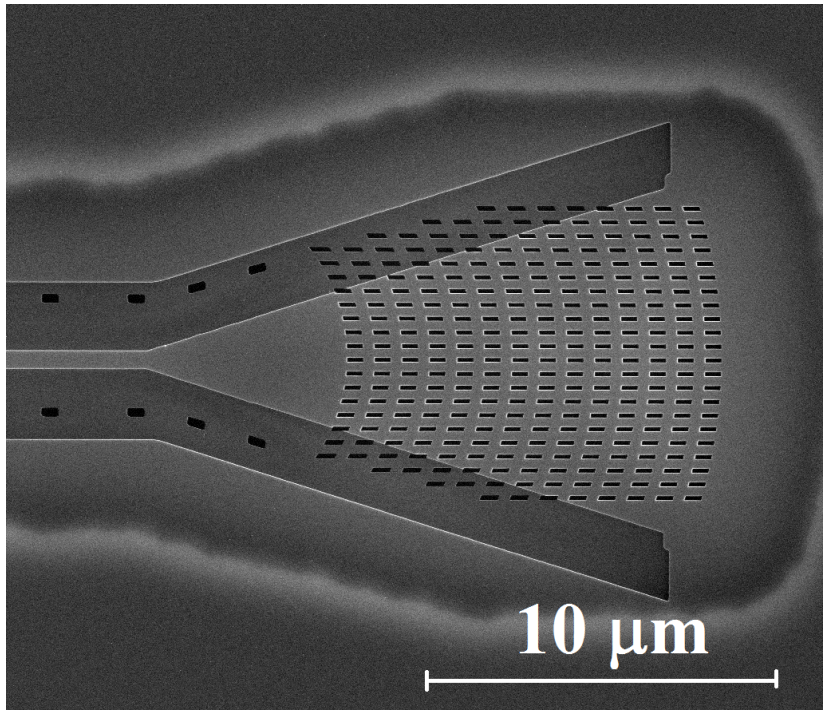

✓ About ~25% maximum coupling efficiency was achieved at 2.75 μm wavelength with an uniform SWG.

[2]

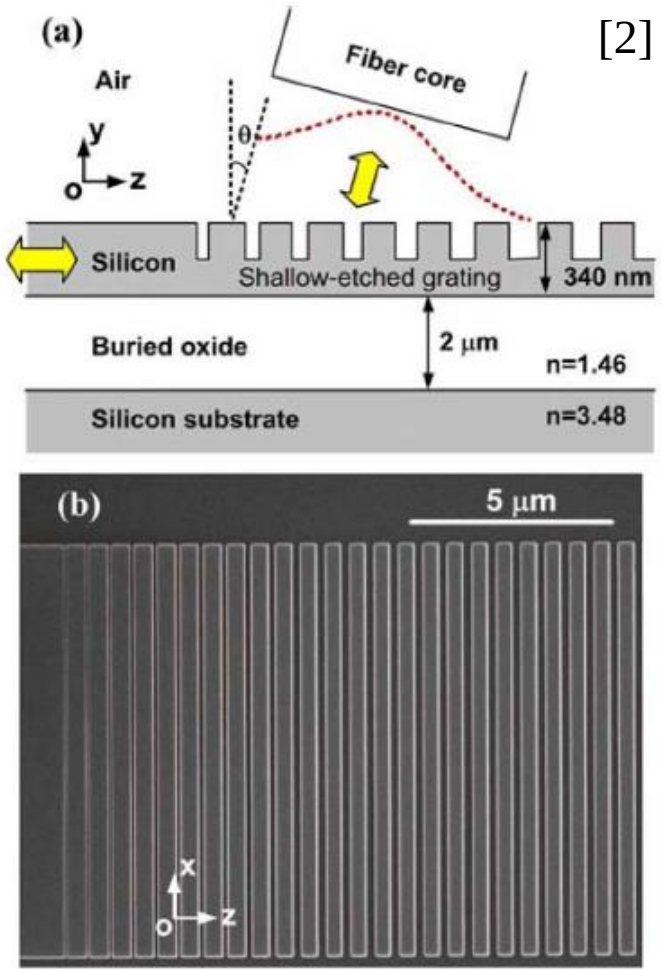

[1] Z. Cheng, et al., Opt. Lett.37, p. 1217 (April 2012).

[2] X. Chen, et al., IEEE PTL 22, p. 1156, 2010.

Photodetector Measurement

➢ Photodetector characterization at 2.75 μm wavelength.

X. M. Wang, Z. Z. Cheng, J. B. Xu, et al.,
Nature Photonics 7, 888-891, Sept. 15 (2013)

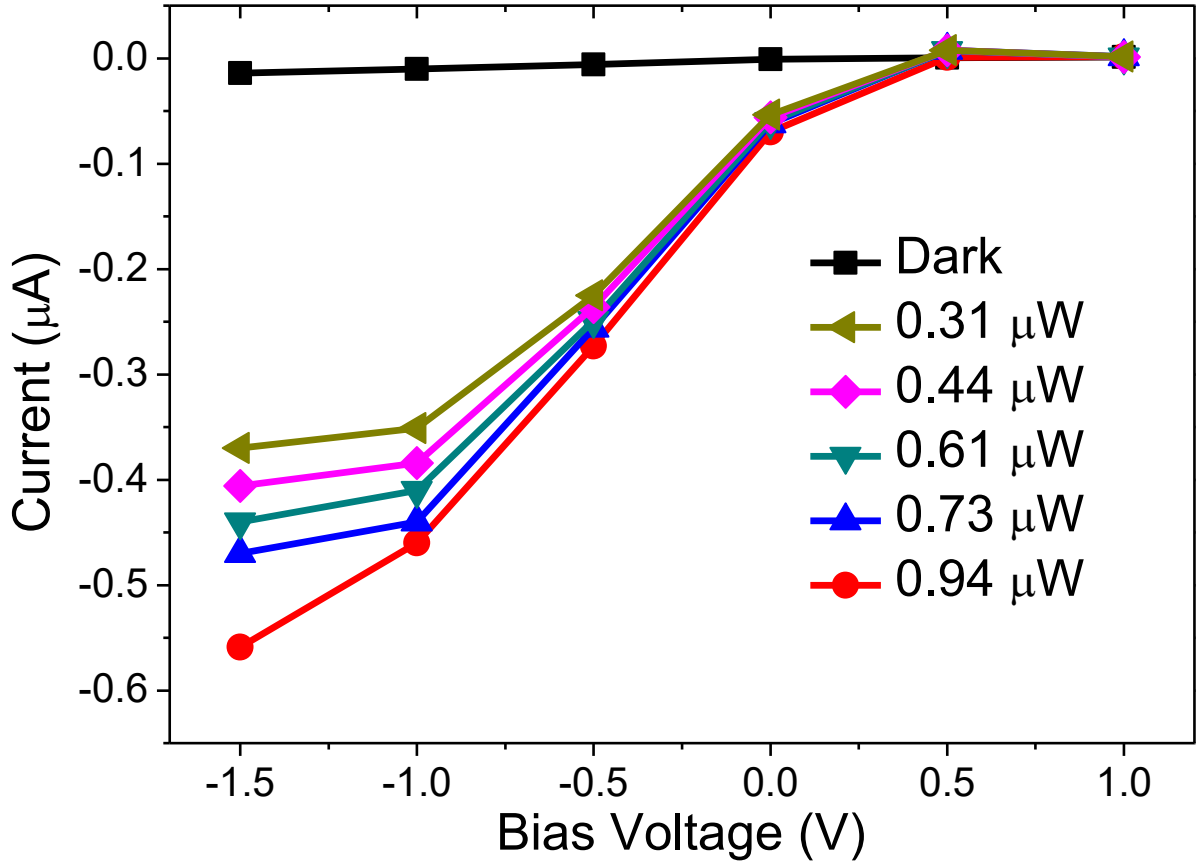

- ✓ The responsivity is measured as **0.130 mA/mW** under room temperature.
- ✓ The ***in-plane absorption*** plays an important role in high responsivity.
- ✓ The sensitivity is comparable with that of currently commercially semiconductor photodetector.

Other Relevant Graphene/Si Detector

Comparison with other graphene photodetectors

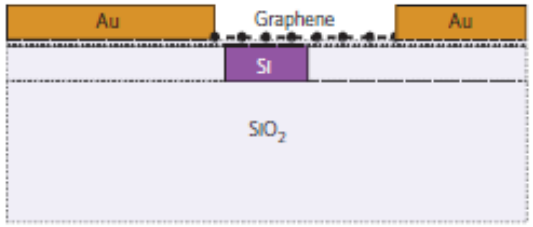

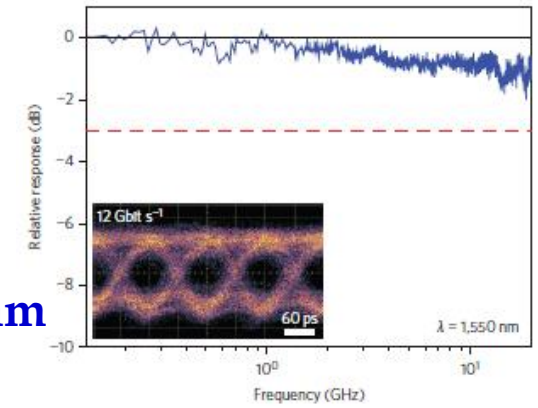

0.108 mA/mW at 1550nm

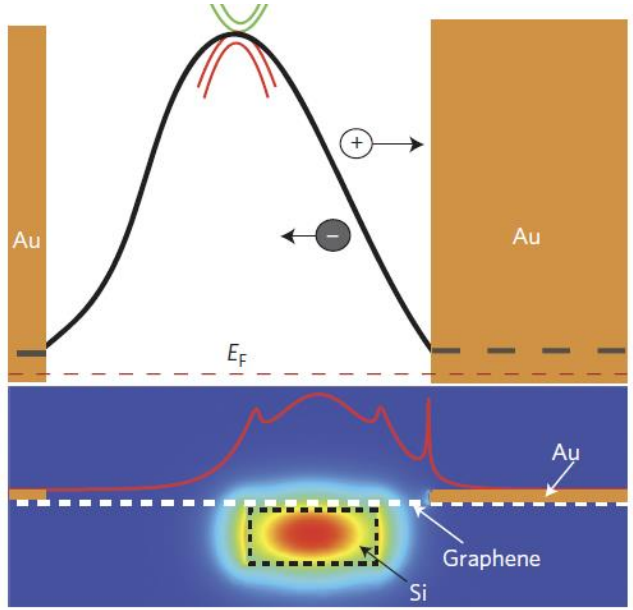

X. Gan *et al*. Nature Photonics 7, 883–887 (2013)

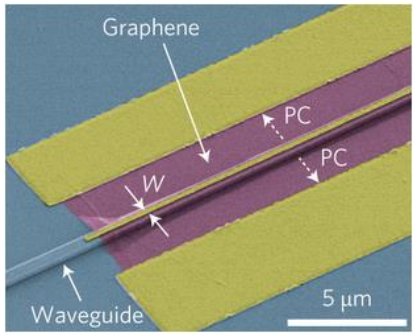

Graphene on SiO_2 silicon waveguide

0.05mA/mW at 1550nm

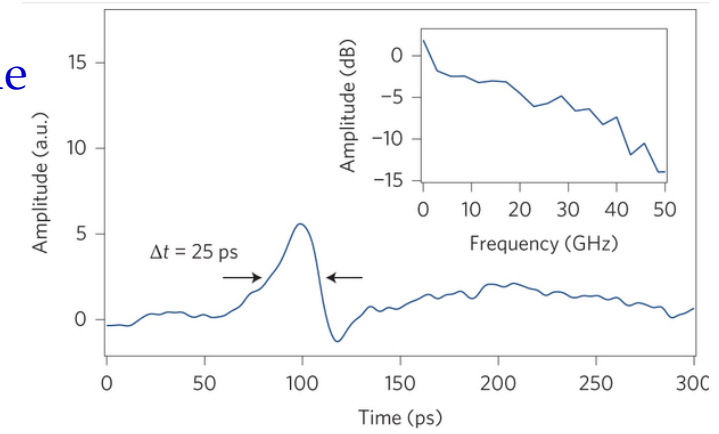

A. Pospischil et al, Nature Photonics 7, 892–896 (2013)

Development by Others

Waveguide-integrated black phosphorus photodetector with high responsivity and low dark current

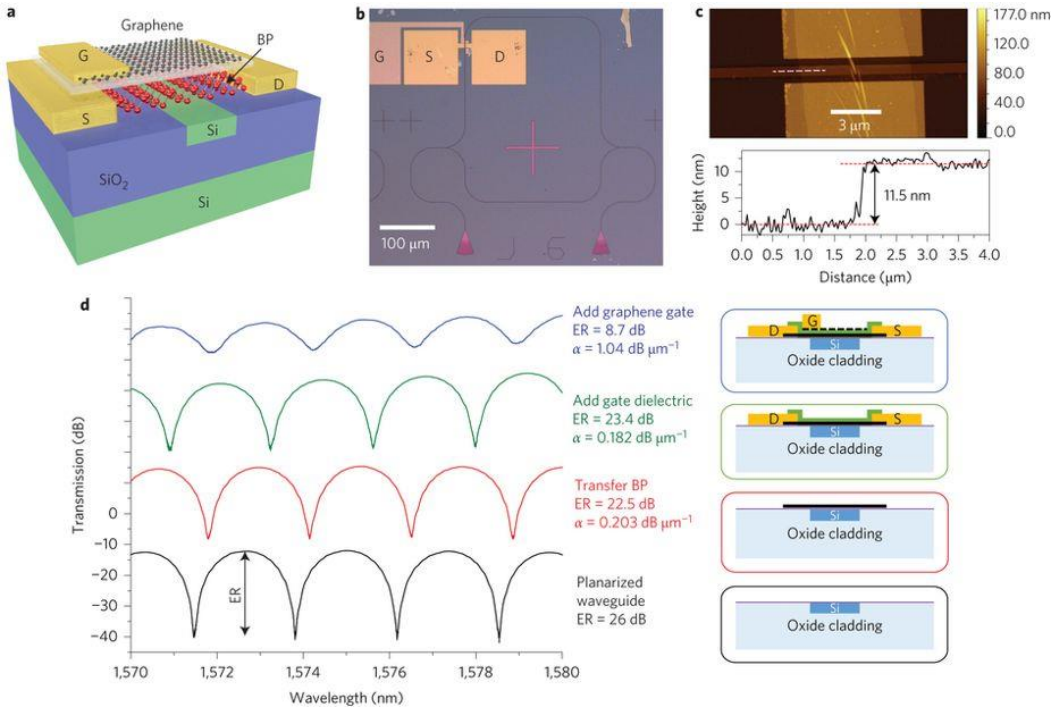

Nathan Youngblood, Che Chen, Steven J. Koester & Mo Li, Nature Photonics **9**, 247–252 (2015)

a, Three-dimensional illustration of the device configuration, featuring a few-layer graphene top-gate. **b**, Optical microscope image of a complete device. A BP field-effect transistor is integrated in one arm of an MZI circuit. G, gate; S, source; D, drain. **c**, Top: atomic force microscope image of the BP with contacts and before the deposition of gate dielectrics and fabrication of the top-gate. Bottom: height profile along the white dashed line in the top panel, showing that the thickness of the BP is 11.5 nm, corresponding to 23 monolayers. **d**, Transmission spectra of the MZI measured after each step of fabrication (shown in the schematics to the right). Spectra have been vertically translated for clarity. From the extinction ratio, the absorption coefficient of each added layer can be determined. Using this method, the absorption coefficient of the BP in the completed device is determined to be 0.182 dB μm^{-1}.

Development by Others

Waveguide-integrated black phosphorus photodetector with high responsivity and low dark current

Nathan Youngblood, Che Chen, Steven J. Koester & Mo Li, Nature Photonics **9**, 247–252 (2015)

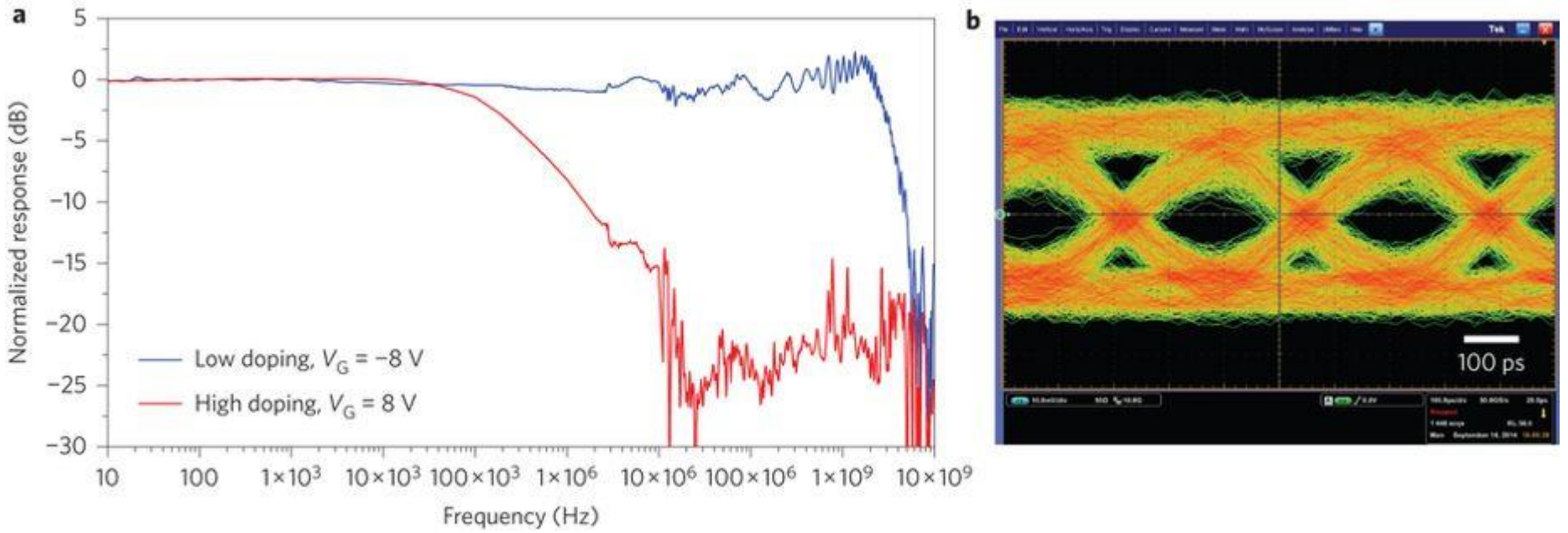

a, The response of the BP photodetector is measured when the BP is gated to low and high doping. At low doping, the response is broadband with a cutoff frequency of 3 GHz, which is limited by the RC bandwidth of the contact pads and the input impedance of the preamplifier. At high doping, the response rolls off at 0.2 MHz, indicating that the photoresponse is of a thermal origin, as expected from the bolometric effect. b, Receiver eye diagram at a data rate of 3 Gbit s^{-1} measured with the BP photodetector. Scale bar, 100 ps.

Development by Others

High-speed and high-responsivity hybrid silicon/black-phosphorus waveguide photodetectors at 2 μm

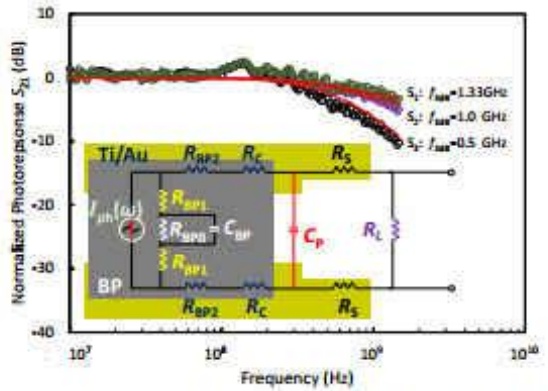

Figure 5 | Measured frequency responses and the equivalent circuit model of hybrid silicon/BP waveguide photodetectors. Measured results for the normalized frequency responses of the three samples when operating at V_{bias} = 2.0 V. **Inset,** Established equivalent circuit model for the present photodetectors. **Red line,** Frequency responses calculated by using the equivalent circuit model with the fitted parameters (red line).

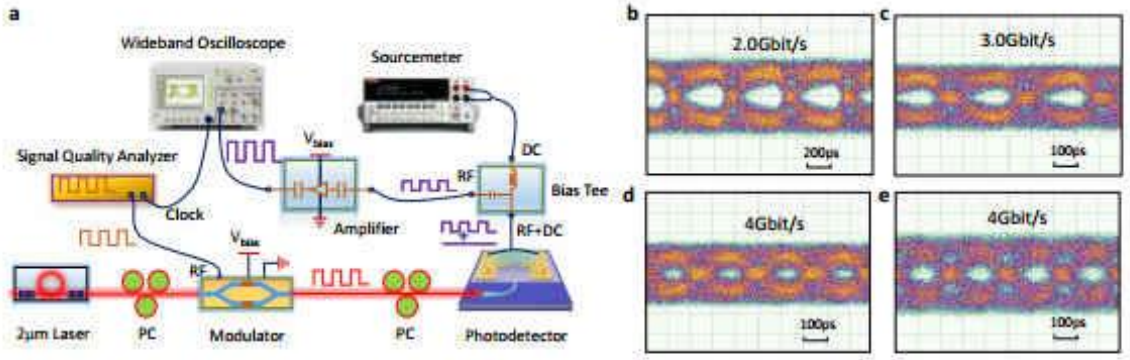

Figure 6 | Measurement of eye-diagrams for the hybrid BP waveguide photodetector (Sample S_3). **a,** Experimental setup for measuring eye-diagrams of the present hybrid silicon/BP waveguide photodetectors. **b-e,** Measured eye-diagrams with different bit rates. (b) 2.0 Gbit/s at 2 V; (c) 3.0 Gbit/s at

Yanlong Yin, & Daoxin Dai, et al., https://arxiv.org/ftp/arxiv/papers/1811/1811.01628.pdf (2018)

Silicon photonics is being extended from the near-infrared (near-IR) window of 1.3-1.5 μm for optical fiber communications to the mid-infrared (mid-IR) wavelength-band of 2 μm or longer for satisfying the increasing demands in many applications. Mid-IR waveguide photodetectors on silicon have attracted intensive attention as one of the indispensable elements for various photonic systems. Previously high-performance waveguide photodetectors on silicon were realized for the near-IR window of 1.3-1.5 μm by introducing another semiconductor material (e.g., Ge, and III-V compounds) in the active region. Unfortunately, these traditional semiconductor materials do not work well for the wavelength of ~2 μm or longer because the light absorption becomes very weak. As an alternative, two-dimensional materials provide a new and promising option for enabling active photonic devices on silicon. Here black-phosphorus (BP) thin films with optimized medium thicknesses (~40 nm) are introduced as the active material for light absorption and silicon/BP hybrid ridge waveguide photodetectors are demonstrated with a high responsivity at a low bias voltage. And up to 4.0 Gbps data transmission is achieved at 2μm.

New Development by Others

50 GBit/s Photodetectors Based on Wafer-Scale Graphene for Integrated Silicon Photonic Communication Systems

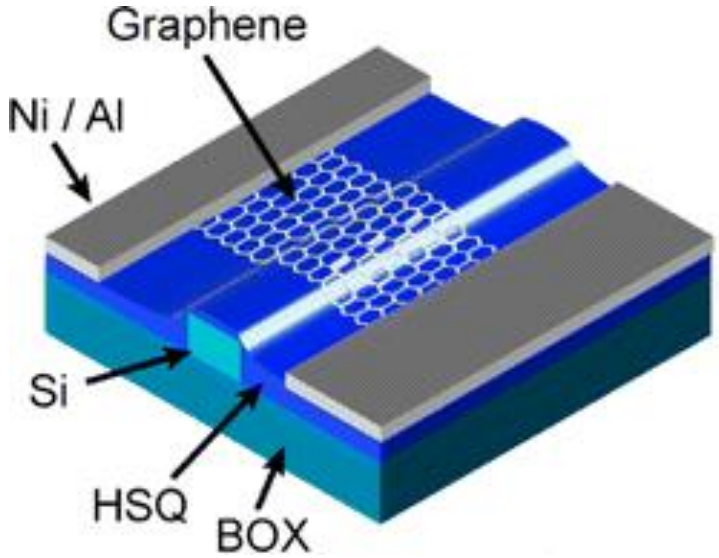

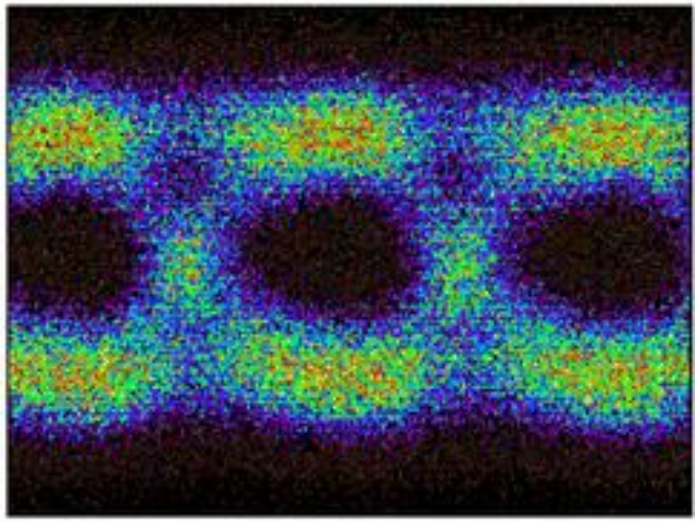

Daniel Schall, et al., ACS Photonics 1 (9), pp 781–784 (2014); Advanced Microelectronic Center Aachen, Germany

The integration of electronic and optic components on one chip is one of the most attractive routes to further increase the system performance. By using in-plane configuration, they present the fabrication of photodetectors based on CVD-grown graphene on silicon photonic waveguides. The devices operate bias-free in the C-band at 1550 nm and show an extrinsic −3 dB bandwidth of 41 GHz. They demonstrate that these detectors work at data rates up to 50 GBit/s with excellent signal integrity.

Photodetector based on PC

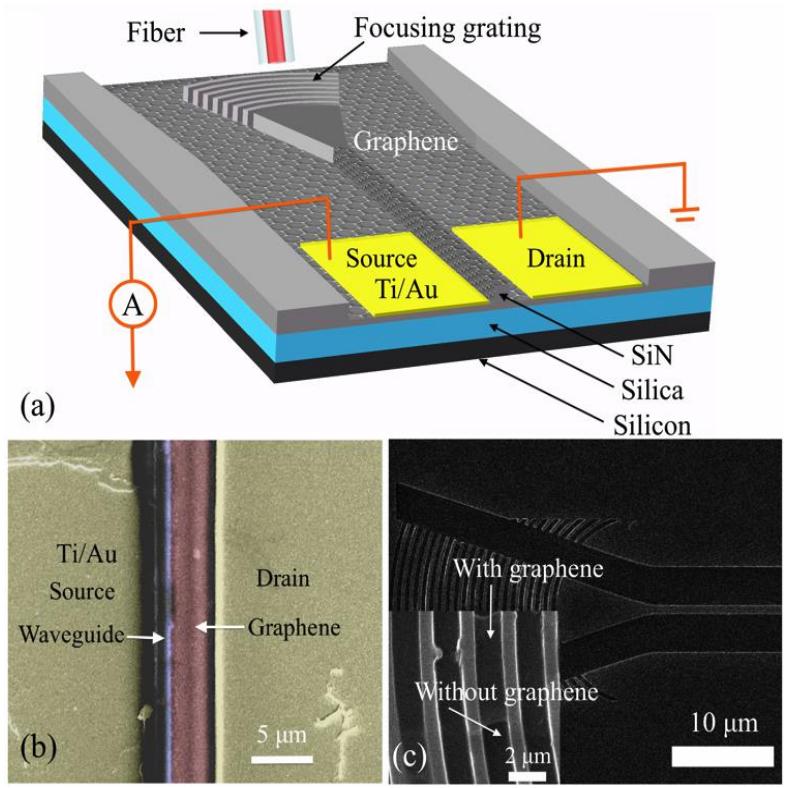

J. Q. Wang, et al.,
Journal of Applied Physics, 2015

A maximum internal responsivity **of 126 mA/W** with dynamic response of 1K Hz at 1.55 μm.

(a) Schematic illustration of the graphene-on-SiN waveguide photodetector (b) SEM image of the device. A monolayer of graphene (red) is transferred on top of the SiN waveguide (purple). Two electrodes made of titanium/gold (yellow) were arranged asymmetrically along the waveguide. (c) SEM image of the focusing grating coupler of the devices and zoom-in SEM image of the region with and without the graphene on top. From the zoom-in picture, the graphene sheet can be identified.

2D Waveguide Devices

Bound States in the Continuum (BICs)

3D view

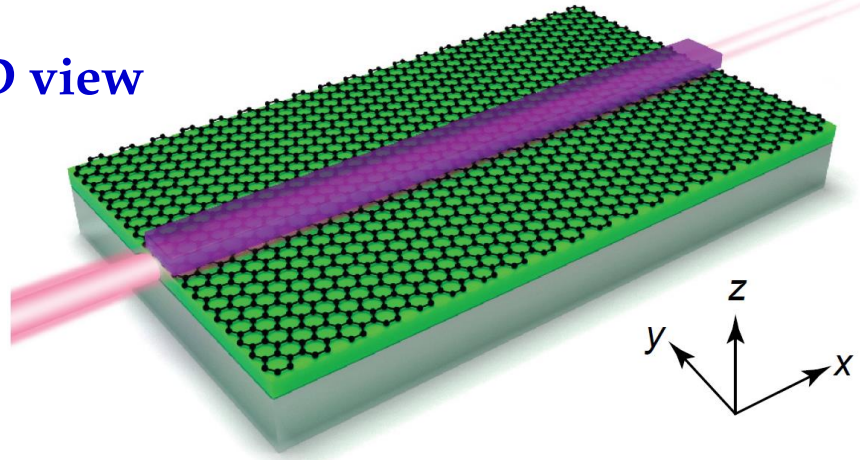

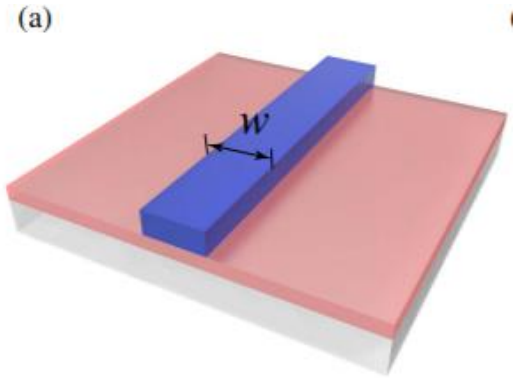

polymer dielectric SiO_2

BIC perfectly confined in the continuous spectrum

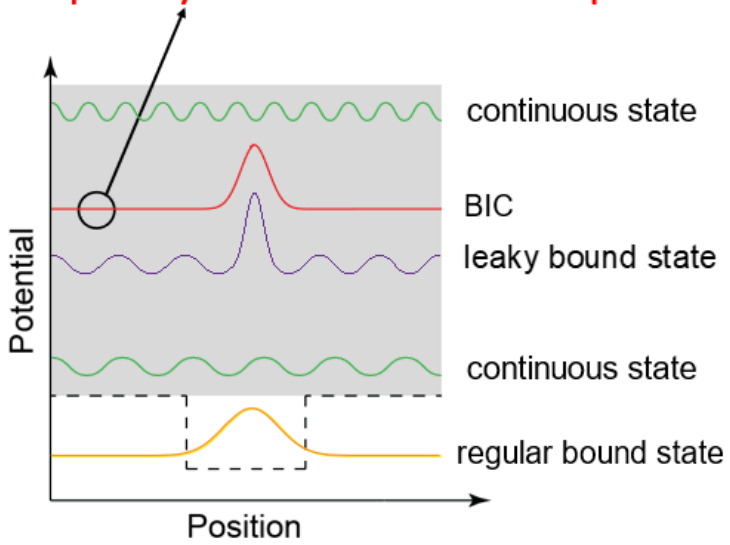

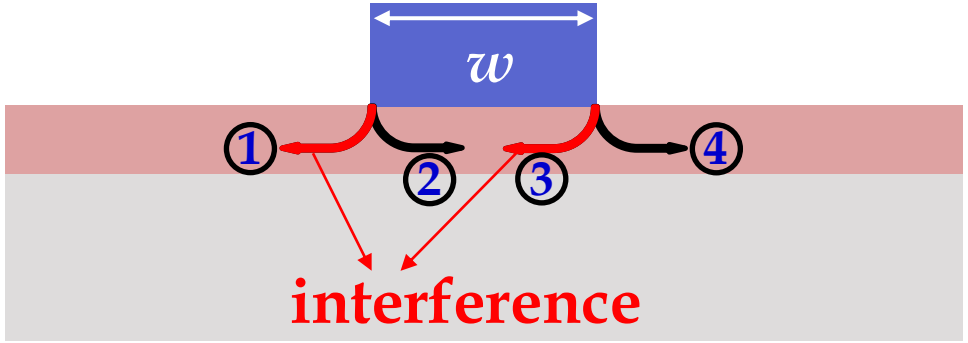

Radiation loss reduced to zero when channels 1(2) and 3(4) have destructive interference and cancel with each other.

Z. Yu†, Y. Wang†, J. B. Xu, X. K. Sun, H. K. Tsang, *et al.* Advanced Optical Materials 7, 1901306, 2019

Device Characterization

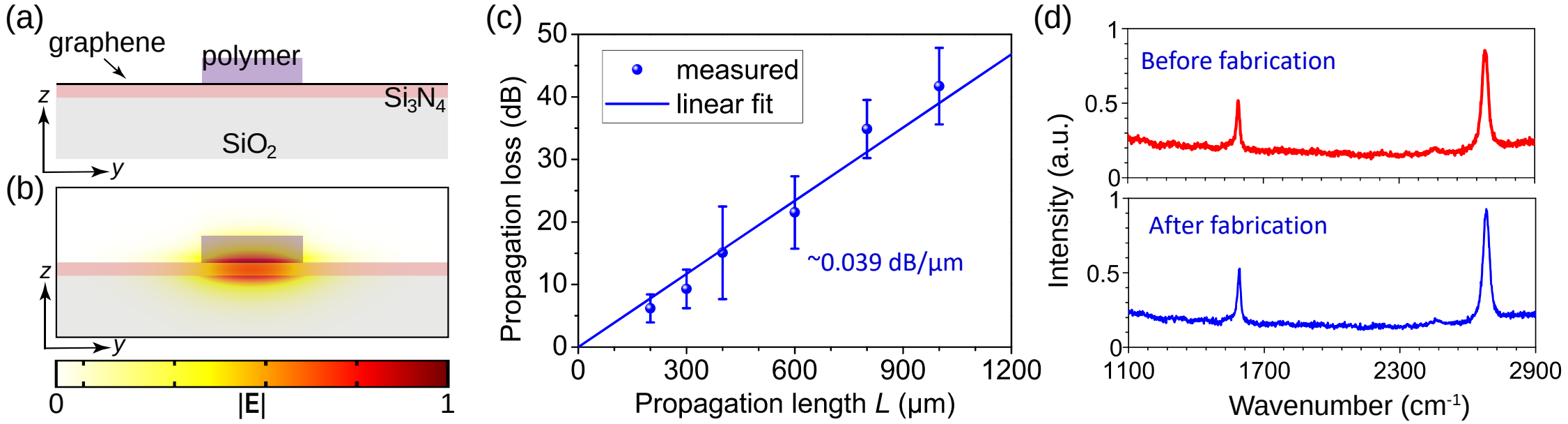

Z. Yu†, Y. Wang†, JBX, X. K. Sun*, *et al.* Advanced Optical Materials 7, 1901306, 2019

Y. Wang, JBX, H. K. Tsang, *el al. Conference on Lasers and Electro-Optics (CLEO)*, May 2020

Device Characterization

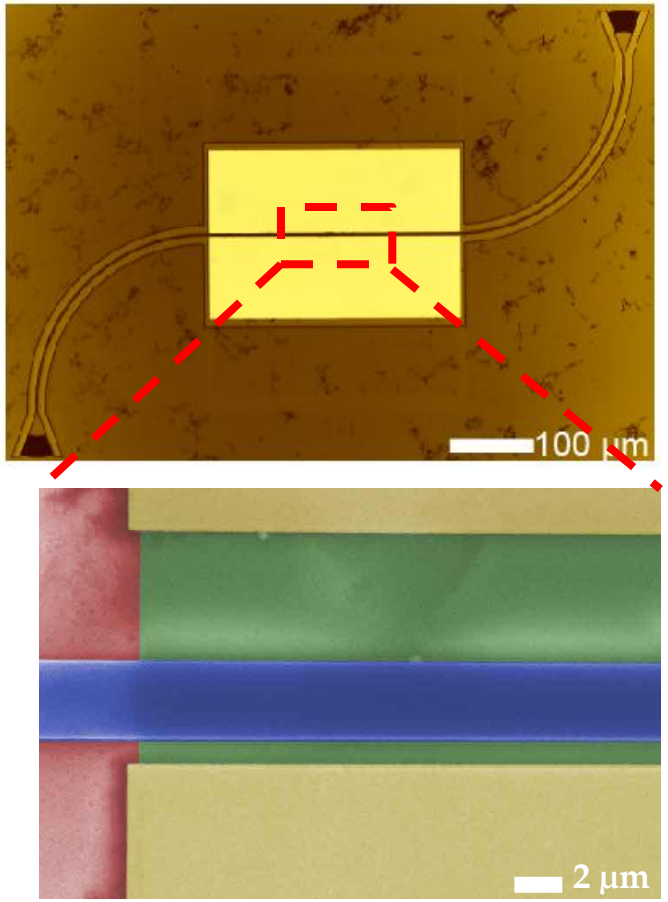

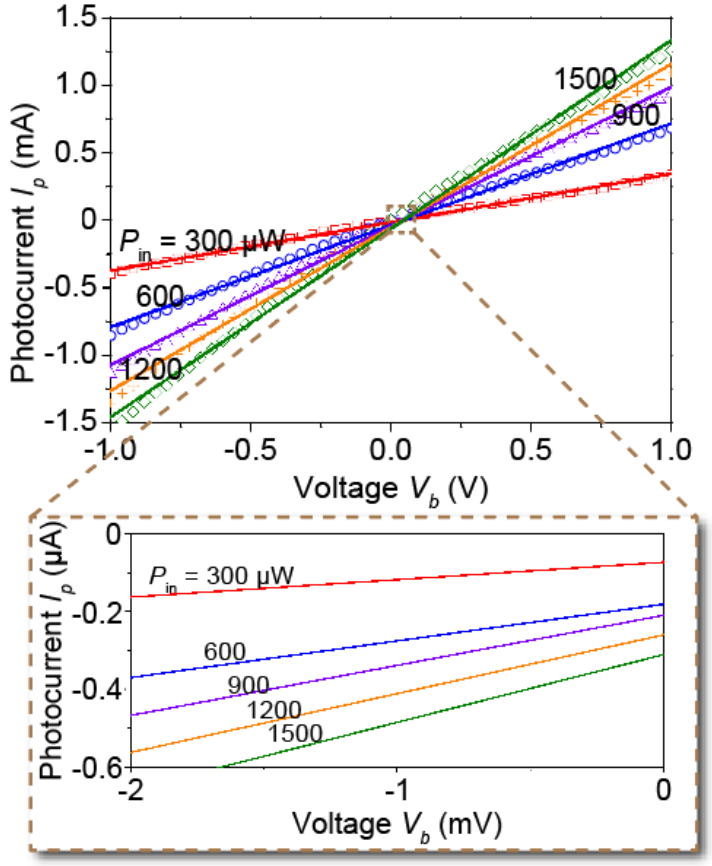

Waveguide width: 2.65 μm

Graphene length: 300 μm

Metal distance to the waveguide:

W_1 = 0.4 μm, W_2 = 4 μm

Responsivity:

~0.65 mA/W at V_b = 0 V,

~1 A/W at V_b = 1 V

Y. Wang, JBX, HK Tsang*, *el al. Conference on Lasers and Electro-Optics (CLEO)*, May 2020

Impulse Response

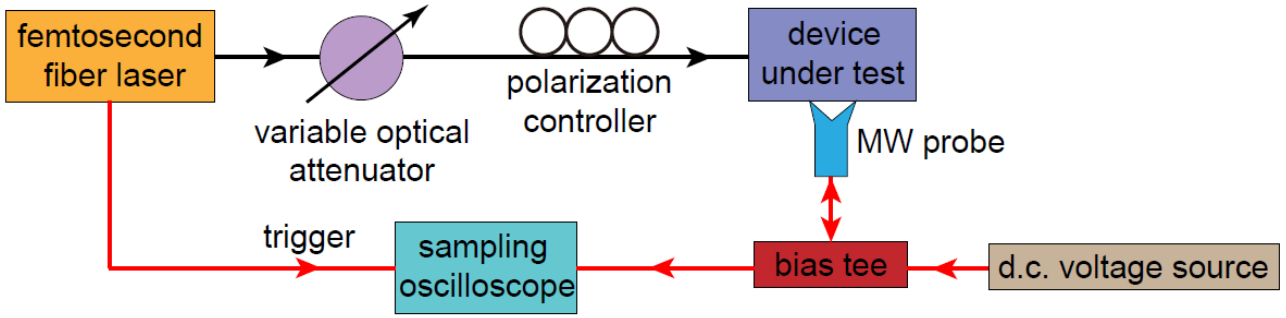

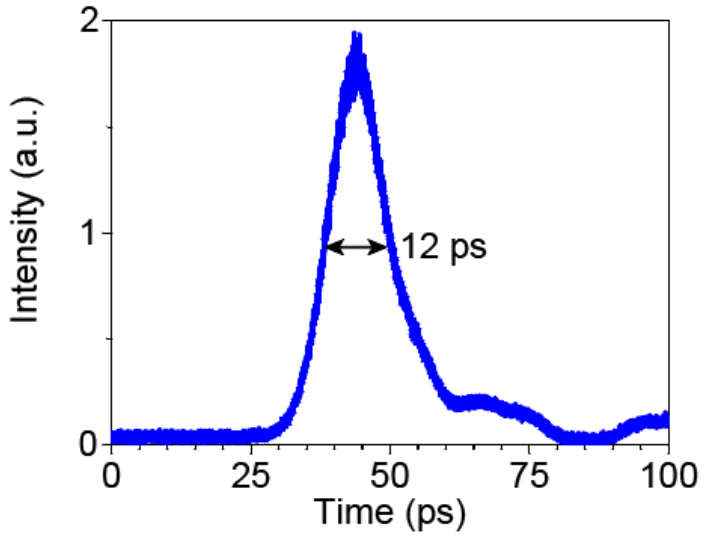

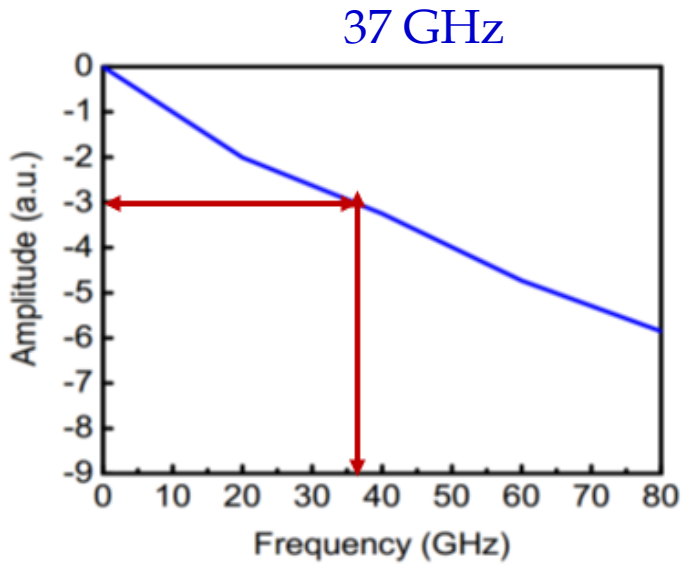

The FWHM of the impulse response Δt ~12 ps

The 3-dB bandwidth of the photodetector:

$\Delta f = 0.441/\Delta t \approx 37$ GHz

Y. Wang, JBX, HK Tsang*, *el al*. *Conference on Lasers and Electro-Optics (CLEO)*, May 2020

Comparison with Others

Reference	Responsivity (mA/W)	Bandwidth (GHz)	Dark current	Structure
[1]	50	18	High	MGM
[2]	130 at λ = 2.75 μm	-	Low	Schottky diode
[3]	100	20	High	MGM
[4]	360	>110	High	MGM
This work	**1000**	**37**	**High**	**MGM**

MGM: metal graphene metal structure

Y. Wang, JBX, HK Tsang*, *el al. Conference on Lasers and Electro-Optics (CLEO)*, May 2020

[1] A. Pospischil *et al.* Nat. Photonics, 7, 892–896 (2013)
[2] X. M. Wang, HKT, JBX, *et al.* Nat. Photonics, 7, 888–891 (2013)
[3] X. T. Gan *et al.* Nat. Photonics, 7, 883–887 (2013)
[4] Y. Ding *et al.* arXiv preprint arXiv:1808.04815, (2018)

PD Waveguide Structures

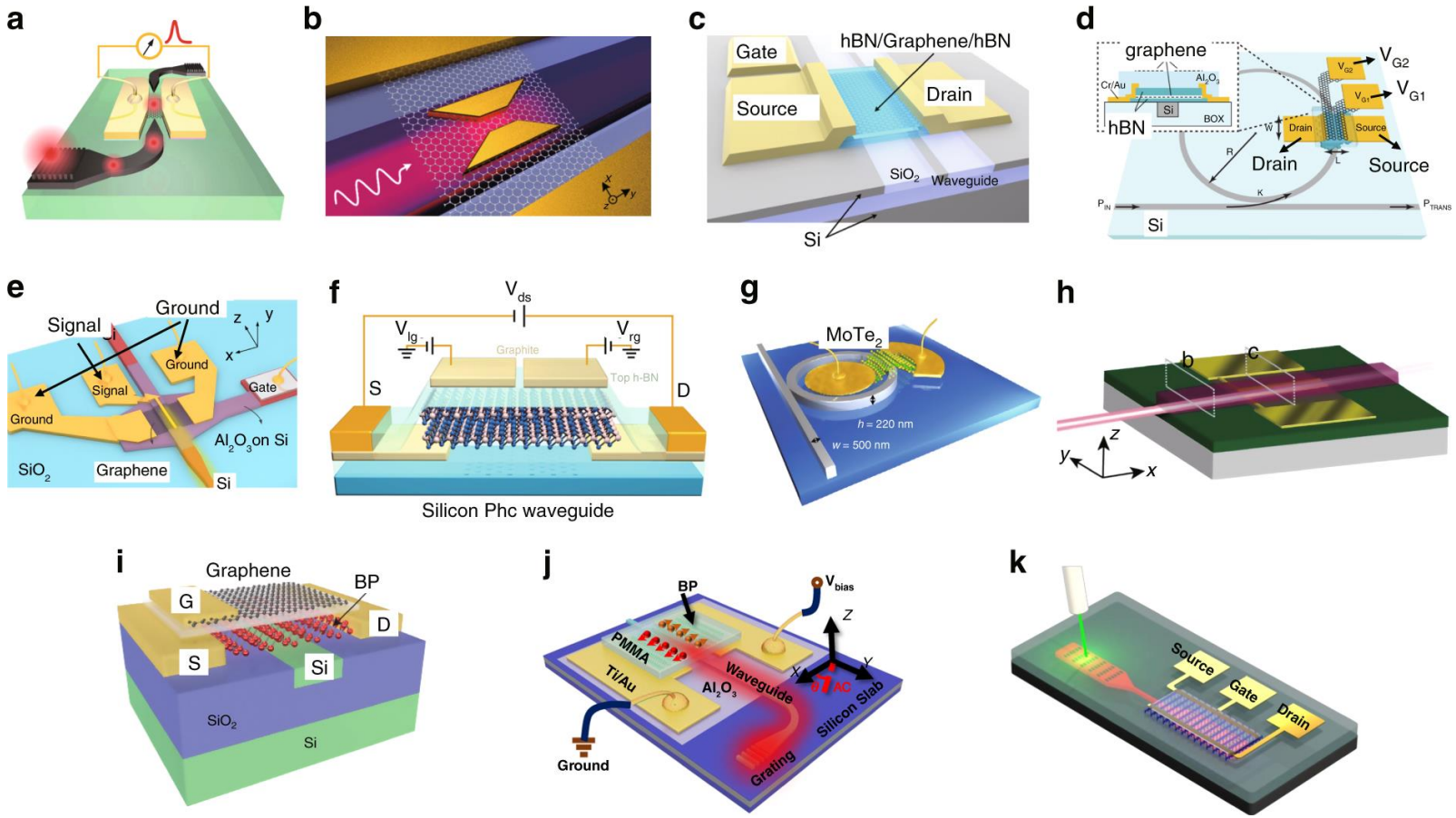

a A graphene plasmonic PD working with the PV effect. b A plasmonically enhanced graphene PD working on the BOL effect. c A horizontally asymmetric graphene PD with one gate electrode based on the PTE effect. d A microring resonator-integrated two-gate graphene PD based on the PTE effect. e The Si-G hybrid plasmonic waveguide PDs operating at 1.55 and 2 μm. f A two-gate $MoTe_2$ PD operating at 1.16 μm based on the PV effect. g A strain-engineered $MoTe_2$ PD integrated on a microring resonator operating at 1.55 μm. h A $PtSe_2$ PD operating at 1.55 μm. i A black-phosphorus PD operating at 1.55 μm with 3 GHz bandwidth. j A black-phosphorus PD operating at 2 μm. k A PG effect-based black phosphorus PD operating at the wavelength band of 3.68–4.03 μm.

40 GHz Waveguide-Integrated 2D $PtSe_2$ PD

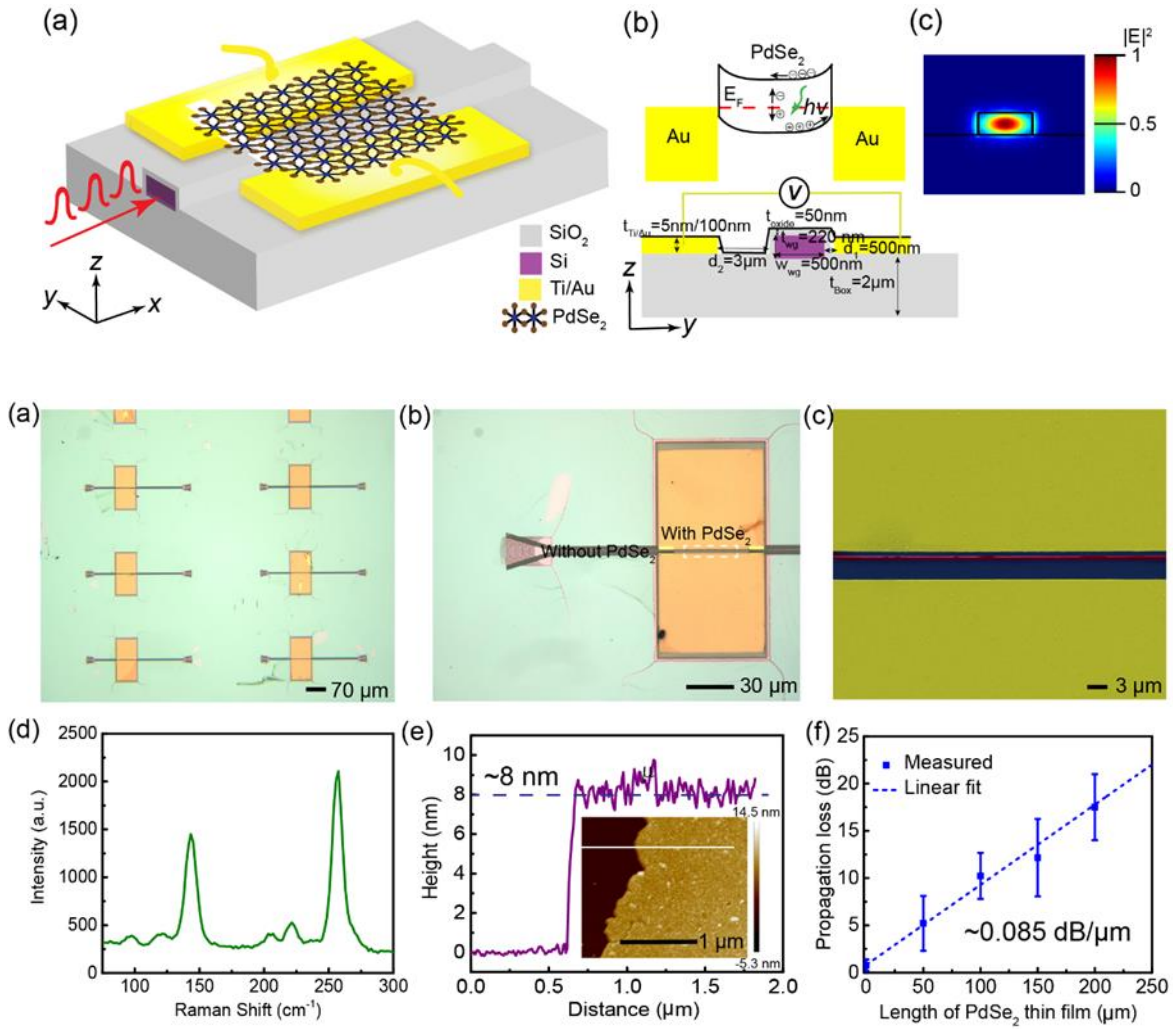

Y. Wang, YQ Zhou, JBX, HK Tsang*, Appl. Phys. Lett., May 2022
https://doi.org/10.1063/5.0091625

40 GHz Waveguide-Integrated 2D $PtSe_2$ PD

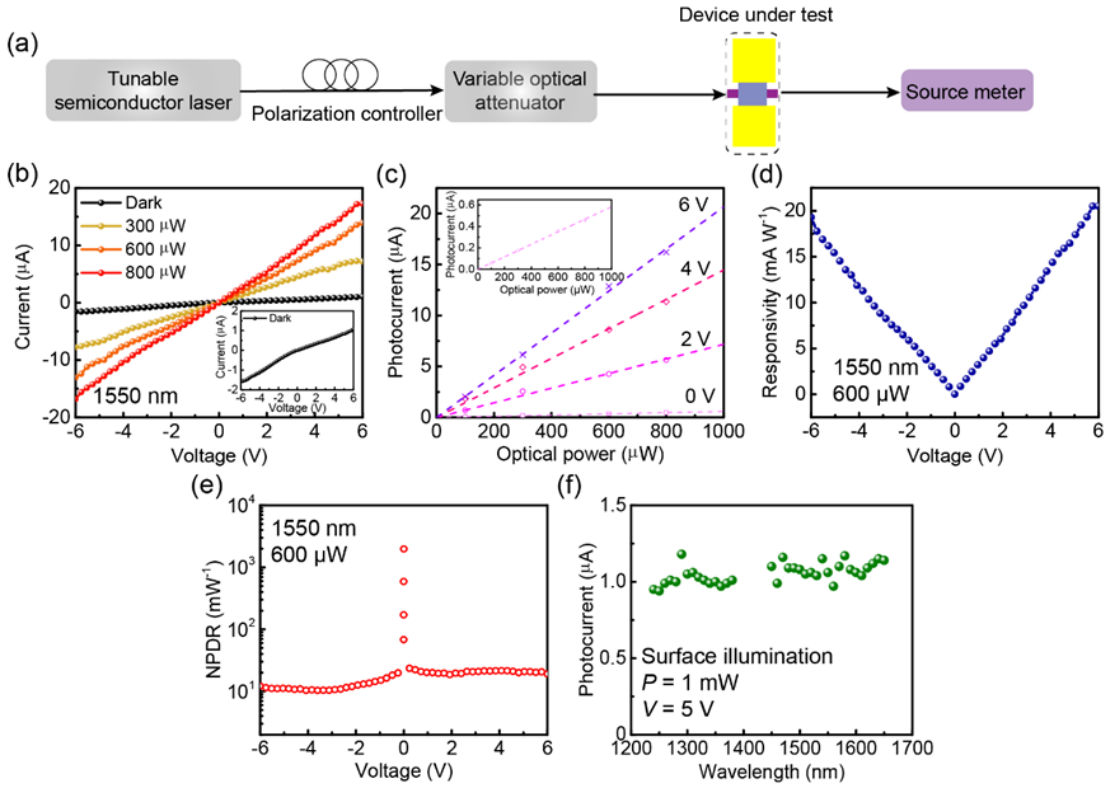

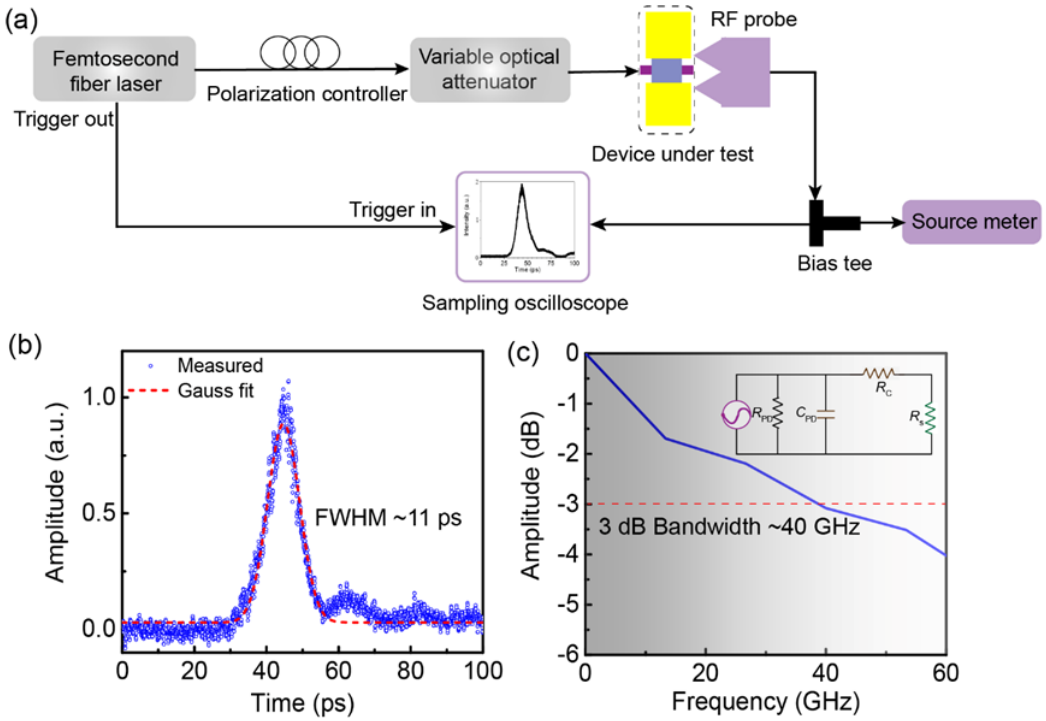

Y. Wang, YQ Zhou, JBX, HK Tsang*, Appl. Phys. Lett., May 2022
https://doi.org/10.1063/5.0091625

Outline

- Introduction and Background
- Graphene-Silicon Hybrid Detectors based on Photodiode Mode
- **Graphene-Silicon Hybrid Detectors based on Photoconductor Mode**
- Graphene based THz Modulator
- Conclusions

Graphene Schottky Junction

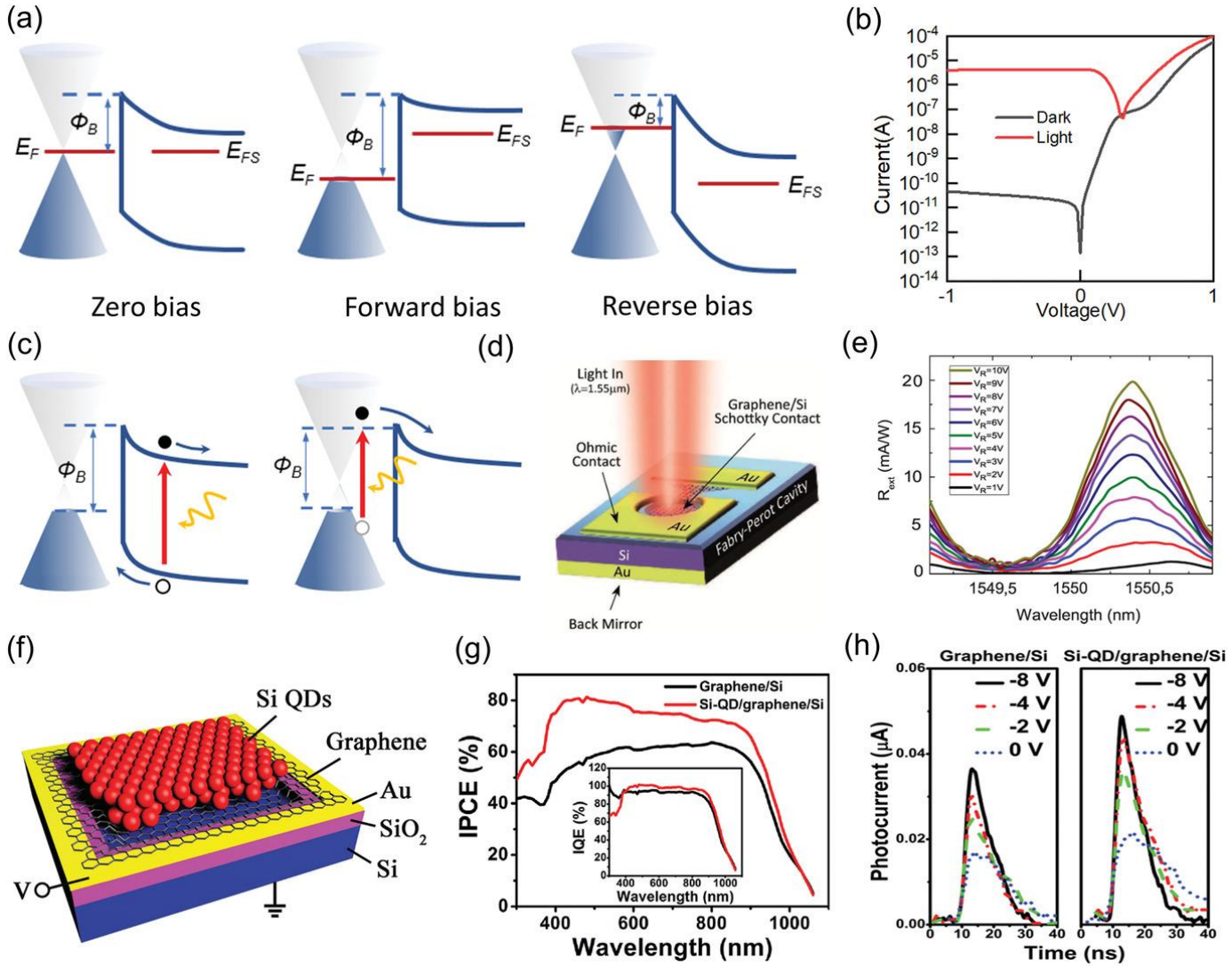

L. Gao, X.R. Wang, Y. Xu, et al., Advanced Materials, First published: 08 July 2019, DOI: (10.1002/adma.201902039)

2D Enhancement Schemes

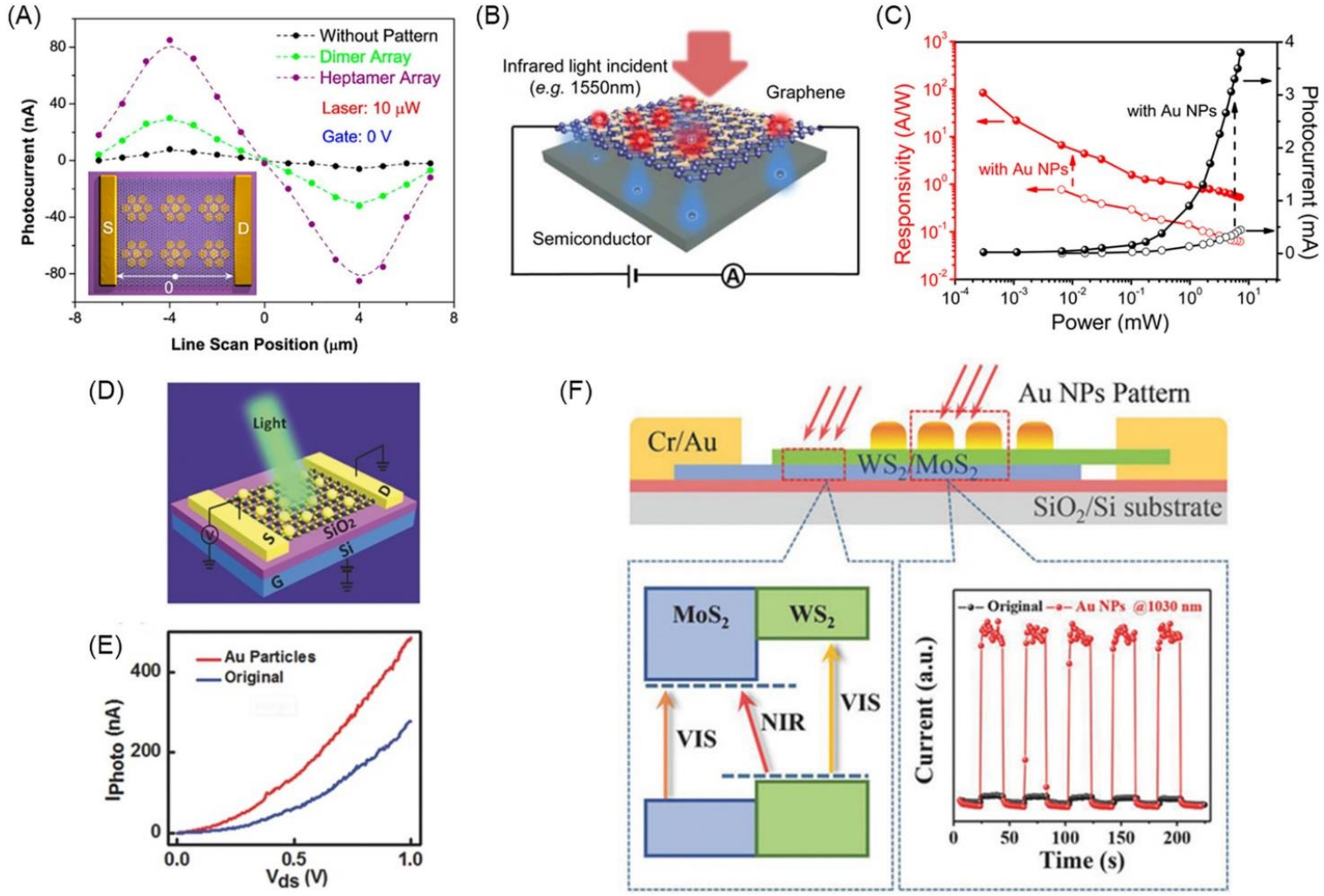

Li Tao, Zefeng Chen, Zhiyong Li, Jiaqi Wang, Xin Xu, Jian-Bin Xu, *InfoMat*, Sept 2020
https://doi.org/10.1002/inf2.12148

Hybrid Gr Device Structures

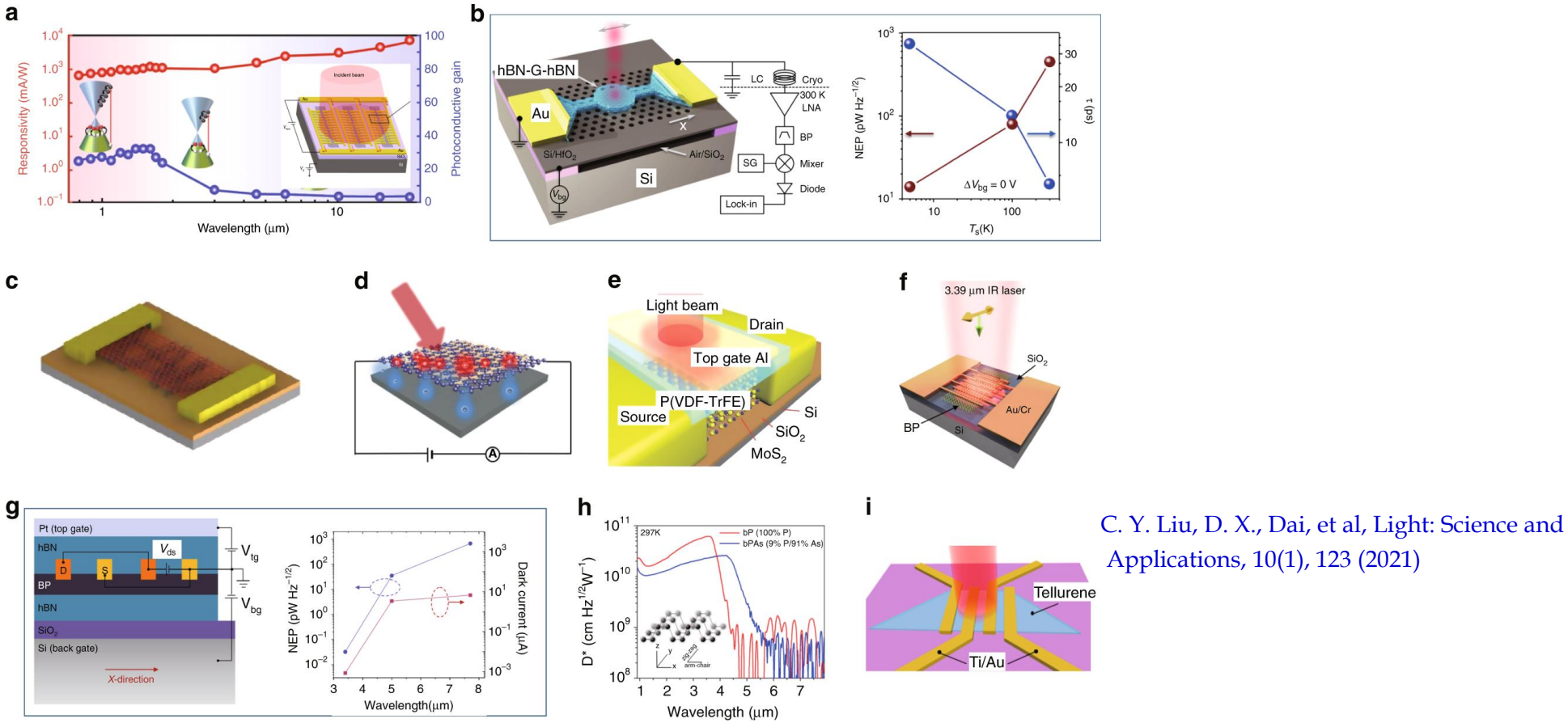

C. Y. Liu, D. X., Dai, et al, Light: Science and Applications, 10(1), 123 (2021)

a A wide-band plasmonic enhanced graphene PD and the measured responsivity/photoconductive-gain. b A cavity-coupled graphene bolometer with Johnson noise read-out. Left: the 3D schematic. Right: the NEP and thermal relaxation time of hot electrons as a function of lattice temperature. c A metal-graphene+X-metal configuration PD, for which X is carbon nanotube. d A short-wave infrared graphene PD with a plasmonic enhanced structure on channel. e A ferroelectric polarization gating MoS2 photodetector with an operation wavelength extended to 1.55 μm. f A mid-infrared black-phosphorus PD with a high gain. g A mid-infrared black-phosphorus PD with an operation wavelength extended to 7.7 μm by applying a vertical electric field. Left: the 3D schematic. Right: the NEP and dark current at different wavelengths. h The specific detectivities of the mid-infrared black phosphorus PD and black-PAs-alloy PD as a function of wavelength. i A short-wave infrared tellurene PD.

Hybrid Gr Device Structures

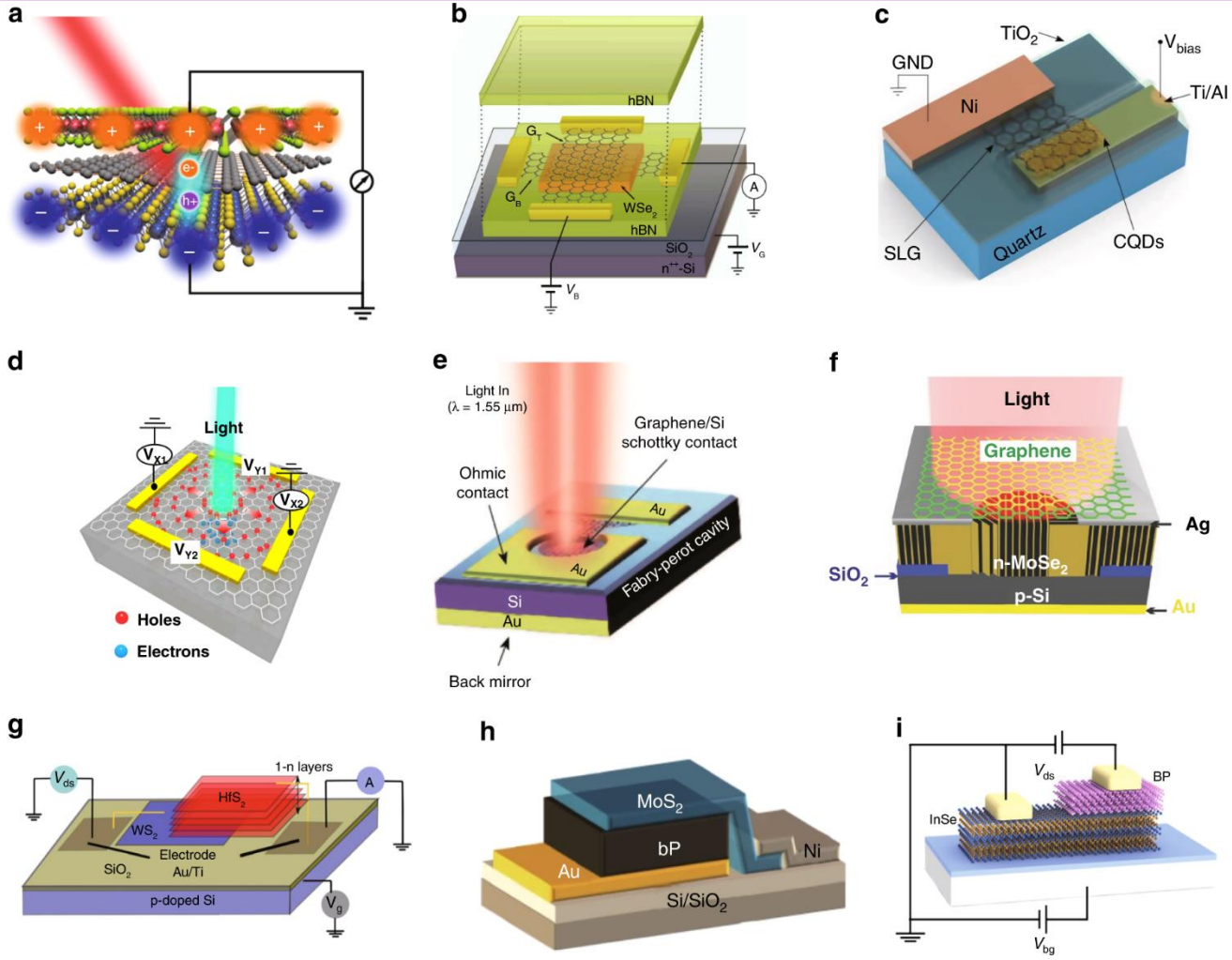

C. Y. Liu, D. X., Dai, et al, Light: Science and Applications, 10(1), 123 (2021)

a A MoS_2-G-WSe_2 PD. b A G-WSe_2-G PD with the IPE effect .c A colloidal quantum dot-graphene (CQD-G) hybrid PD with tunneling layer. d A G-Si heterostructure position-sensitive PD operating at near-infrared wavelengths. e A G-Si PD operating at 1.55 μm. f A G/vertical-$MoSe_2$/Si heterojunction PD. g A mid-infrared WS_2-HfS_2 heterostructure PD based on interlayer excitons. h A mid-infrared BP-MoS2 heterostructure PD. i A mid-infrared BP-InSe avalanche photodetector.

Gr/Si Photodetector in Conductor Mode

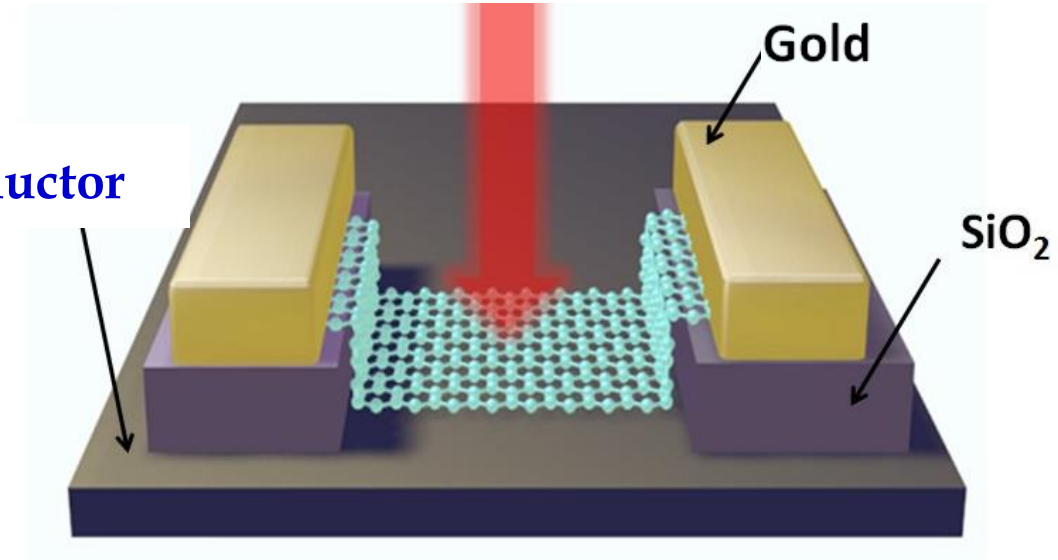

Graphene — High Mobility

Graphene — Broadband absorption from visible to infrared

(2.2 μm for E_F of 0.6 eV)

Semiconductor — Provide photo-induced carriers through light absorbtion

Z. F. Chen, JBX, et al., *Advanced Optical Materials*, 2015

Energy Band Structure

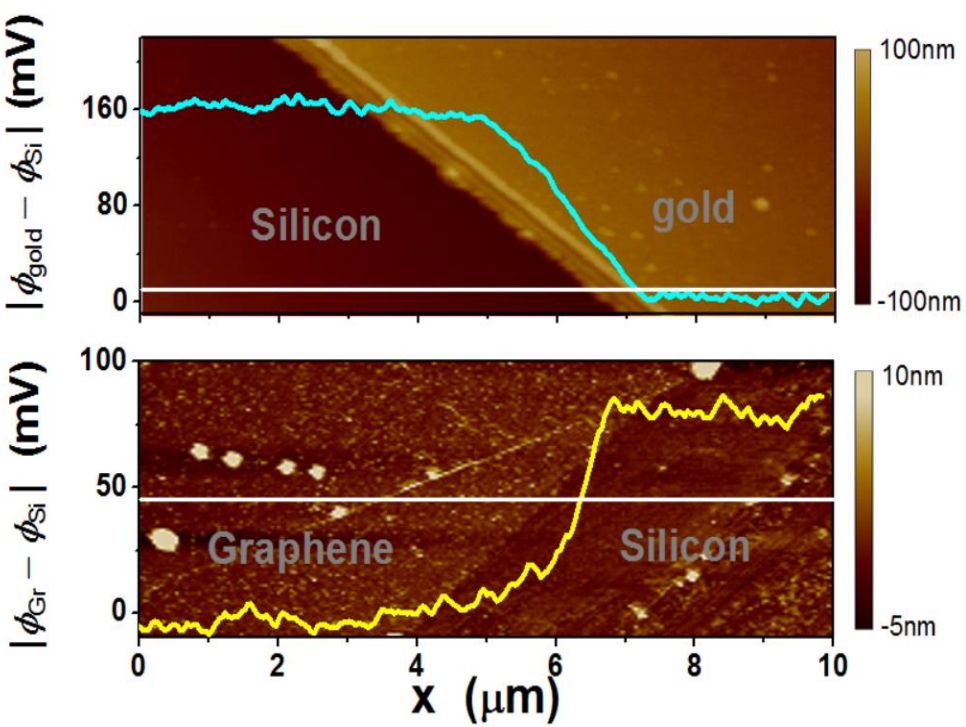

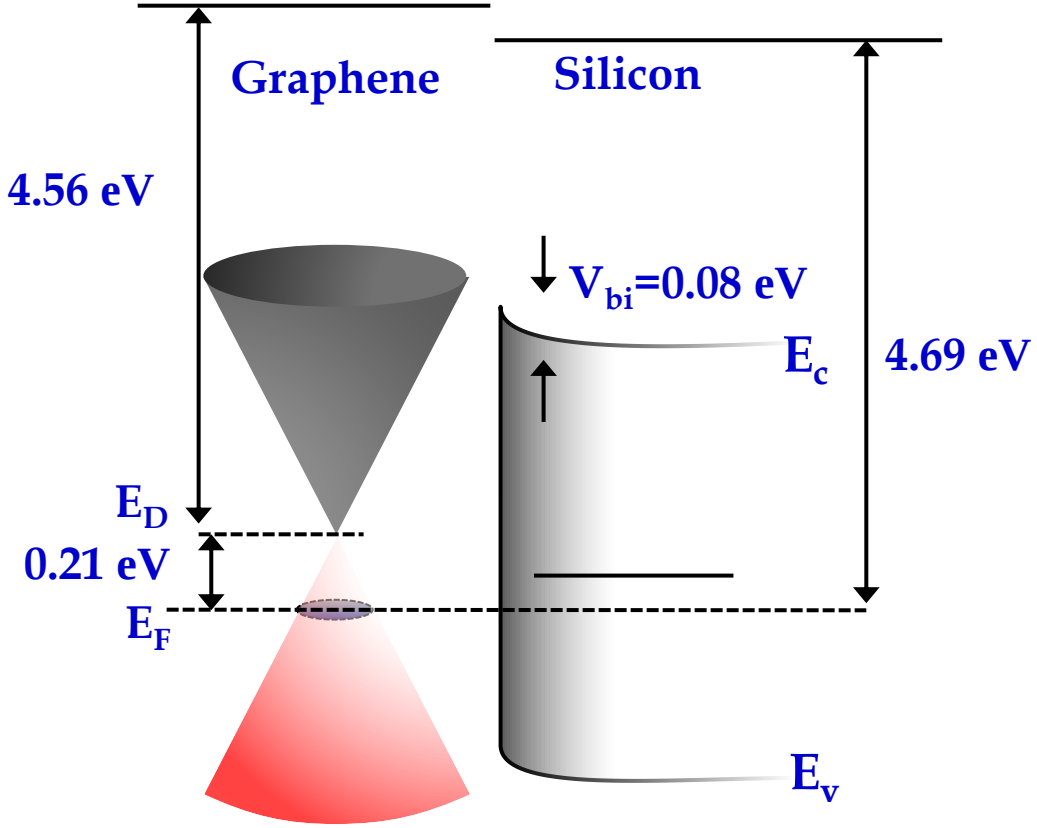

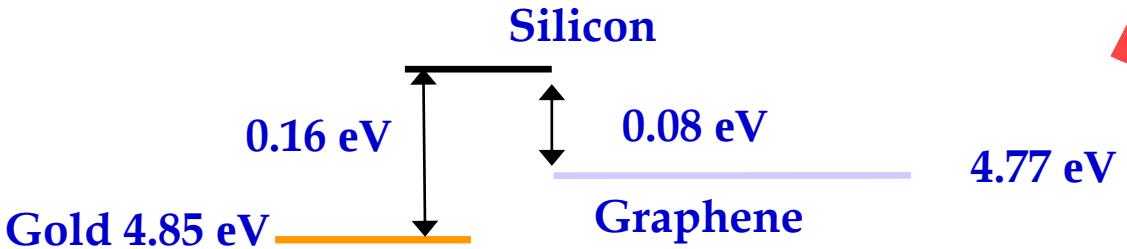

Left: Surface potential of graphene-silicon heterostructure measured by KP-AFM.

Right:Energy band diagram of graphene/silicon heterostructure

Photoresponse

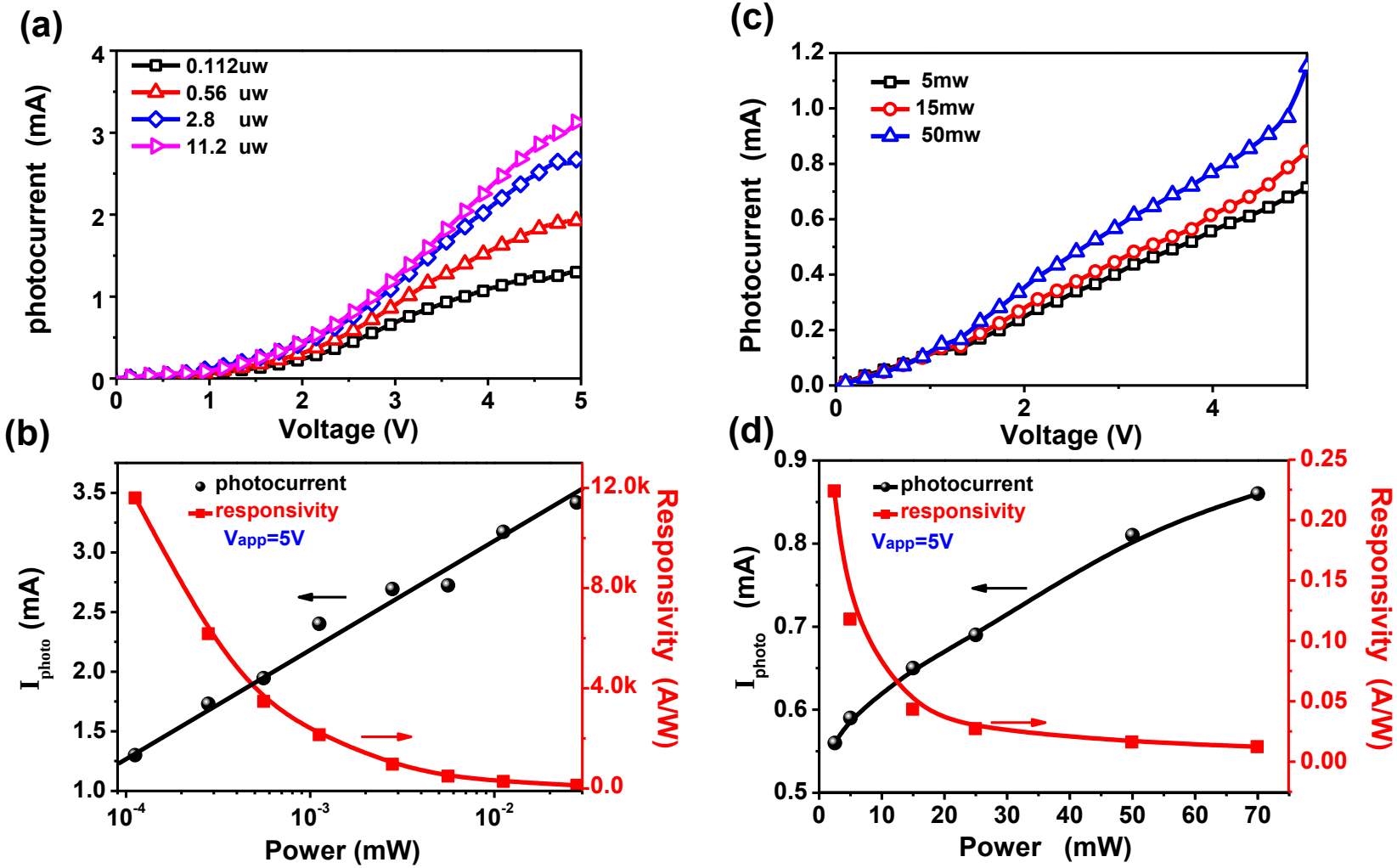

Wavelength of 632 nm

1.1×10⁴ A/W

Wavelength of 1.55 μm

0.23 A/W

Built-in Field & Carrier Density

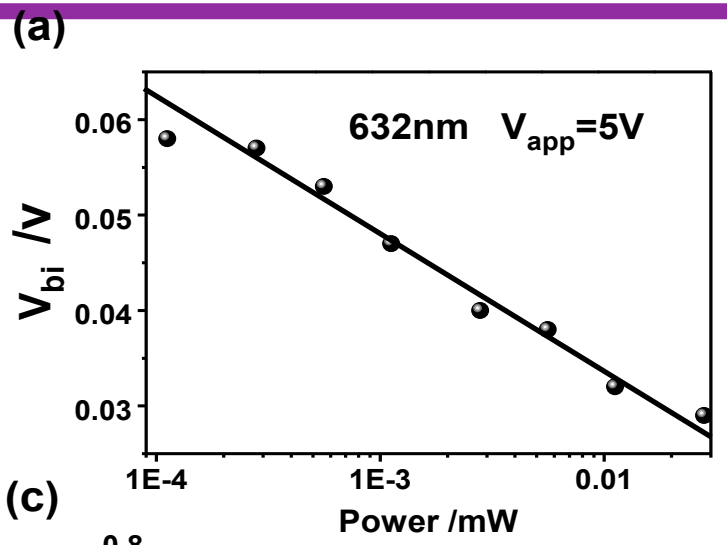

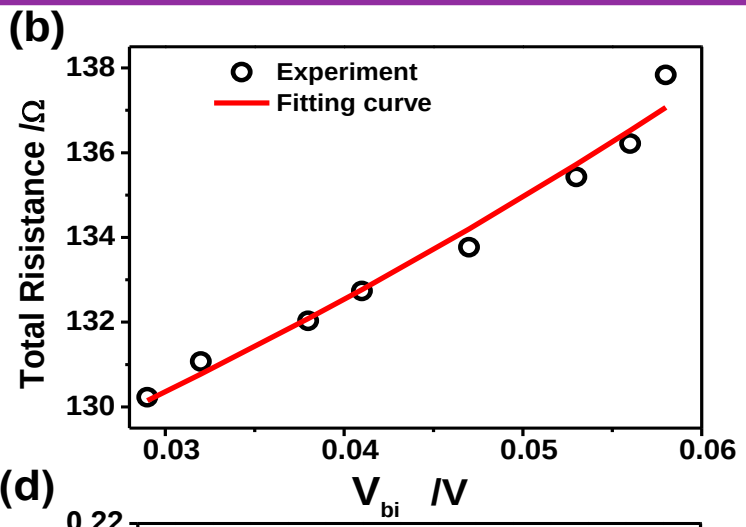

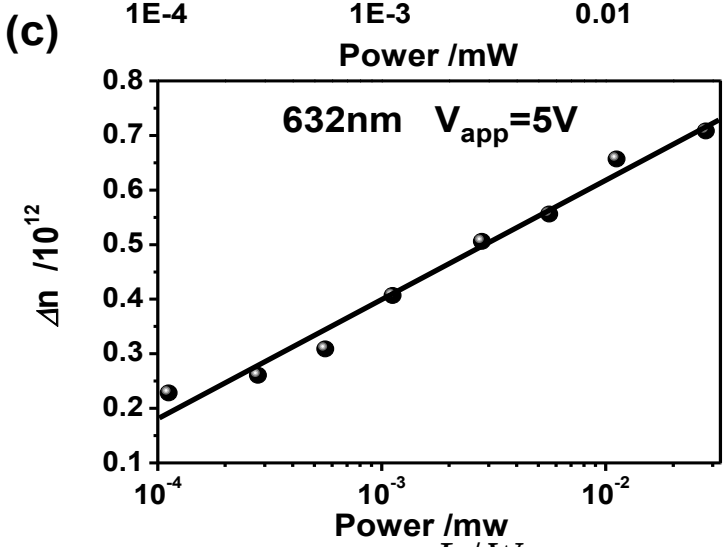

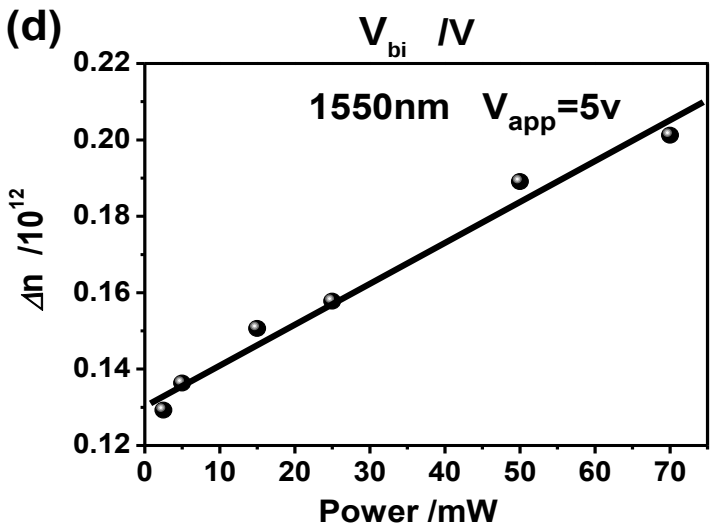

$$R_{total} = R_{contact} + R_{channel} = R_{contact} + \frac{L/W}{(n+\Delta n)e\mu}$$

$$E_{F\ dark} + \Delta\Phi_{Bi} = E_F = 11.65\sqrt{(n+\Delta n)/(10^{10}\mathrm{cm}^{-2})}$$

$R_{contact} = 270\ \Omega$, n=3.2 × 10^{12} cm^{-2}

μ=1.6 × 10^{3} $cm^2V^{-1}s^{-1}$

Plasmonic Enhancement

Surface Plasmonics: Collective oscillations of the free electron gas density → light trapping effect

(1) In a nanoparticle

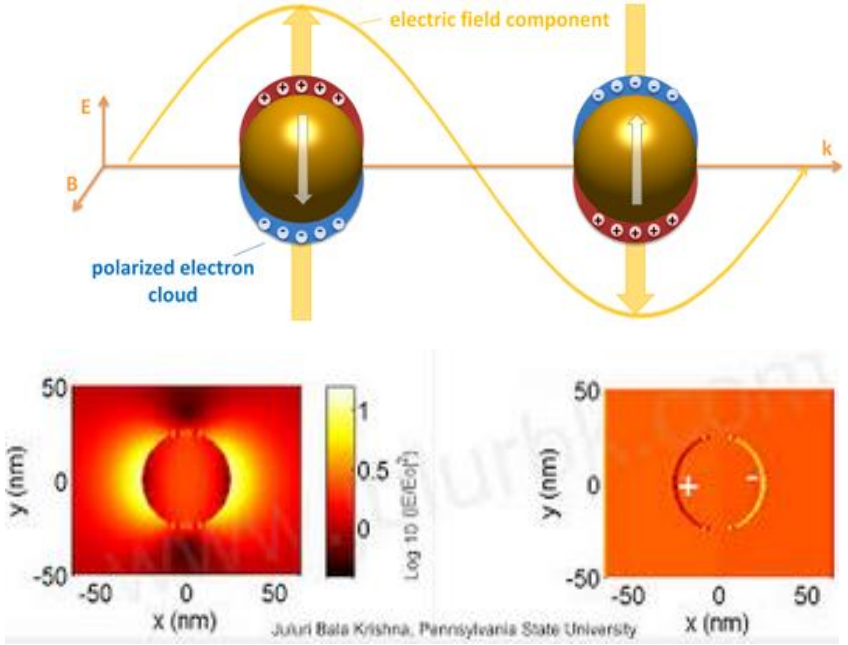

- trapping effect at the surface
- short wavelength (Au ~530nm)

(2) in peridic nano/microstructure

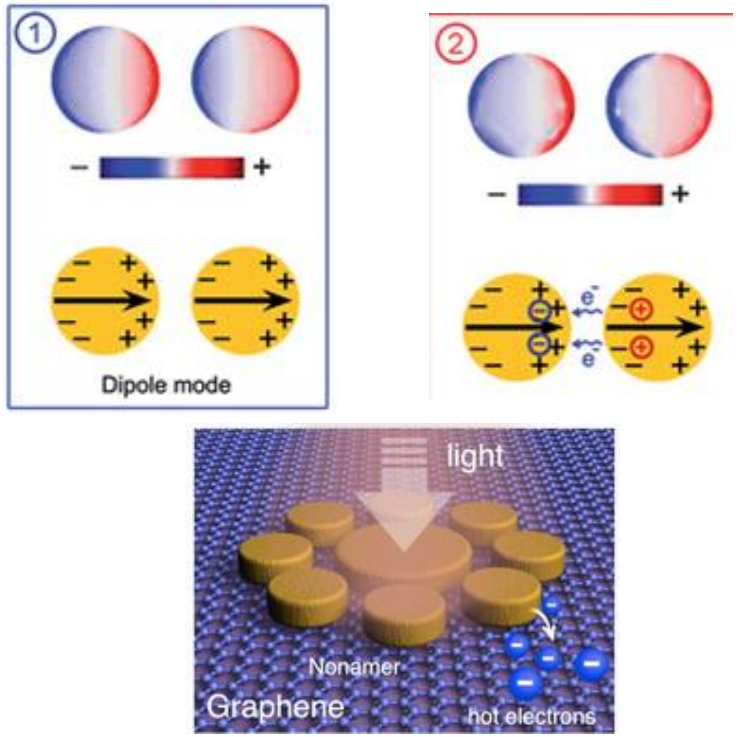

- trapping effect between structure
- resonance wavelength depend on the structure

Transmission

Tunable size of gold particle through baking the PS sphere monolayer

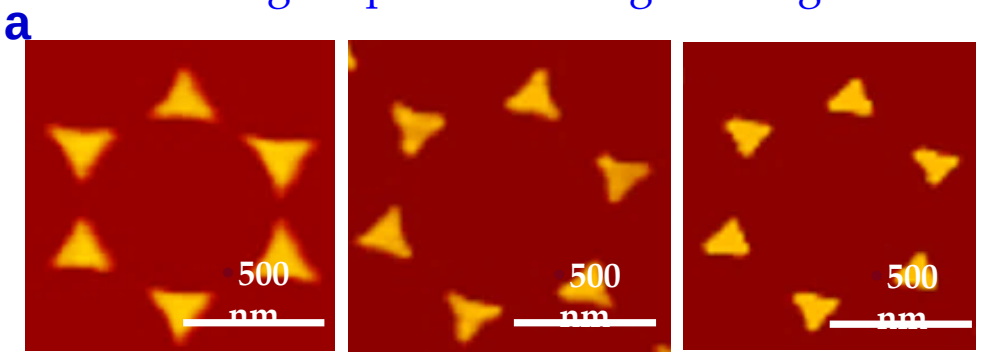

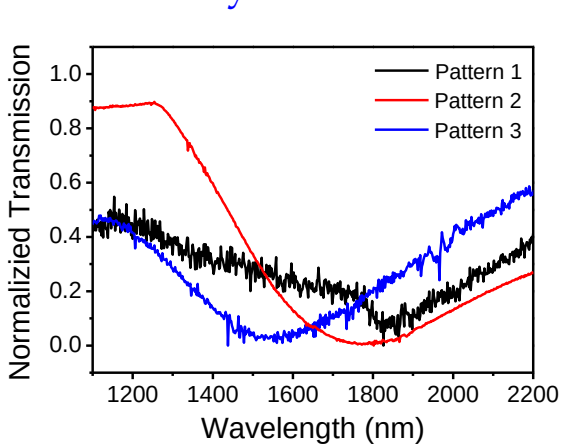

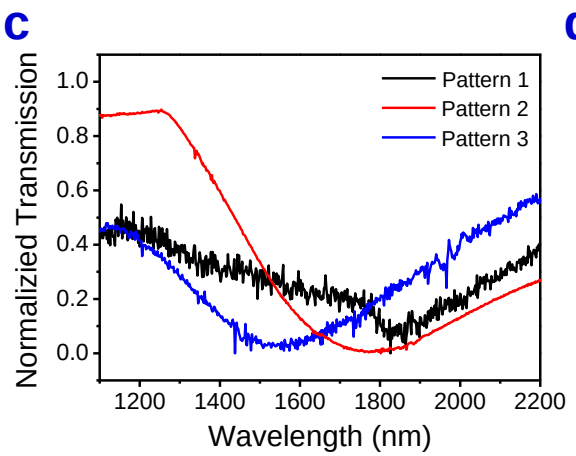

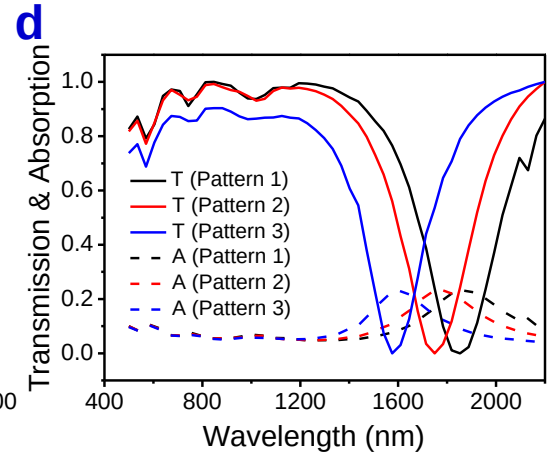

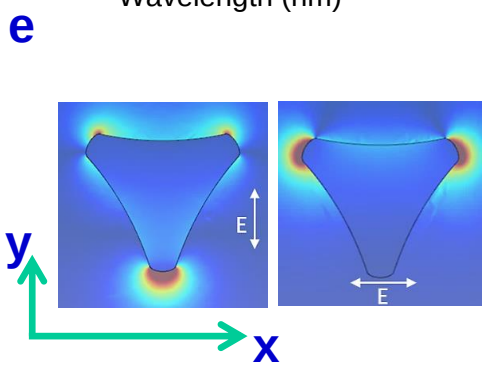

- The plasmonic peak is depended on the size. (from 1.45 μm to 1.85 μm)
- Experimental results consist with simulation
- The light intensity enhanced by 10 times
- TE/TM mode have same results (triangle belongs to C_{3v} symmetry group)

$$n_{eff\,(g)} = \sqrt{(\alpha\varepsilon_{air} + (1-\alpha)\varepsilon_{glass})} \approx 1.22$$

$$n_{eff\,(s)} = \sqrt{(\alpha\varepsilon_{air} + (1-\alpha)\varepsilon_{silicon})} \approx 2.48$$

idea case: $\lambda = n_{eff} * \pi d/2$

Photoresponsitivity

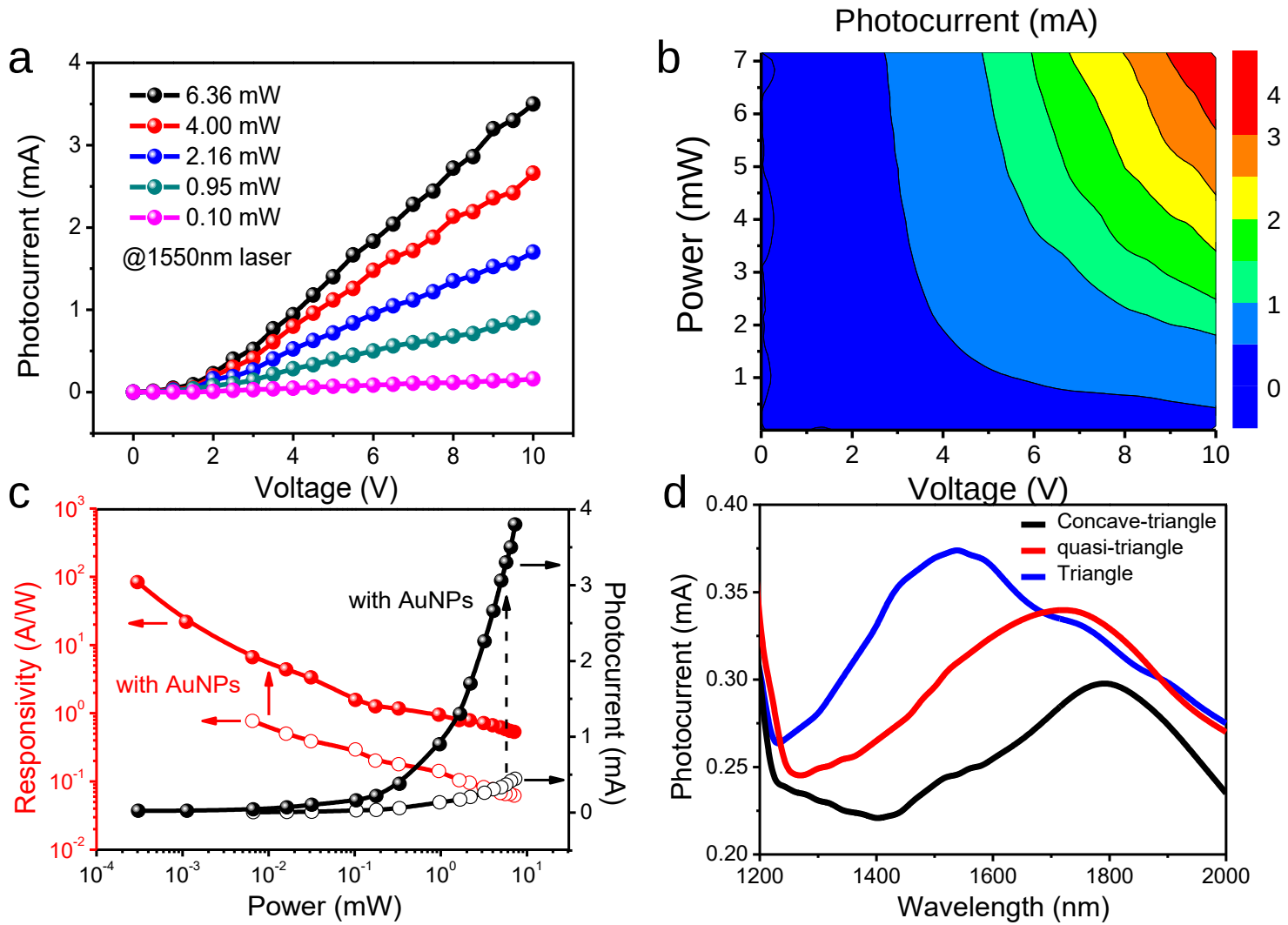

- With Au NPs photoresponse improve about 10 times
- Maximum photocurrent corresponds to the plasmonic peaks

Z. F. Chen, JBX, et al., ACS Nano 2017

Photocurrent Mapping

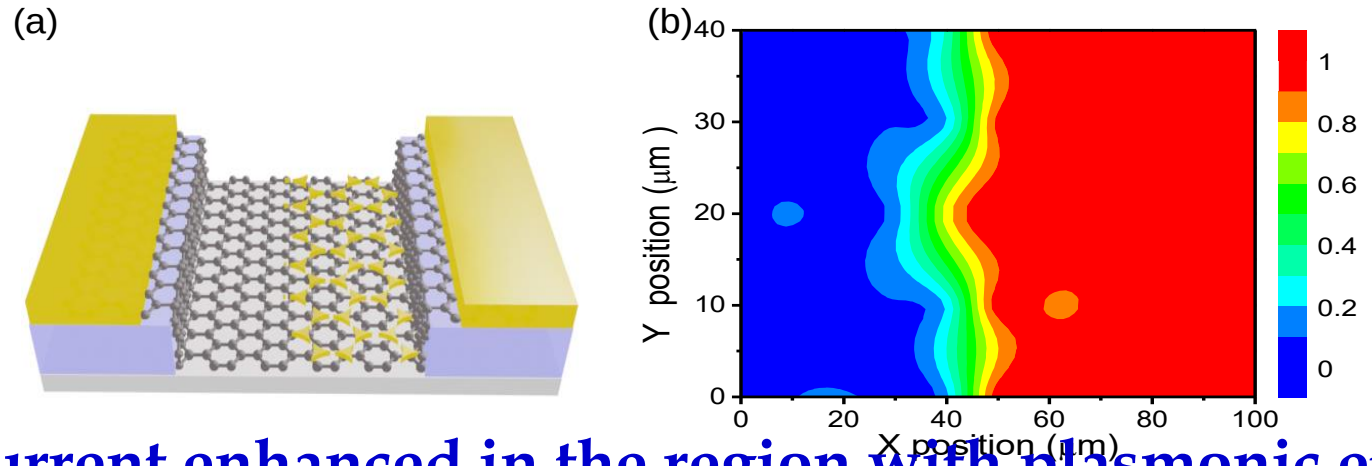

- **Photocurrent enhanced in the region with plasmonic effect**

Broadband response

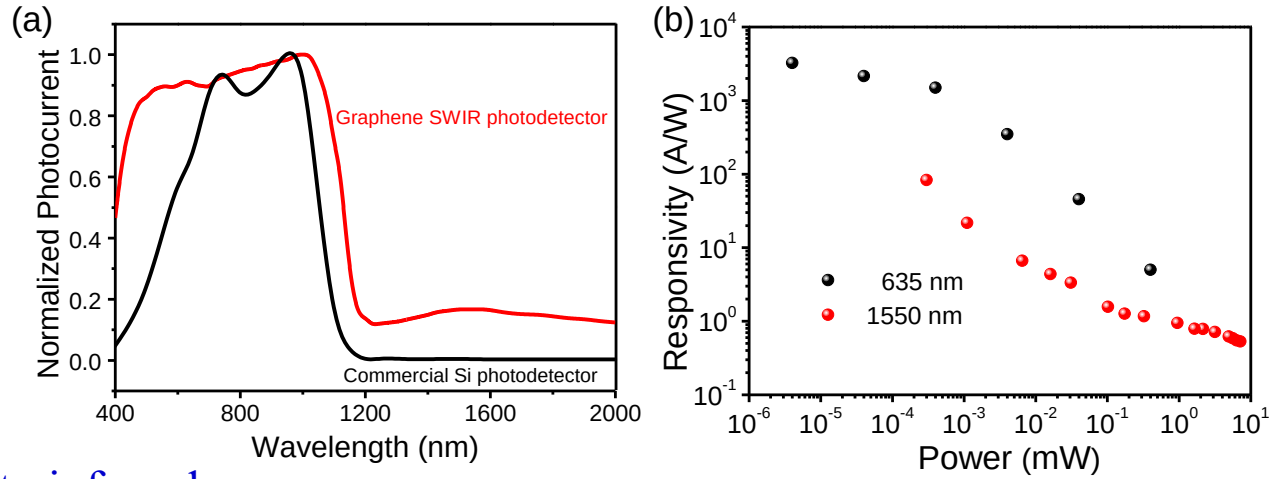

- From visible light to infrared
- Photocurrent before 1100nm much higher (silicon provide carriers)

Z. F. Chen, JBX, et al.,
ACS Nano 2017

Hybrid Graphene Tunneling Photoconductor

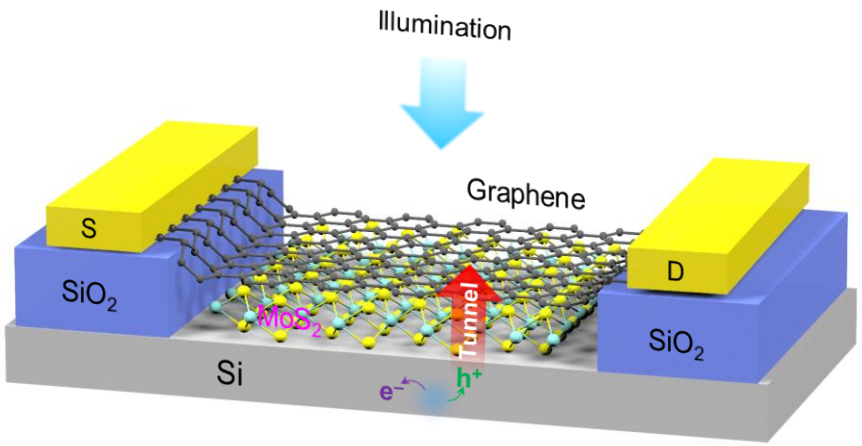

- **Bulk Si: photo-active material**
- Monolayer MoS_2: passivation layer for reducing interface states; retaining graphene's intrinsic electrical properties; and providing a tunneling barrier for photocarriers in Si to transfer into graphene
- Graphene: High-mobility channel for ultra-high photoconductive gain

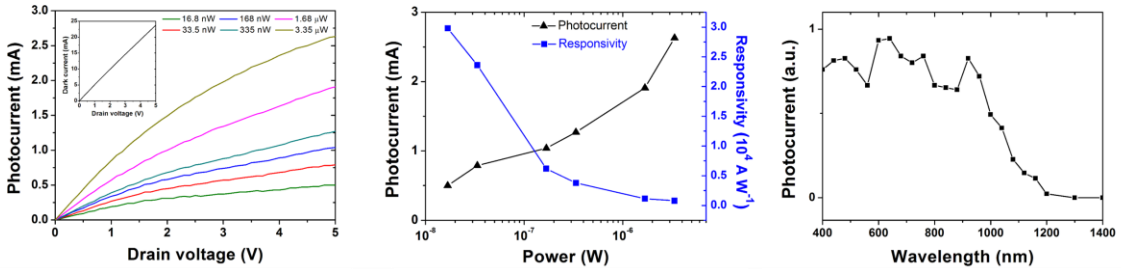

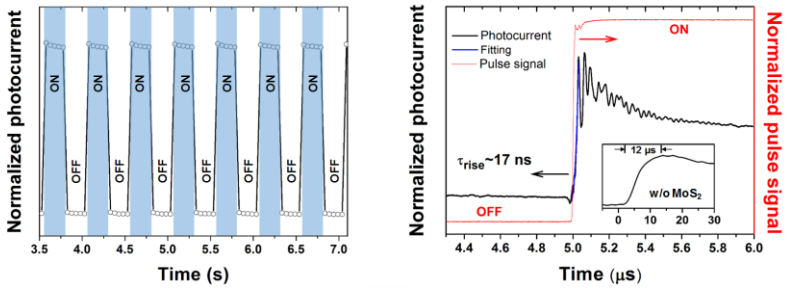

•**Switching performance**

- **High responsivity up to 3×10^4 A/W (635 nm, 3.35 μW);**
- **Broadband response from visible to NIR;**
- **Ultra-short response time (rising time ~17 ns), 3 orders of magnitude improved than device w/o MoS2**

L. Tao, JBX, et al, NPJ 2D Materials 1, 19 (2017)

Development by Others

Plasmonic for infrared photodeteoctor

Plasmonic Silicon Quantum Dots for Ultrabroadband Graphene Photodetection

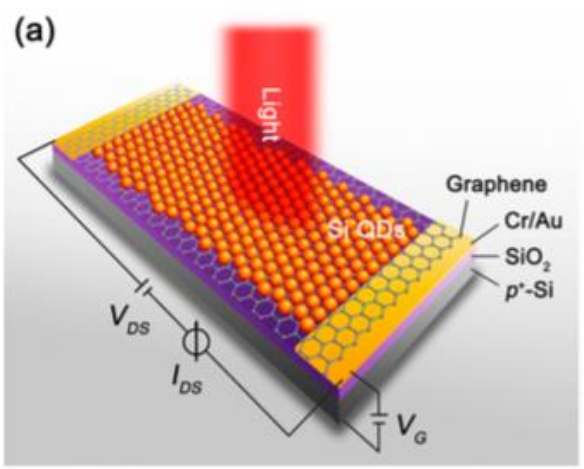

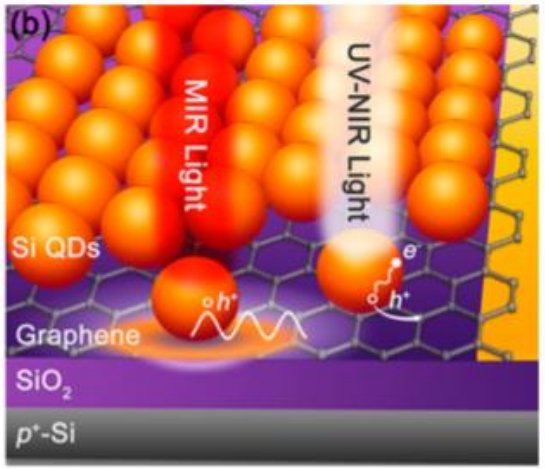

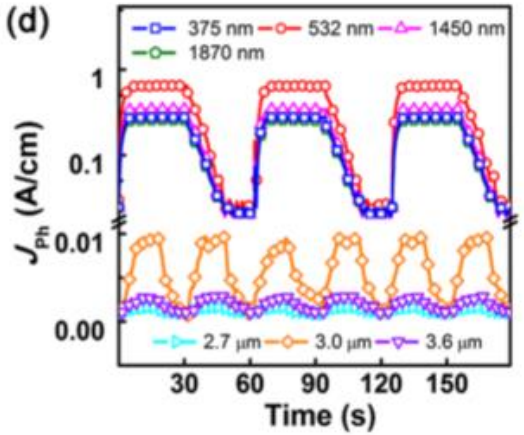

Zhenni Yin, ACS Nano, 11 (10), 9854(2017)

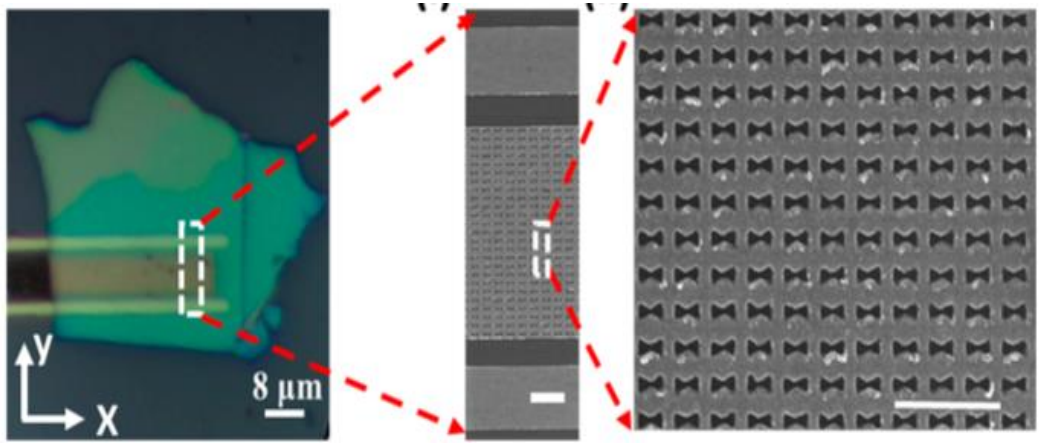

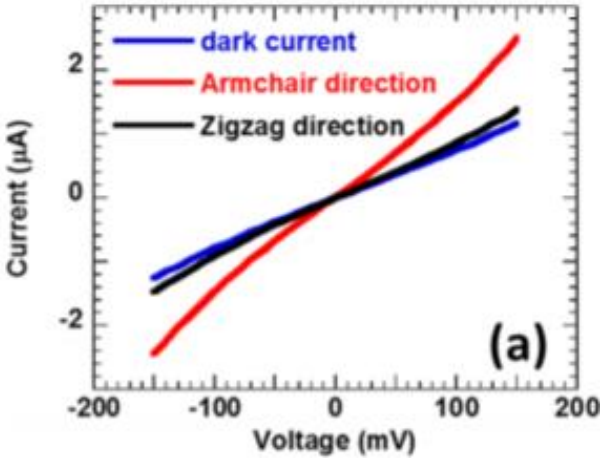

Prabhu K. Venuthurumill, et al, ACS Nano, 12 (5), 4861(2018)

Hybrid Phototransistors

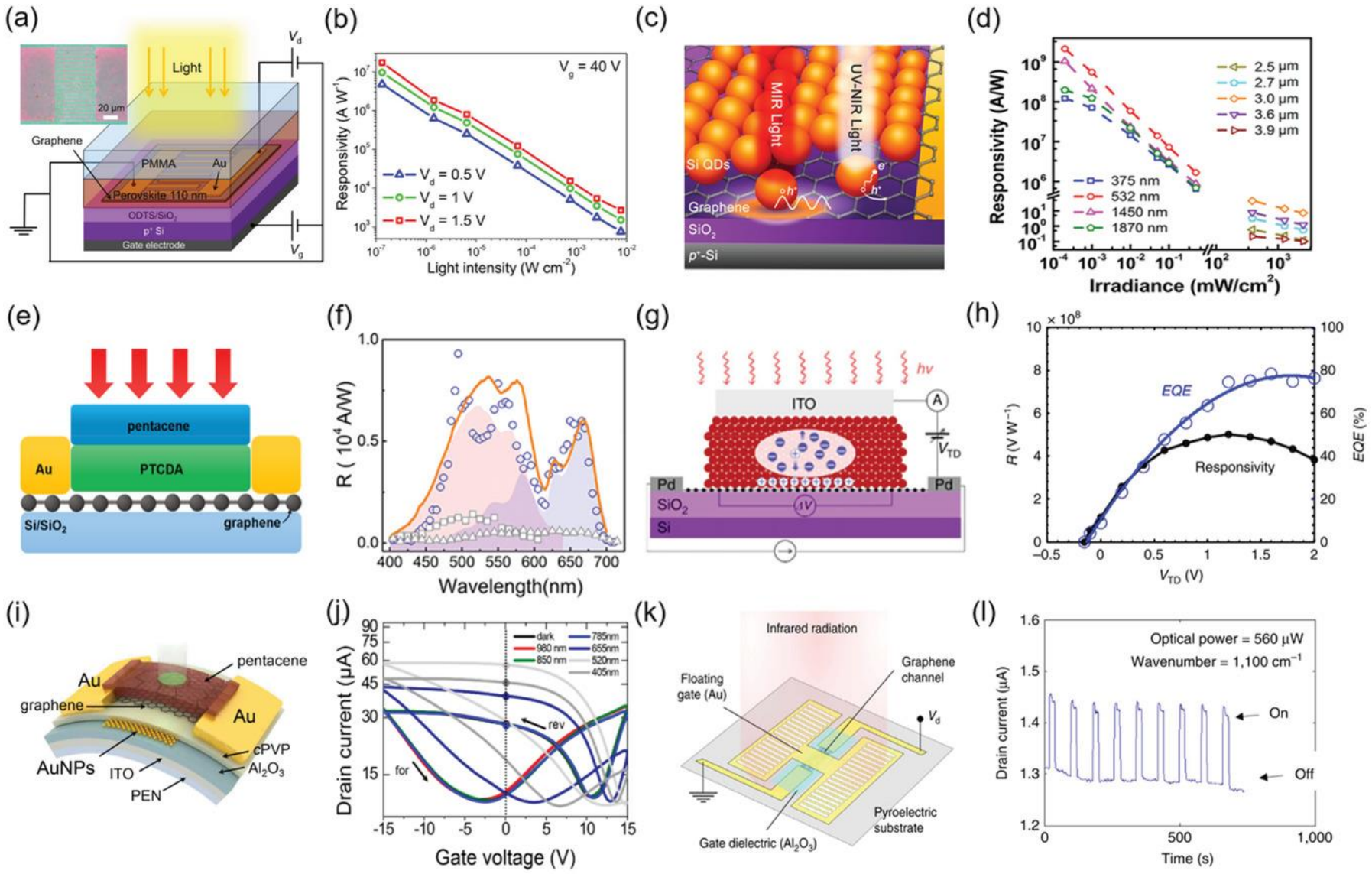

Advanced Materials, First published: 08 July 2019, DOI: (10.1002/adm.201902039)

New Development by Others

Broadband image sensor array based on graphene-CMOS integration

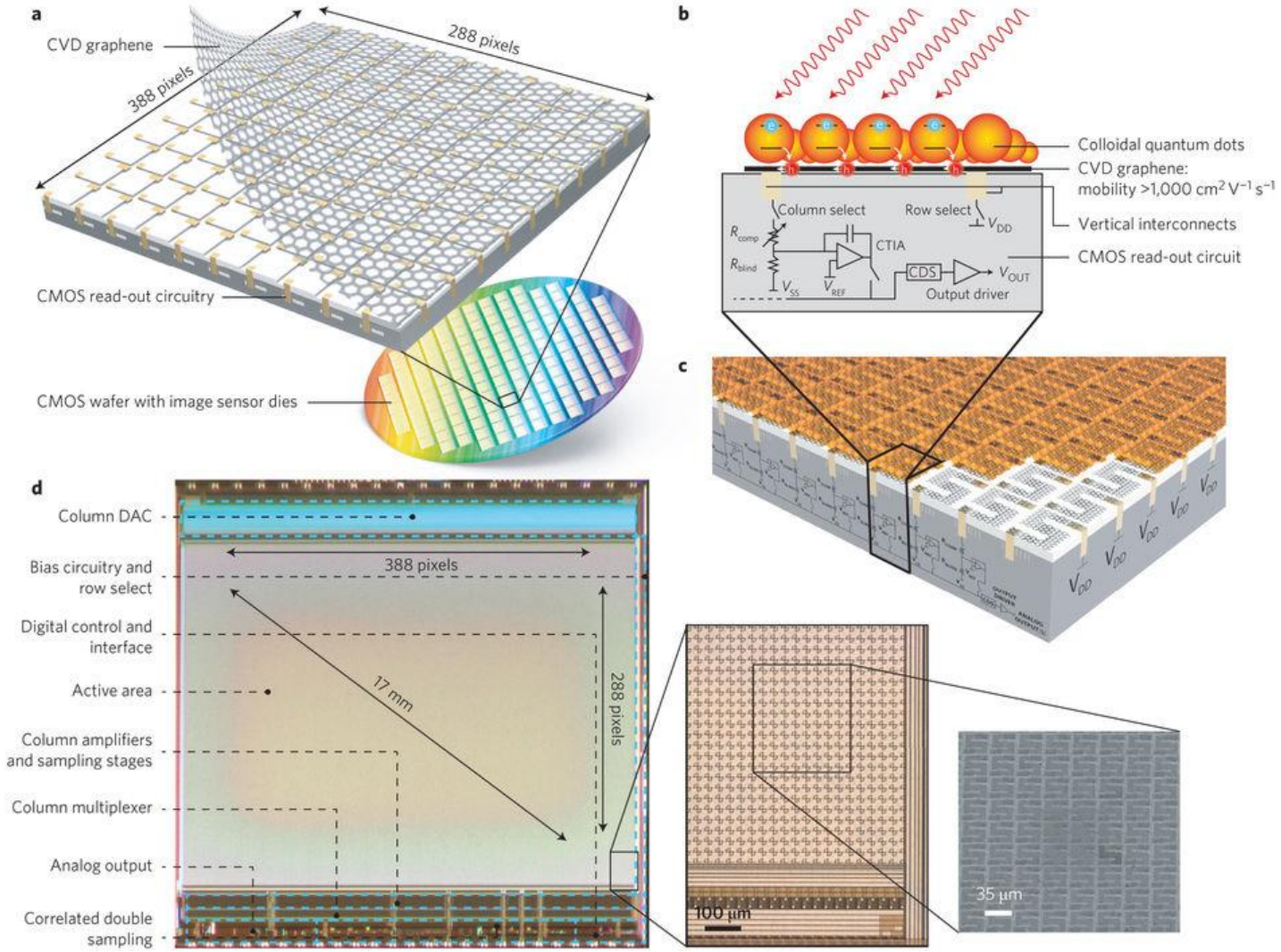

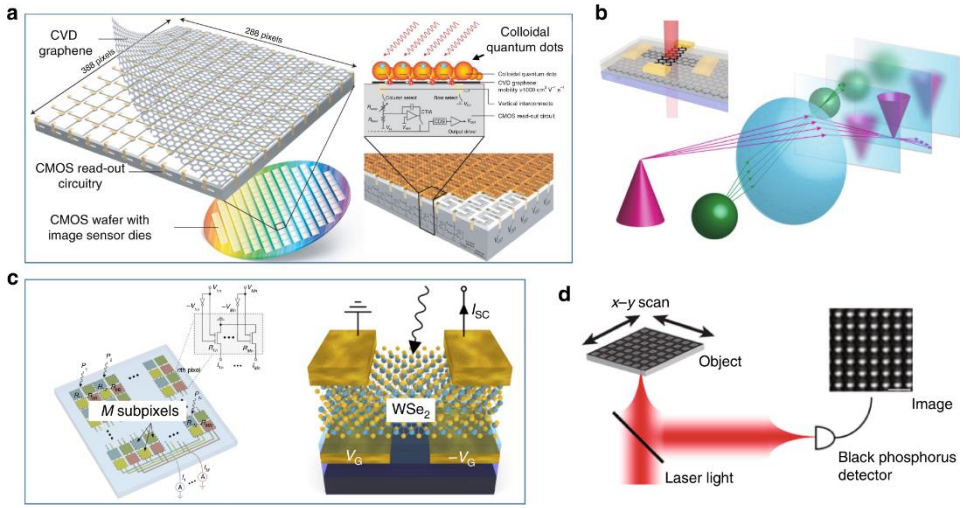

Stijn Goossens, Frank Kobben, et al.,
Nature Photonics 11, 366–371 (2017)

New Development by Others

Broadband image sensor array based on graphene-CMOS integration

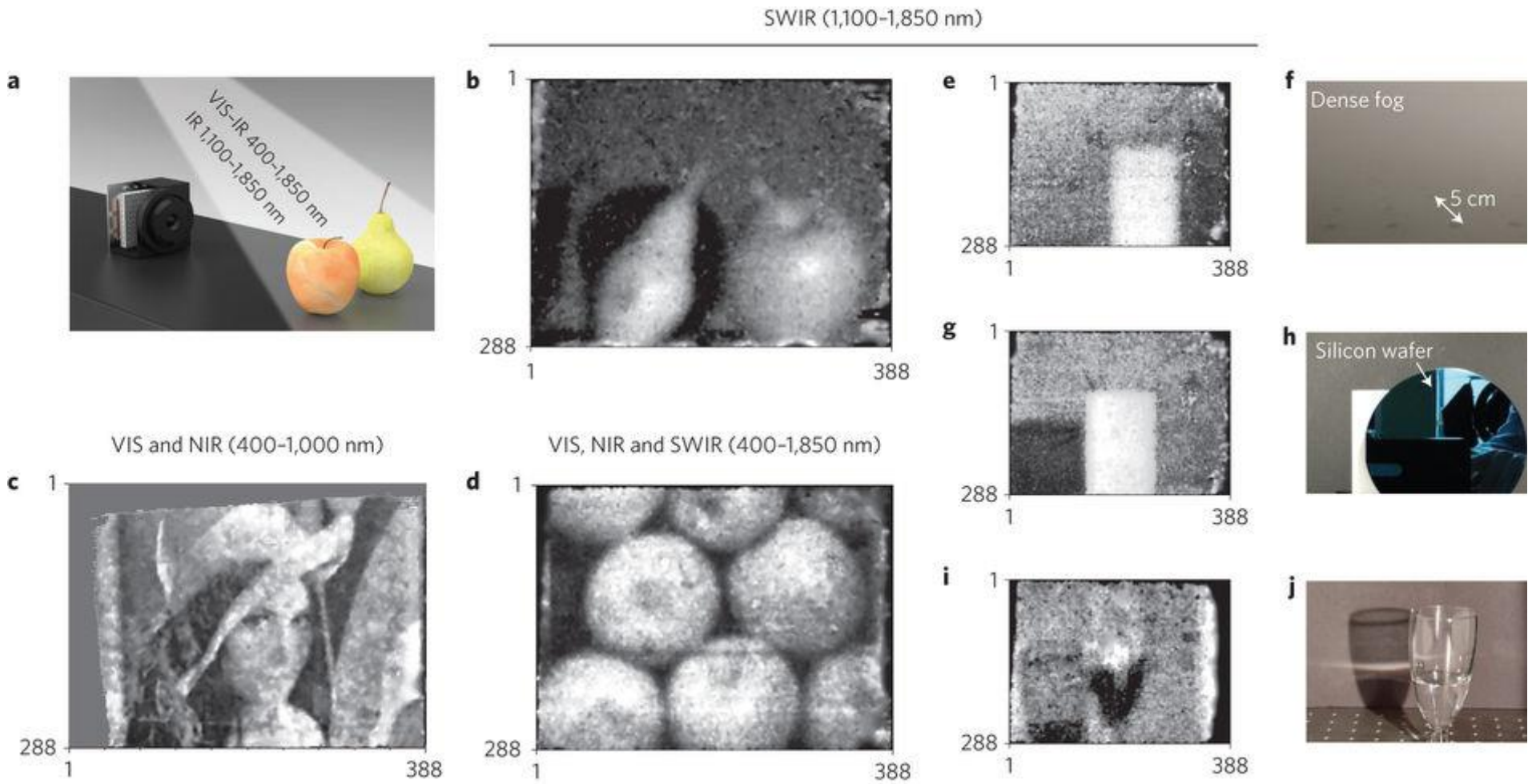

Stijn Goossens, Frank Kobbens, et al., Nature Photonics 11, 366–371 (2017)

Future Portable Broadband Imager

Source: https://www.youtube.com/watch?v=szL-ejdpNgU

Graphene-Silicon Based Full-Band Imager

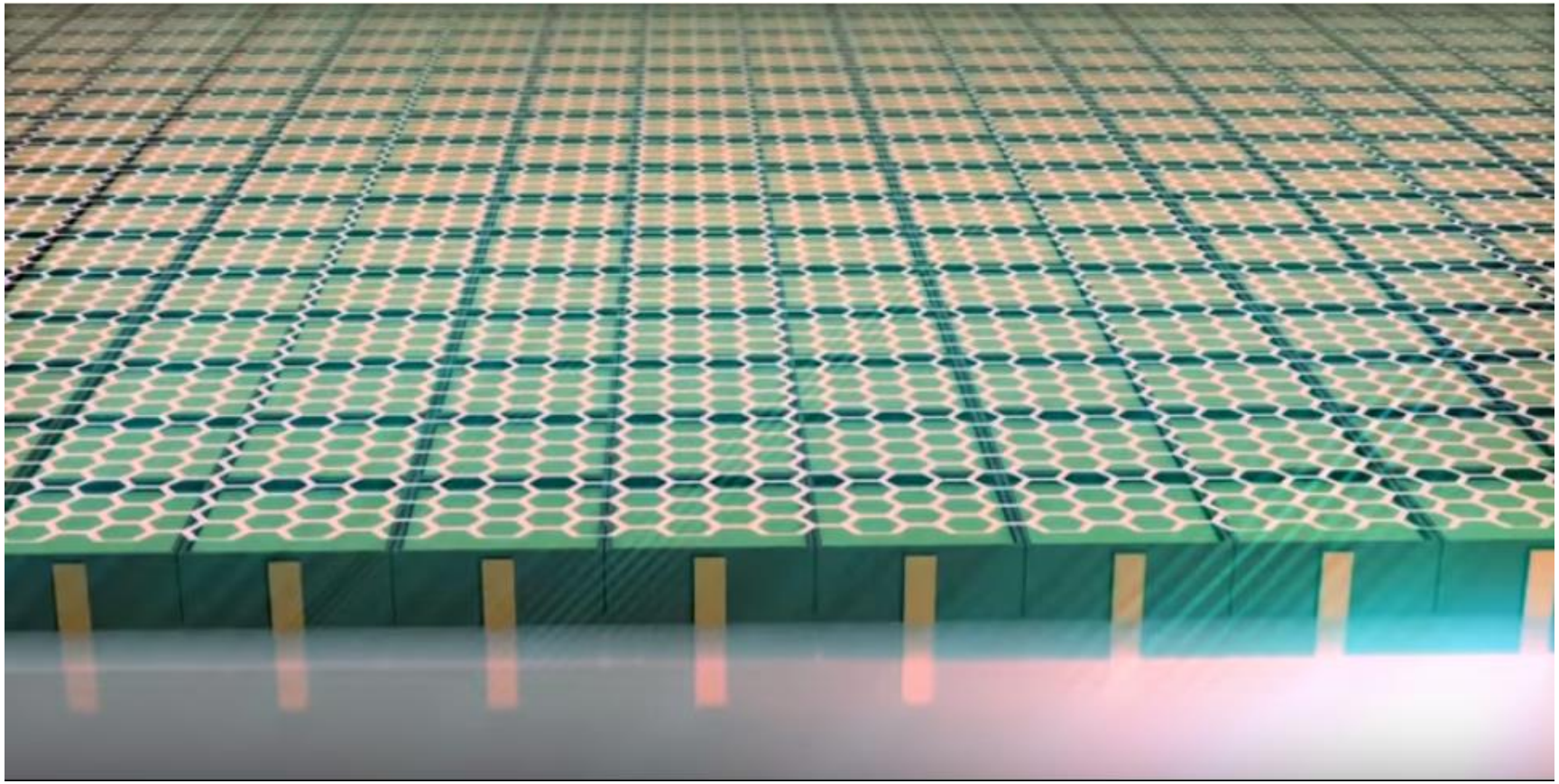

Figure of Merit

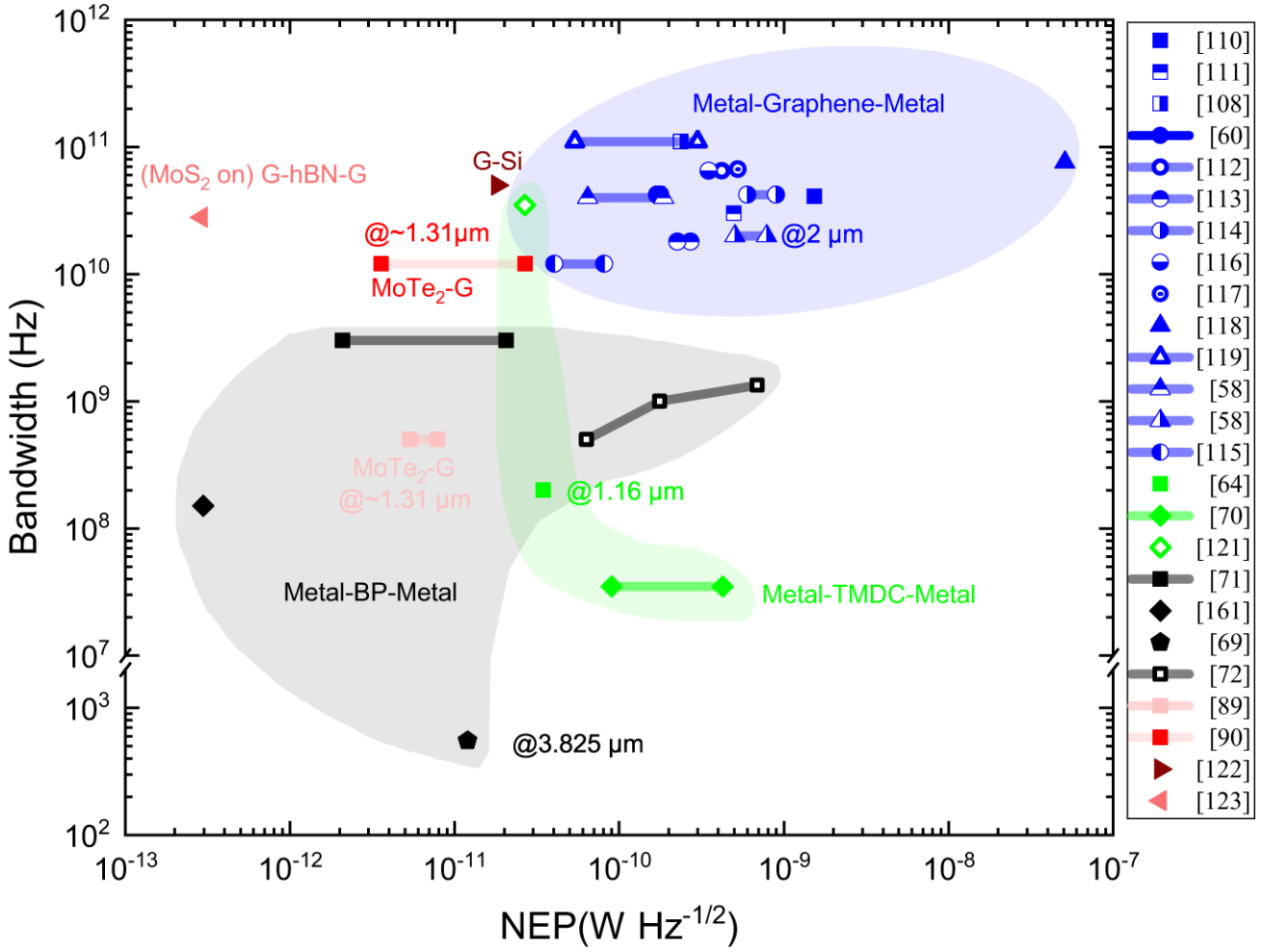

■: photovoltaic (PV) effect, ●: photo-thermoelectric (PTE) effect, ▲: bolometric (BOL) effect, ◆: photoconductive (PC) effect, ⬟: Photo-gating (PG) effect, ◄: tunneling effects, ►: internal photon emission.(IPE) effect; blue: metal-graphene-metal (M-G-M); green: metal-TMDC-metal; black: metal-BP-metal; red: 2DM-heterostructure

C. Y. Liu, D. X., Dai, et al, Light: Science and Applications, 10(1), 123 (2021)

Highly Polar. Sensitive Infrared Photodetector BP/WSe_2

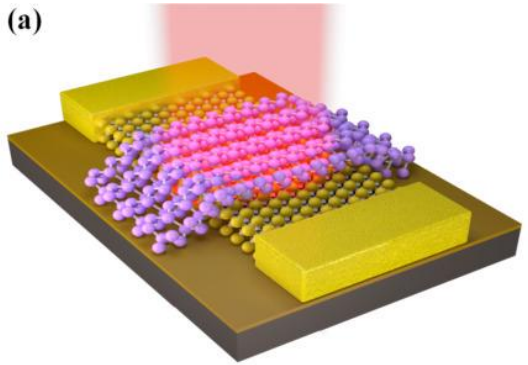

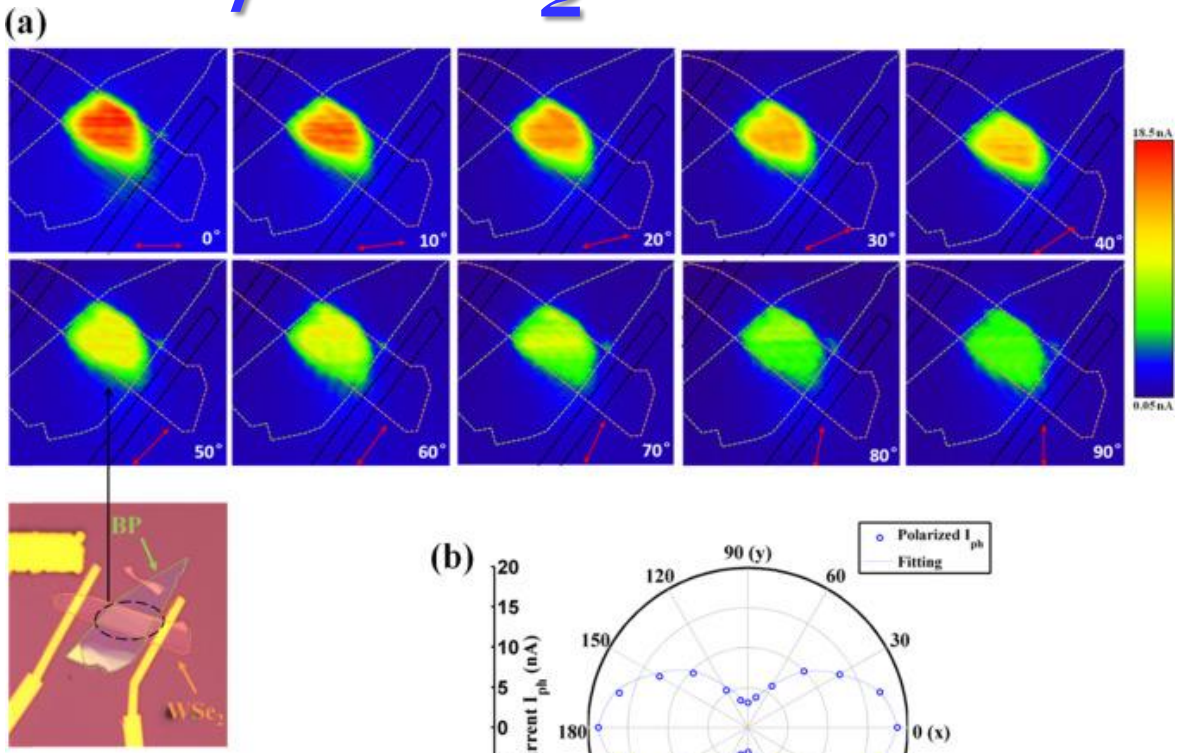

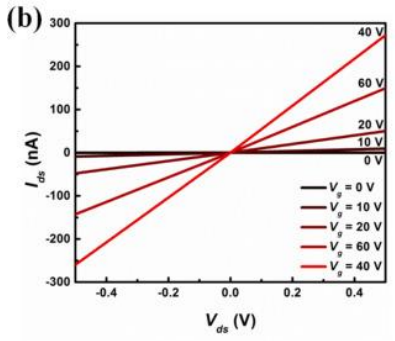

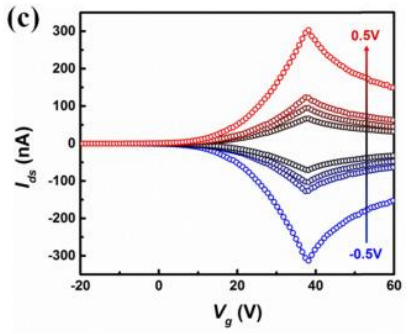

Lei Ye, Peng Wang, Wenjin Luo, Fan Gong, Lei Liao, Tiande Liu, Lei Tong, Jianfeng Zang, Jianbin Xu, Weida Hu

Nano Energy 37, 2017, 53–60, http://dx.doi.org/10.1016/j.nanoen.2017.05.004

Routes to Commercialization

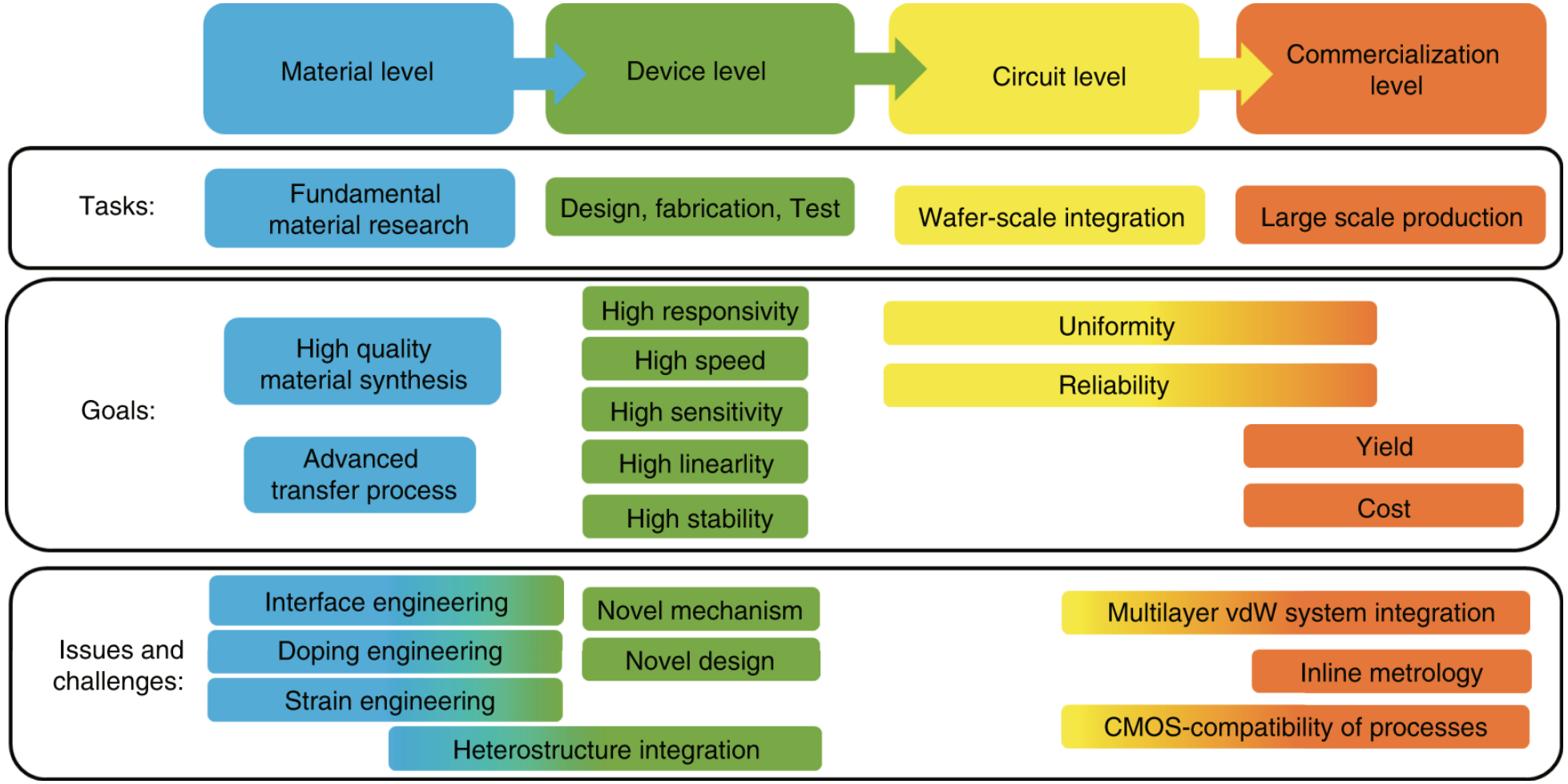

The tasks, goals, and issues and challenges are summarized from the perspective of the material level, the device level, the circuit level, as well as the commercialization level.

C. Y. Liu, D. X., Dai, et al, Light: Science and Applications, 10(1), 123 (2021)

Enhanced Schemes for Planar Structures

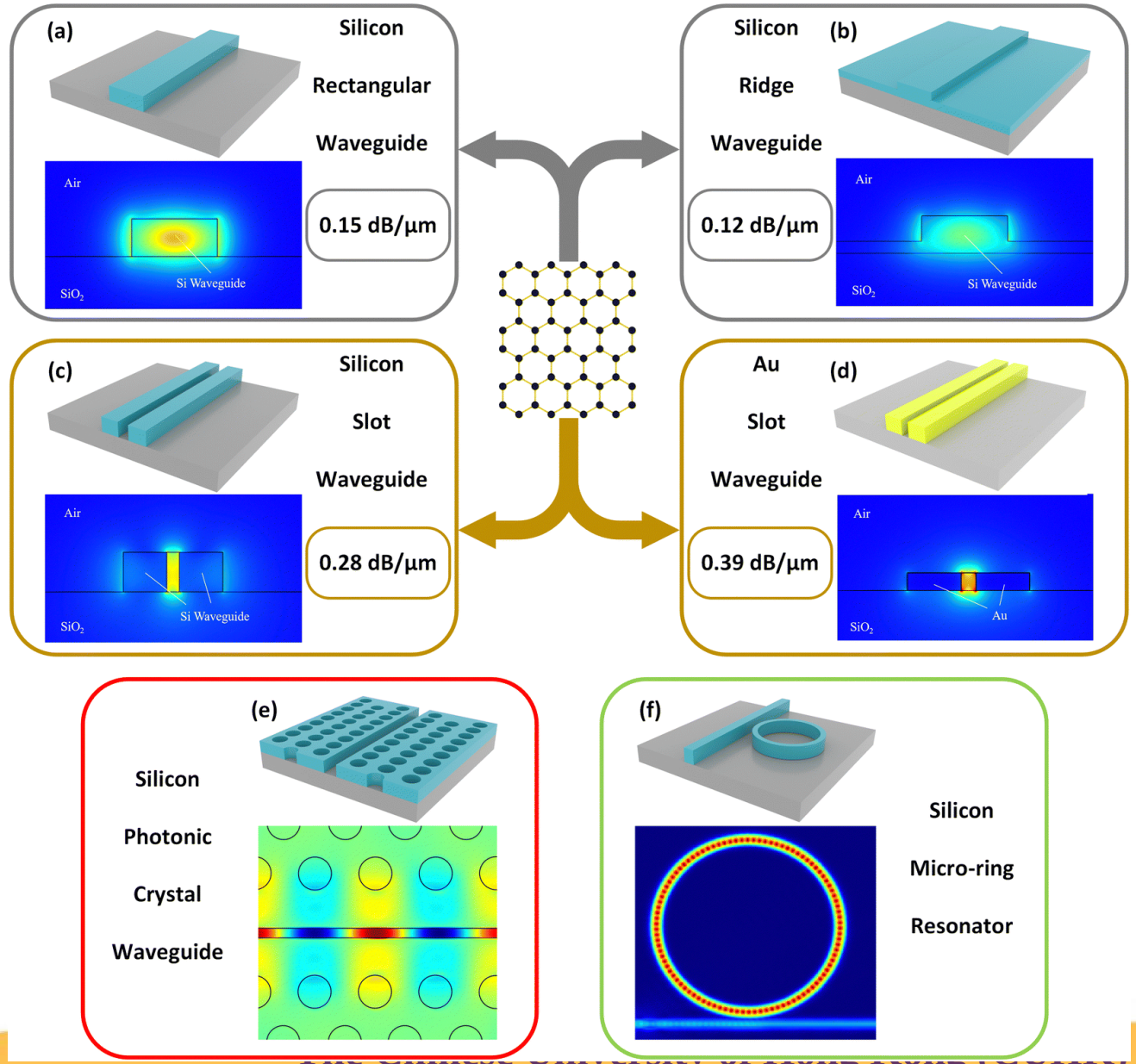

Commonly used waveguide structures in on-chip photonic devices together with their optical field distributions and the calculated optical absorption coefficients of monolayer graphene covered on some waveguide structures: (a) silicon rectangular waveguide. Height: 220 nm, width: 500 nm, and absorption coefficient: 0.15 dB μm^{-1}. (b) Silicon ridge waveguide. Height: 220 nm, width: 500 nm, ridge height: 70 nm, and absorption coefficient: 0.12 dB μm^{-1}. (c) Silicon slot waveguide. Height: 220 nm, width: 550 nm, slot width: 70 nm, and absorption coefficient: 0.28 dB μm^{-1}. (d) Au SPP slot waveguide. Height: 90 nm, width: 2500 nm, slot width: 70 nm, and absorption coefficient: 0.39 dB μm^{-1}. (e) Silicon PhC waveguide. (f) Silicon MRR. Each of these waveguides contributes to improving the optical absorption of 2DMs, and also has different advantageous properties.

On-chip two-dimensional material-based waveguide-integrated photodetectors
X He, Y Wang, Z Peng, Z Li, X Yu, L Xu, X Huang, X Meng, W Shi, X Gao, J. B. Xu, et al., Journal of Materials Chemistry C 12, 2279-2316 (2024)

Development by Others

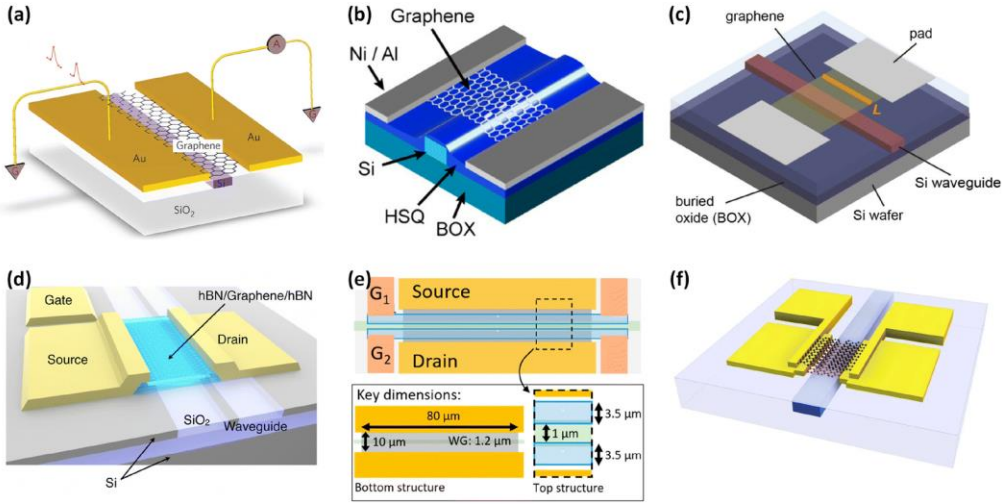

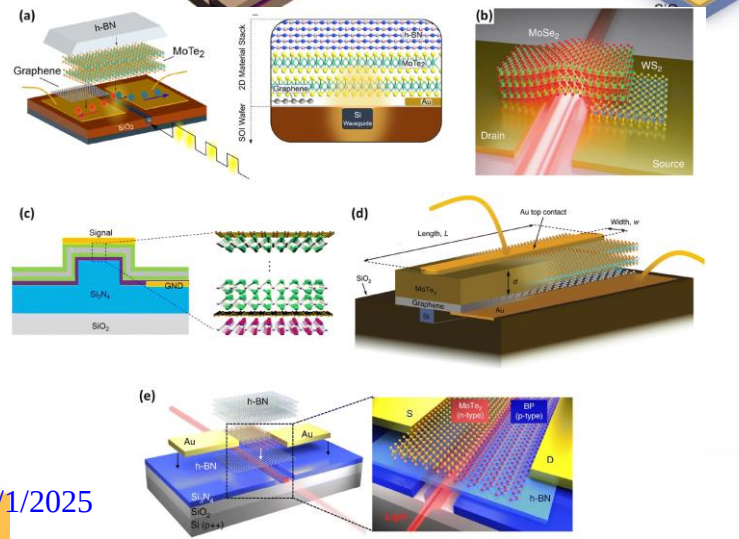

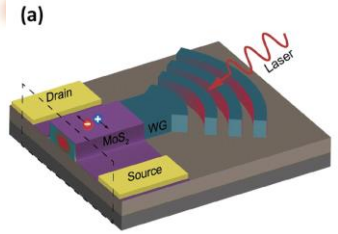

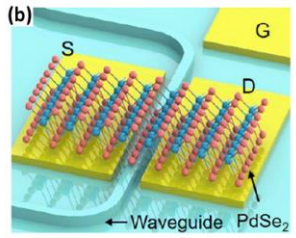

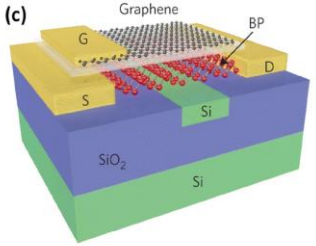

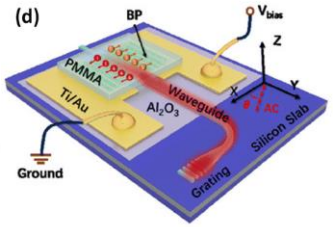

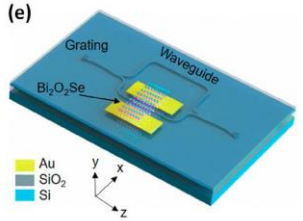

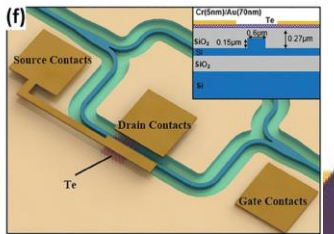

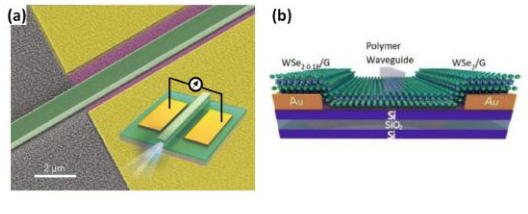

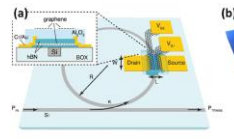

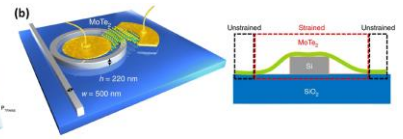

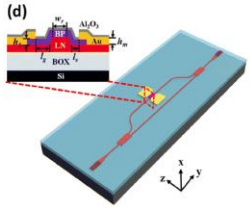

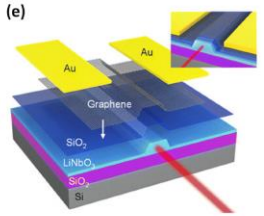

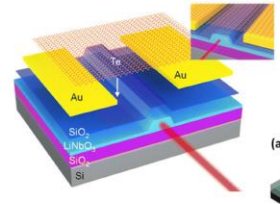

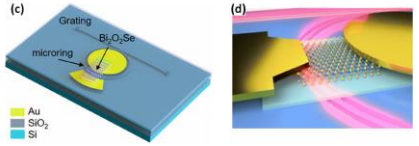

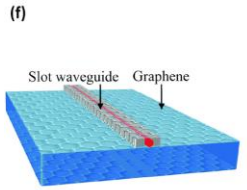

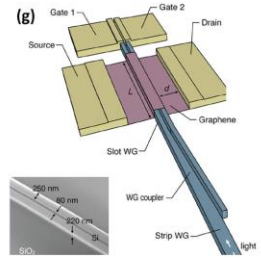

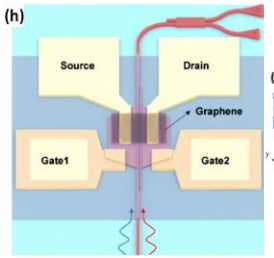

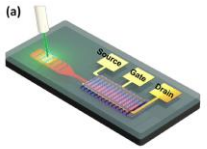

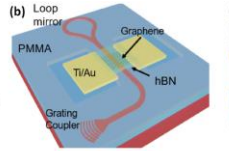

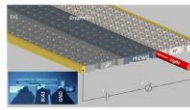

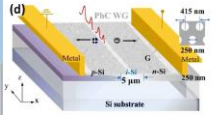

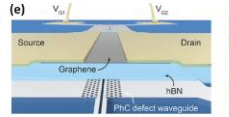

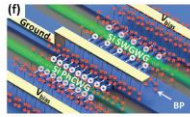

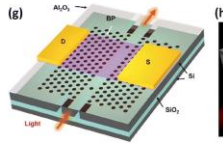

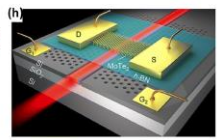

On-chip two-dimensional material-based waveguide-integrated photodetectors
X He, Y Wang, Z Peng, Z Li, X Yu, L Xu, X Huang, X Meng, W Shi, X Gao, J. B. Xu, et al.,
Journal of Materials Chemistry C 12, 2279-2316 (2024)

Summary of PDs

2DM WI PDs	Operating wavelengths	Mechanism	Material	Structure	2DMs	Bias voltage	Responsivity	Bandwidth	Dark current	Ref.
Visible	647 nm	PG	Si_3N_4	Rectangular	MoS_2	1 V	>1000 A W^{-1}	>20 Hz	Few nA	193
	765–785 nm	PV	$LiNbO_3$	Ridge	Graphene	0 V	8 mA W^{-1}	40 GHz	5 nA	186
	1500–1630 nm						17.27 mA W^{-1}			
	780 nm	PC, PG	Si_3N_4	Rectangular	$MoSe_2$–WS_2	2 V	1 A W^{-1}	20 MHz	50 pA	198
Near- infrared	1.26–1.265 μm	PC	Silicon	MRR	Bi_2O_2Se	2 V	1.83 A W^{-1}	—	15.3 nA	196
	1.26–1.31 μm	PC	Silicon	Ridge	Bi_2O_2Se	2 V	3.5 A W^{-1}	—	72.9 nA	
	1.26–1.32 μm	PV	Silicon	PhC	$MoTe_2$	1 V	400 mA W^{-1}	34 GHz	<90 pA	228
	1.26–1.565 μm	PV	Silicon	Ridge	$PtSe_2$	5 V	1.76 A W^{-1}	1.5 GHz	79.9 μA	194
	1.265–1.33 μm	PV, PG	Silicon	Rectangular	$MoTe_2$–graphene	3 V	200 mA W^{-1}	>24 GHz	Few μA	200
	1.3–1.4 μm	BOL, PV	Ti/Au	SPP Slot	Graphene	0.5 V	670 mA W^{-1}	—	—	215
	1.31 μm	PV, PG	Silicon	Rectangular	$MoTe_2$–graphen	3 V	23 mA W^{-1}	1 GHz	Few nA	173
	1.31–1.65 μm	PV, PTE	Silicon & Au	hybrid SPP	Graphene	0 V	30 mA W^{-1}	18 GHz	None	183
	1.45–1.59 μm	PV	Silicon	Rectangular	Graphene	1 V	108 mA W^{-1}	>20 GHz	—	182
	1.48–1.58 μm	IPE	Silicon	PhC	Graphene	4 V	0.8 mA W^{-1}	5 GHz	None	224
	1.48–1.62 μm	BOL	Silicon & Au	Hybrid SPP	Graphene	0.4 V	500 mA W^{-1}	>110 GHz	Few mA	209
	1.5–1.63 μm	PV, PC	Si_3N_4	Rectangular	BP-$MoTe_2$	1 V	709 mA W^{-1}	1 GHz	<7 nA	201
	1.5–1.63 μm	PC	$LiNbO_3$	Ridge	Te	0.5 V	7 A W^{-1}	2 GHz	<300 μA	186
	1.5–1.63 μm	IPE	Si_3N_4	MRR	MoS_2	1 V	154.6 mA·W^{-1}	—	<2.5 μA	231
	1.5–1.8 μm	PTE, PV	Silicon	Rectangular	Graphene	1.2 V	360 mA W^{-1}	42 GHz	—	189
	1.52–1.58 μm	PV, PC	$LiNbO_3$	Ridge	BP	2 V	2.64 A W^{-1}	1.97 GHz	<1.5 mA	185
	1.55 μm	PV	Silicon	Rectangular	Graphene	0 V	16 mA W^{-1}	41 GHz	None	187
	1.55 μm	PV	Silicon	Rectangular	BP	0.4 V	135 mA W^{-1}	>3 GHz	220 nA	174
	1.55 μm	PV	Silicon	PhC	BP	0.5 V	125 mA W^{-1}	>1.42 GHz	<20 nA	227
	1.55 μm	PV	Au	SPP Slot	Graphene	2.2 V	360 mA W^{-1}	>110 GHz	—	214
	1.55 μm	PTE, PV, BOL	Silicon	Slot	Graphene	0.3 V	76 mA W^{-1}	65 GHz	—	204
	1.55 μm	PTE, PC	Silicon	PhC	Graphene	0.4 V	170 mA W^{-1}	>18 GHz	—	226
	1.55 μm	PTE	Silicon	Slot	Graphene	2 V	273 mA W^{-1}	—	—	89
	1.55 μm	PTE	Silicon	Rectangular	Graphene	0 V	3.5 V W^{-1}	70 GHz	None	191
	1.55 μm	PTE	Si_3N_4	Rectangular	Graphene	0 V	6 V W^{-1}	>67 GHz	None	190
	1.55 μm	PTE	Au	SPP Slot	Graphene	0 V	12.2 V W^{-1}	42 GHz	None	213
	1.55 μm	PC, PG	Au	SPP Slot	BP	1.5 V	10 A W^{-1}	150 MHz	—	216
	1.55 μm	PC	Polymer & Au	Hybrid SPP	$PtSe_2$	8 V	12 mA W^{-1}	35 GHz	317 nA	210
	1.55 μm	PC	Au	SPP Slot	Graphene	0.4 V	130 mA W^{-1}	>70 GHz	3.52 mA	219
	1.55 μm	PC	$LiNbO_3$	Ridge	BP	0.3 V	148 mA W^{-1}	3.5 MHz	—	203
	1.55 μm	PC	Silicon	MRR	$MoTe_2$	2 V	500 mA W^{-1}	35 MHz	<100 nA	230
	1.55 μm	IPE	Silicon	PhC	Graphene	0 V	11 mA W^{-1}	>50 GHz	None	225
	1.55 μm	IPE	Si_3N_4 & Au	Hybrid SPP	MoS_2	0.3 V	15.7 mA W^{-1}	>1.37 GHz	Few μA	211
	1.55 μm	IPE	Silicon & Au	Hybrid SPP	Graphene	1 V	370 mA W^{-1}	—	3 μA	207
	1.55 μm	BOL, PTE	Silicon	Rectangular & Mirror Reflector	Graphene	0.3 V	25 mA W^{-1}	17 GHz	—	223
	1.55 μm	BOL	Silicon	Rectangular	Graphene	1 V	1 mA W^{-1}	>76 GHz	—	188
	1.55 μm	BOL	Silicon & Au	Slot & SPP Slot	Graphene	1.9 V	603.92 mA W^{-1}	78 GHz	—	218
	1.55587 μm	PTE	Silicon	MRR	Graphene	0 V	90 V W^{-1}	12 GHz	None	229
	1.56 μm	DT, F–N tunneling	Si_3N_4	Ridge	MoS_2–graphene–hBN–graphene	10 V	24 mA W^{-1}	28 GHz	13.5 nA	199
	1.6 μm	IPE	Ti	SPP Slot	$MoTe_2$	10 V	23 mA W^{-1}	—	Few μA	221
Mid- infrared	1.55 μm	IPE	Silicon	Ridge	Graphene	6 V	0.147 mA W^{-1}	30 GHz	<100 pA	192
	2 μm						0.0148 mA W^{-1}			
	1.55 μm	PC, BOL	Silicon & Au	Hybrid SPP	Graphene	0.3 V	70 mA W^{-1}	>40 GHz	3 mA	208
	2 μm						400 mA W^{-1}	>20 GHz		
	1.55 μm	PTE	Silicon	Slot	Graphene	0 V	2.81 V W^{-1}	>40 GHz	None	205
	2 μm						2.78–4 V W^{-1}	>22 GHz		
	1.55 μm	PV	Silicon & Au	Rectangular & SPP Slots	BP	2 V	66 A W^{-1}	1.05 GHz	<0.7 mA	217
	2 μm						125 A W^{-1}			
	2 μm	PV	Silicon	Ridge	BP	0.4 V	306.7 mA W^{-1}	1.33 GHz	—	195
	2–2.55 μm	PV	ChG	Rectangular	Graphene	1.5 V	250 mA W^{-1}	—	—	117
	2.015 μm	PC	Silicon	Rectangular	Te	1.5 V	2.3 A W^{-1}	4 GHz	—	75
	2.75 μm	IPE	Silicon	Ridge	Graphene	1.5 V	130 mA W^{-1}	—	None	184
	3.68–4.03 μm	PG	Silicon	Rectangular & Grating	BP	1 V	23 A W^{-1}	—	<250 μA	222
	3.825 μm	PG	Silicon	PhC	BP	0.5 V	11.31 A W^{-1}	—	<30 μA	167

Table 1 Structural and performance metrics of PDs operating in different bands. Note that the material of the SPP waveguide in the table is not labeled with the adhesion layer metal and ChG stands for chalcogenide glass

- Various types of planar PDs with graphene and other 2D materials
- Wavelengths from 1.2 – 8 μm
- High responsivity at RT

On-chip two-dimensional material-based waveguide-integrated photodetectors, X He, Y Wang, Z Peng, Z Li, X Yu, L Xu, X Huang, X Meng, W Shi, X Gao, J. B. Xu, et al., Journal of Materials Chemistry C 12, 2279-2316 (2024)

Outline

- Introduction and Background
- Graphene-Silicon Hybrid Detectors based on Photodiode Mode
- Graphene-Silicon Hybrid Detectors based on Photoconductor Mode
- **Graphene based THz Modulator**
- Conclusions

Introduction to THz Waves

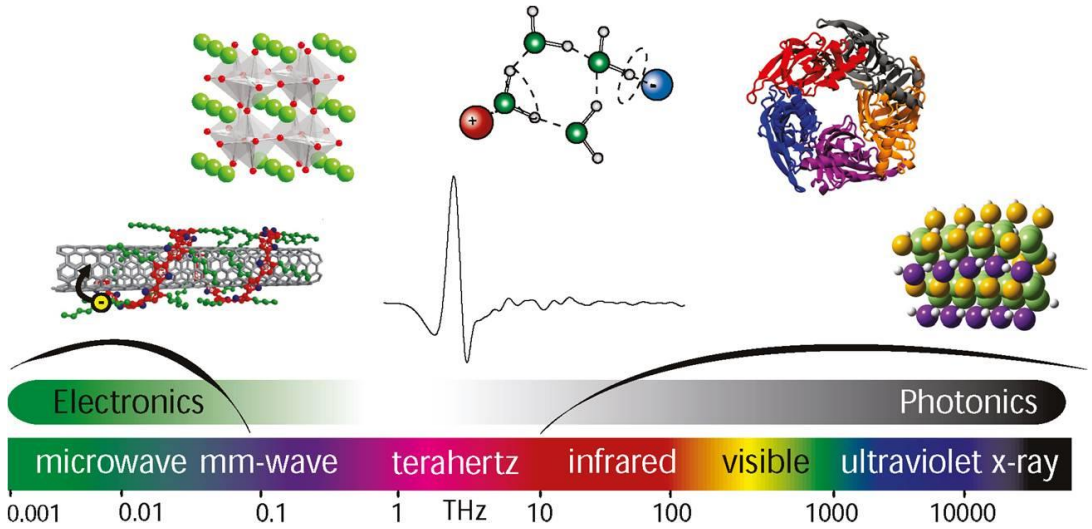

1 THz (10^{12} Hz) ~ 300 μm ~ 33 cm^{-1} ~ 1 ps ~ 4 meV ~ 47 K

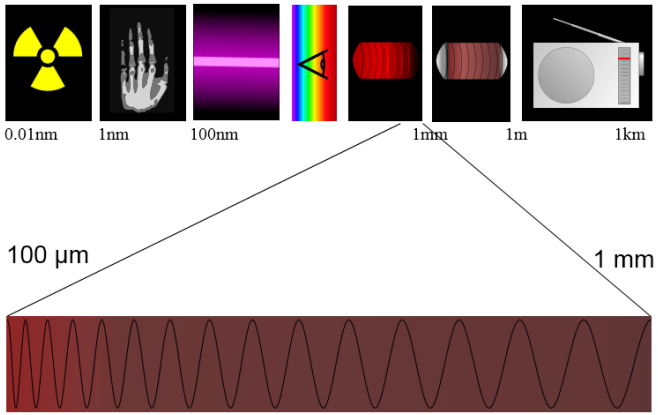

	Features of terahertz waves
Fingerprint	Rotational and vibrational modes of molecules
See-through	Dry and non-metallic materials: Paper, plastic, and textiles
Resolution	THz images provide lot of details for macroscopic objects
Safety	THz photons are non-ionizing; They are not hazardous for humans

J. B. Baxter et al., Anal. Chem. 83, 4342-4368 (2011)

Background

Department of Physics
Microwave Laboratory

Imaging Through Obscuration

650 GHz Active Image

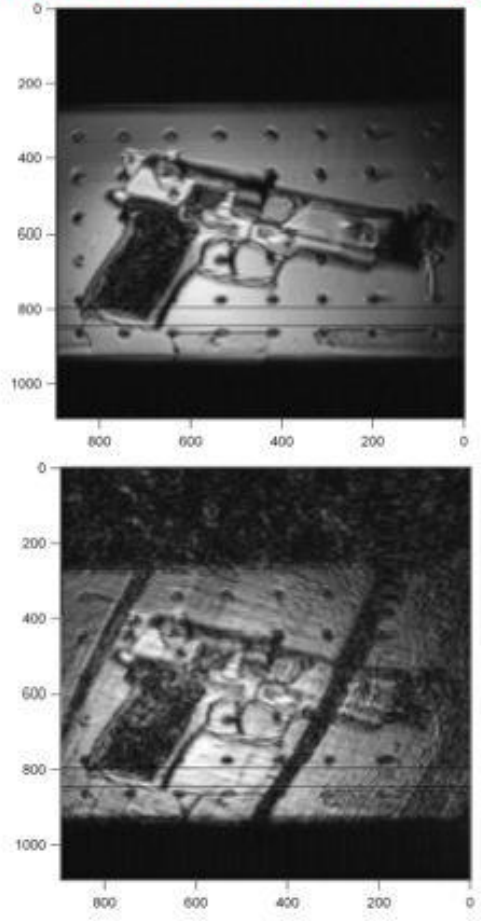

Optical Properties of Gr

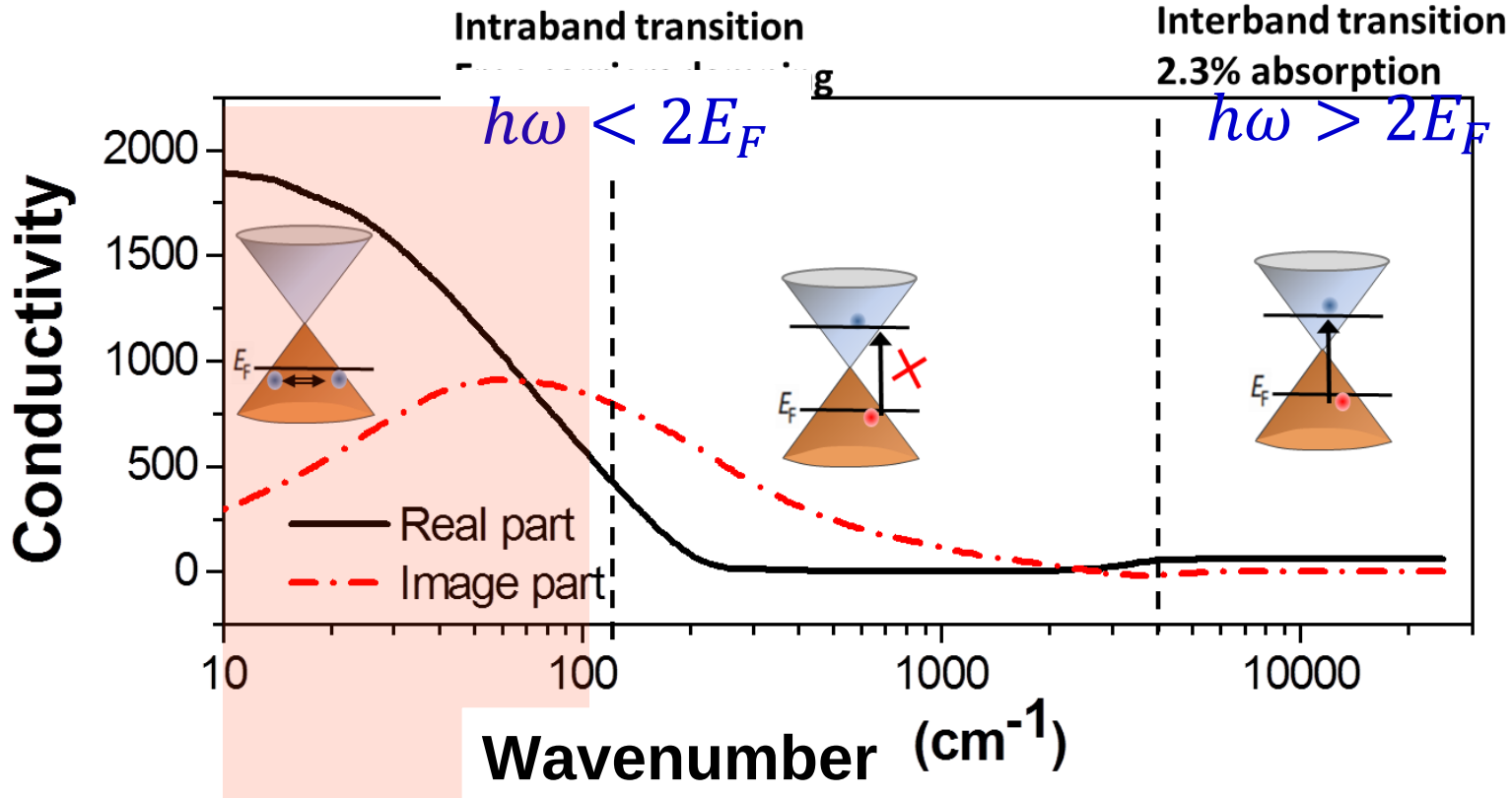

Classical THz Modulator

- **Intensity modulator**

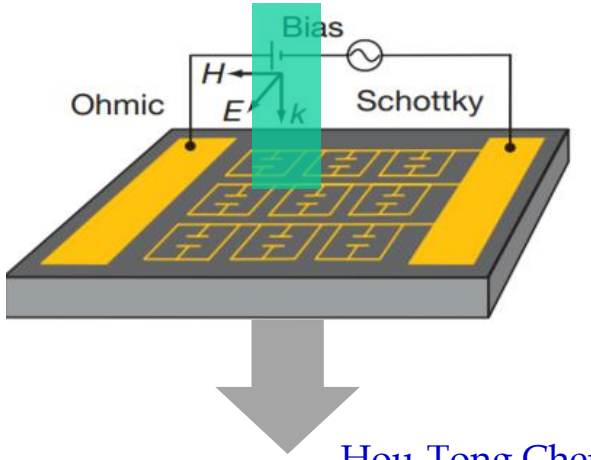

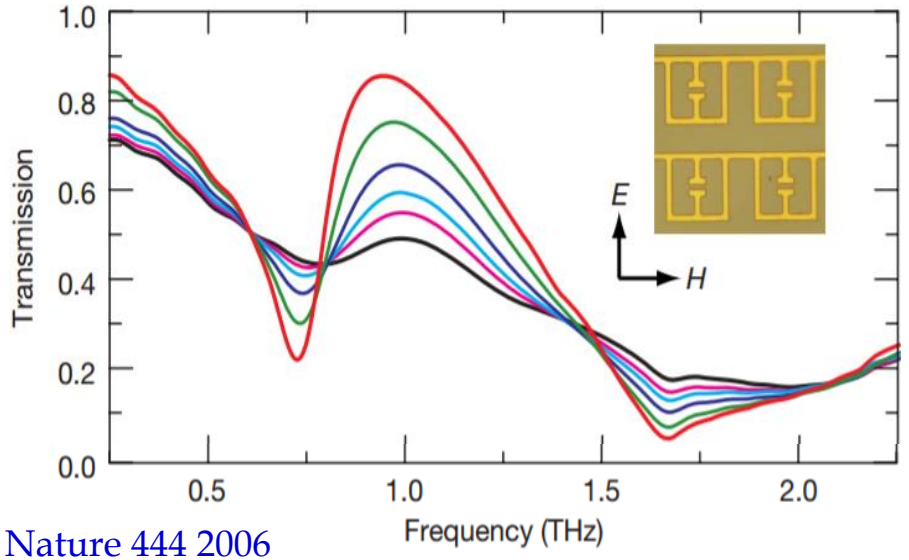

Hou-Tong Chen et al. Nature 444 2006

Modulation depth 50%, frequency limited

- **Phase modulator**

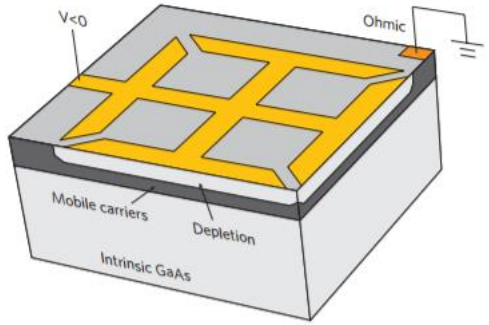

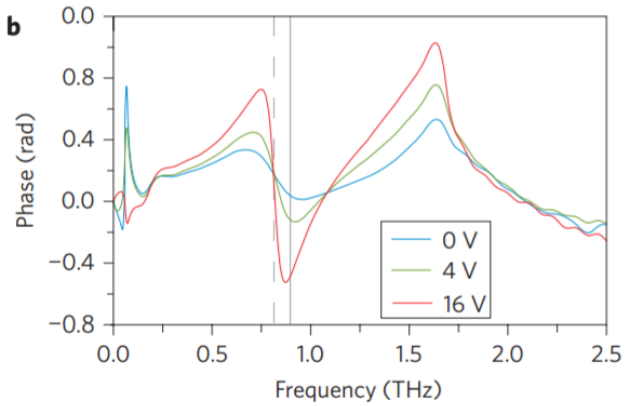

Hou-Tong Chen et al. nature photonic 3 2009

Modulation depth 35º, frequency limited

Gr Based THz Modulator

➢ Phase modulator

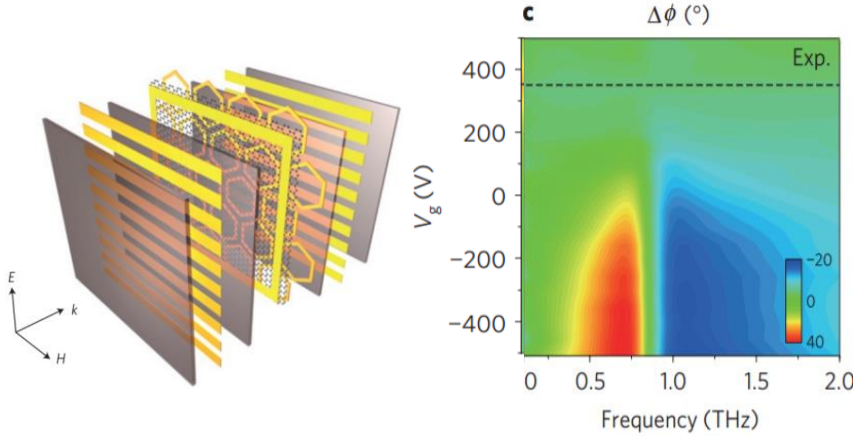

S H Lee et al. Nature materials 11 2012

graphene with metamaterials :

Gate control; 32º; Narrowband

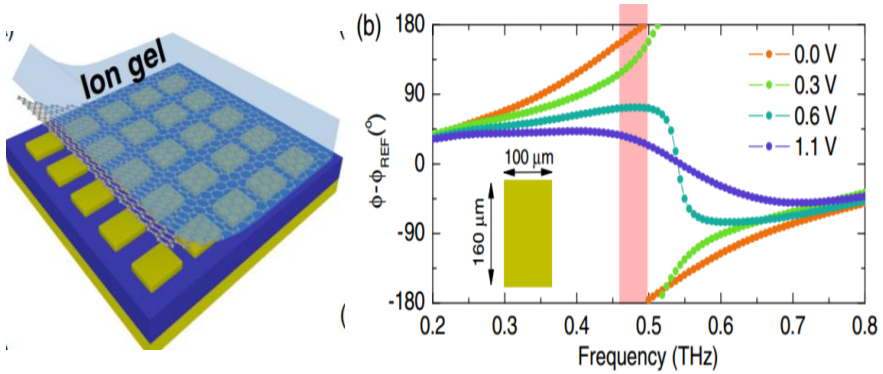

Ziqi Miao et al. Physical review X 5 2015

graphene with metamaterials & ion gel:

Gate control; 180º; Narrowband

Summary

With optical structure: high tenability, but narrow band

With optical pump: difficult integration

Motivation:

Through structure design to get modulator with high tunability, broadband and electric gate

FET THz Intensity Modulator

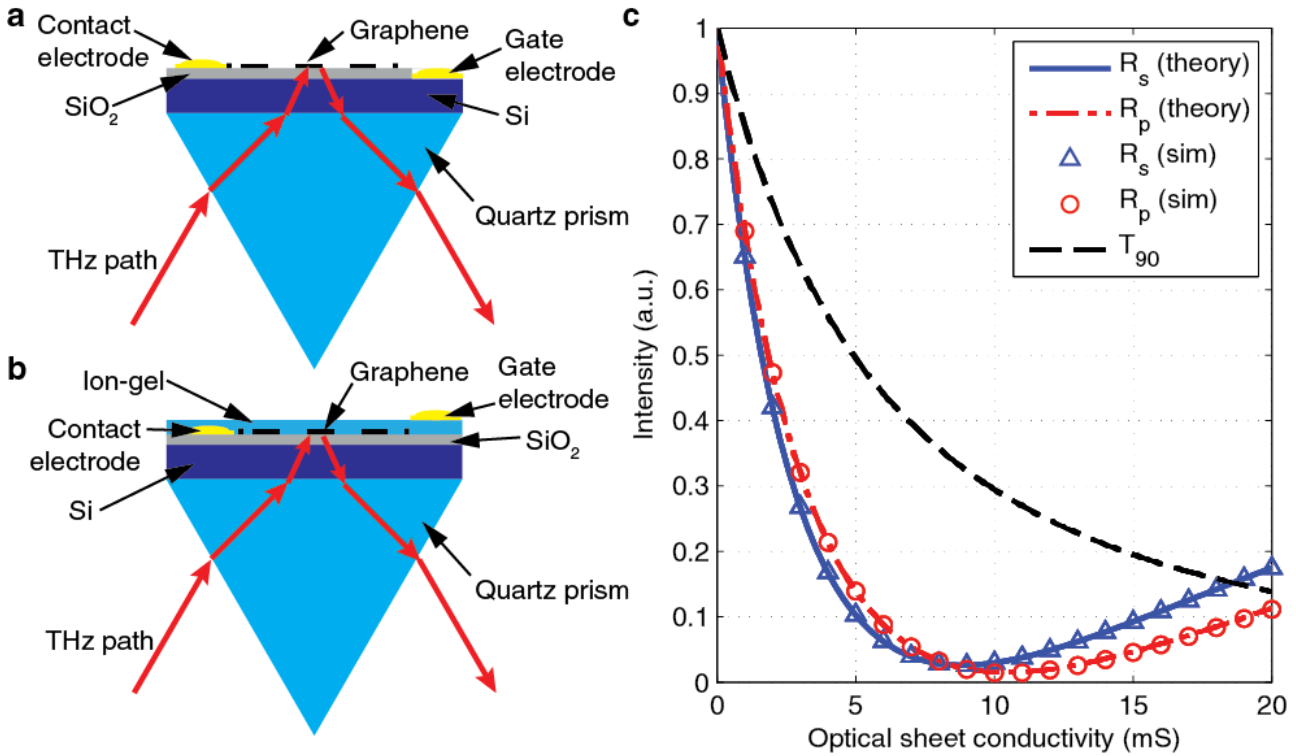

Figure: 2D schematic diagram of (a) our ordinary graphene on SiO_2/Si wafer FET device and (b) our ion-gel graphene device. Both devices are sitting on the top of an equilateral quartz prism. The red arrows in (a) and (b) highlight the path of the THz beam through this structure in the TIR orientation. (c) Theoretical and simulated reflected or transmitted intensity as a function of optical sheet conductivity. The solid blue and red dash-dot lines are the calculated reflectance in s- and p- polarization from an interface with a variable interface sheet conductivity. The incident angle from Si to air is set to 24.6° (this angle is a result of the particular geometry of our system). The squares and triangles represent the corresponding simulation results from COMSOL Multiphysics. The black dashed line represents the theoretical transmittance in normal incidence from air to Si with a conductive interface.

FET THz Intensity Modulator

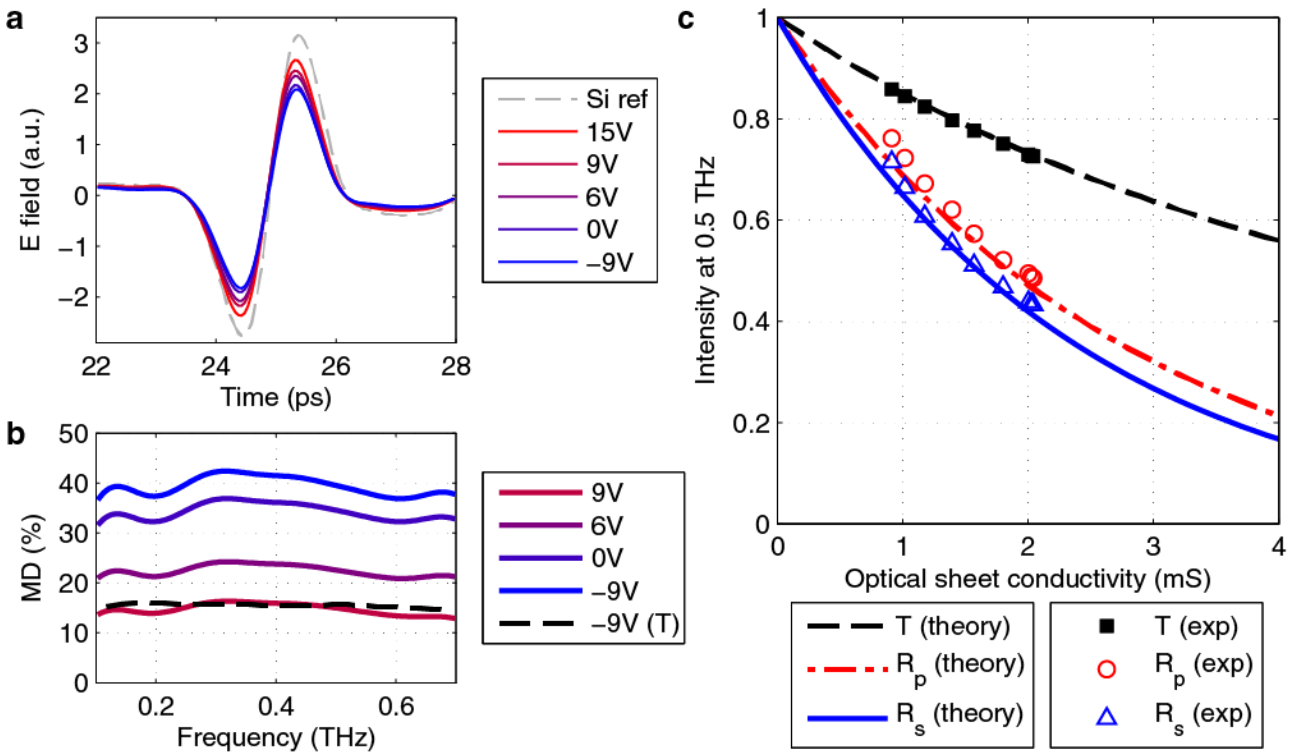

Figure: (a) Reflected time domain waveforms for a SiO_2/Si reference and 5 gate voltages and (b) the modulation depth (MD) for the device in *s*- polarization from 0.1-0.7 THz. The MD was defined relative to the 15 V measurement and the corresponding maximum MD in transmission is shown (black dashed line) for comparison. (c) Transmitted (black solid squares) or reflected *s*- (blue open triangles) and *p*- (red open circles) polarized intensity for 0.5 THz as a function of the measured optical sheet conductivity. The theoretical values are given for comparison (corresponding colored lines).

X. D. Liu, Z. F. Chen, JBX, Emma, Advanced Optical Materials (2017)

THz Phase Modulator

Metal Mirror Reflection (MR)

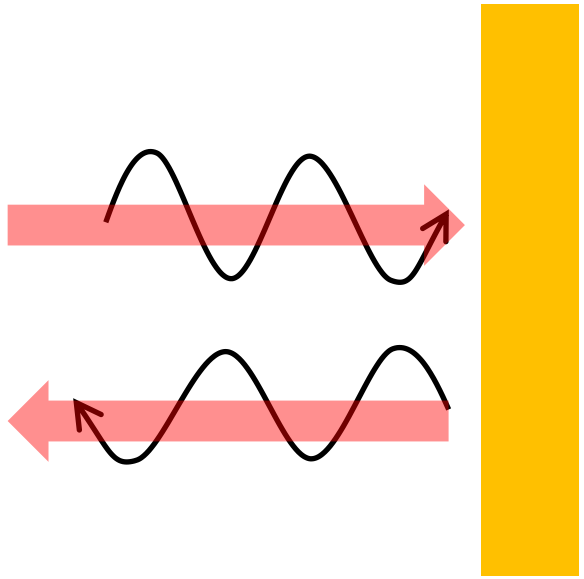

- phase shift is π

Transition

Internal Total Reflection (ITR)

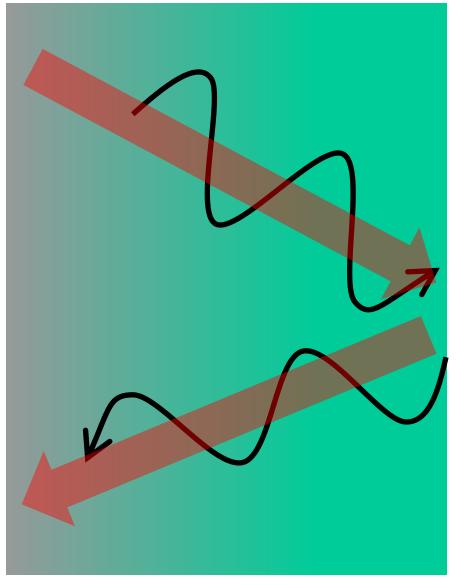

- phase shift is 0

- If a device can be changed from ITR to MR, highly tunable phase modulator can be achieved.

Physical Model

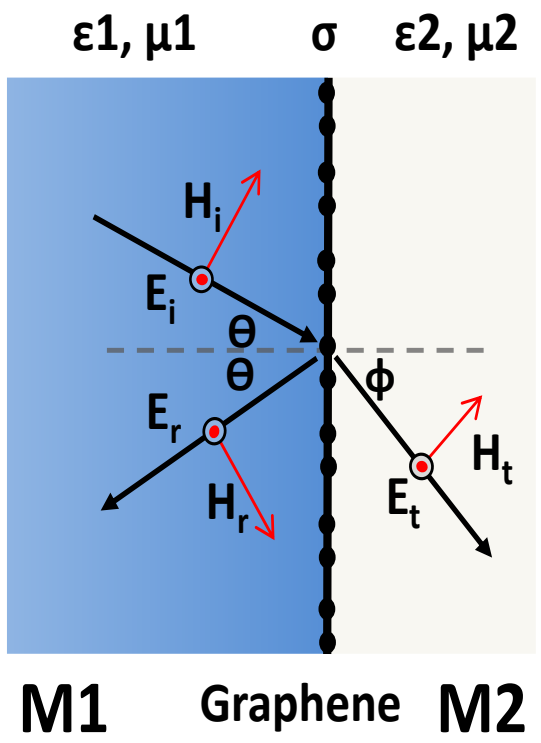

For *s*-polarization light, the boundary conditions:

$$H_i cos\theta_i - H_r cos\theta_i + H_t cos\Phi = -\sigma_s E_t,$$

$$E_t - (E_i - E_r) = 0$$

$$H = nE/Z_0$$

$$n_1 \sin\theta_i = n_2 \sin\Phi,$$ **Total reflection angel θ_i=30°**

$$r_s = \frac{n_1 \cos\theta_i - i \cdot \sqrt{n_1^2 \sin^2\theta_i - n_2^2} - Z_0\sigma_s}{n_1 \cos\theta_i + i \cdot \sqrt{n_1^2 \sin^2\theta_i - n_2^2} + Z_0\sigma_s}$$

r_s is a complex number, and depends on $n_1 cos\,\theta_i$ and $Z_0\sigma_s$

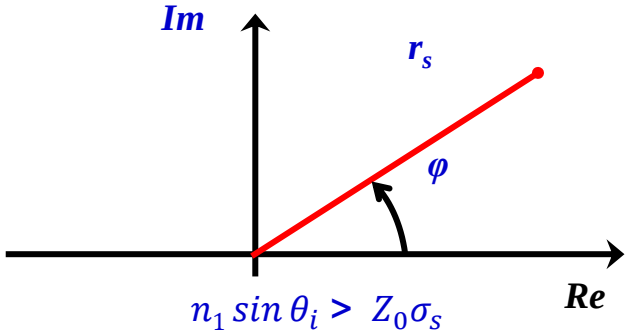

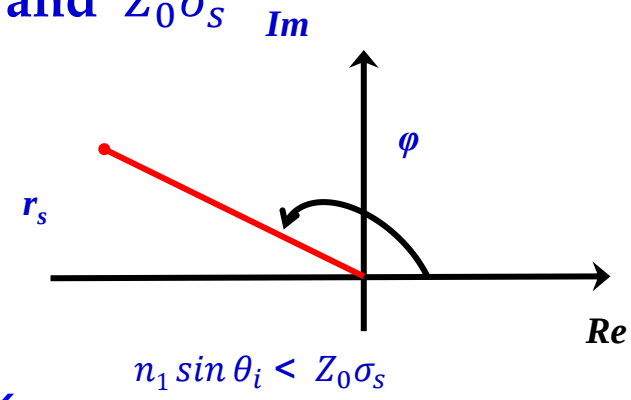

Device Configuration

(a)

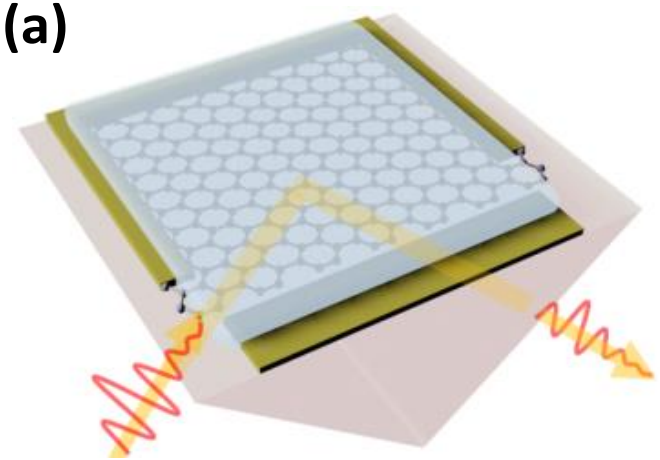

(b)

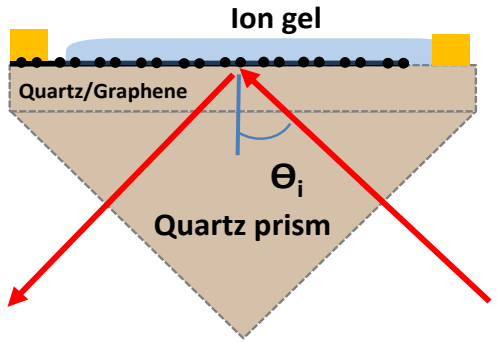

$\theta_i = 45^0$

(c)

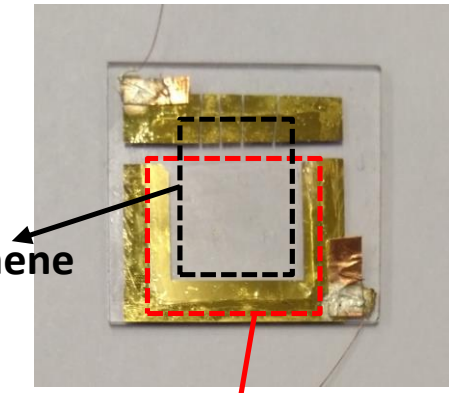

(d)

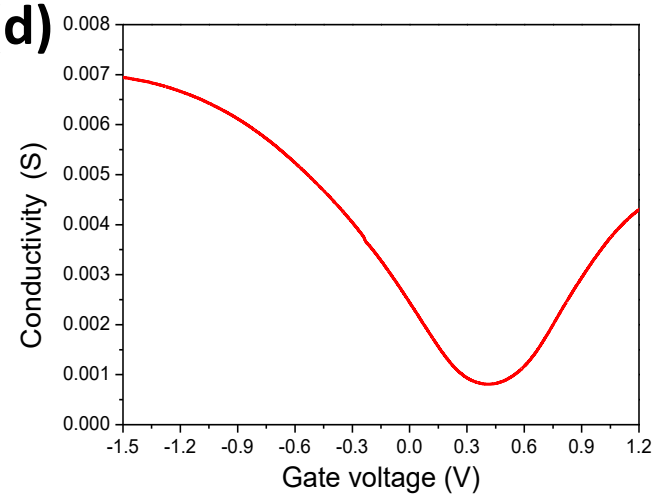

- Quartz prism for get ITR
- Ion-gel gate for highly tunable conductivity of graphene
- Side gate (no additional conductor is introduced into the reflection system)

Device Configuration

(a)

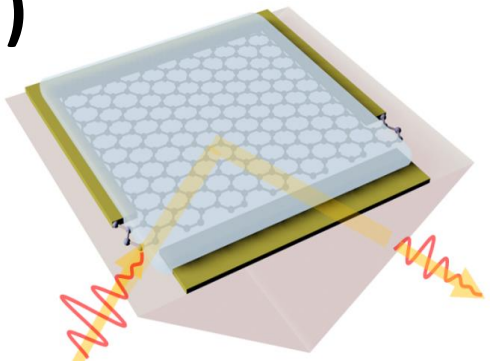

(c)

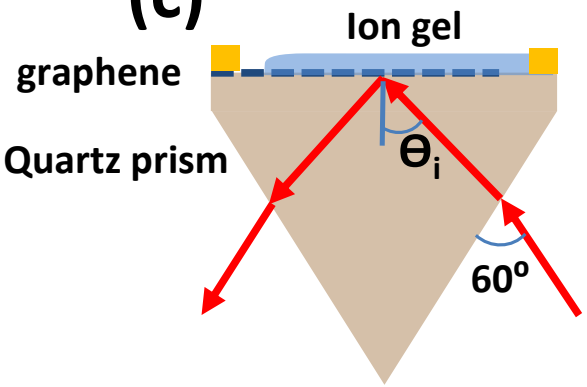

(b)

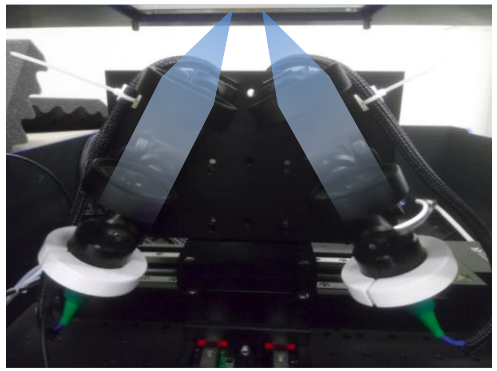

(d)

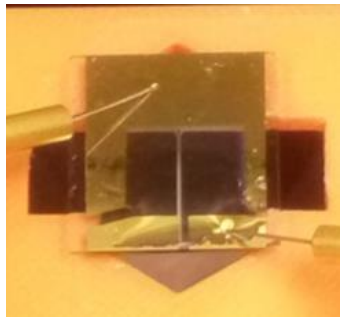

- Quartz prism for IRT
- ion-gel gate for high tunable conductivity of graphene
- ion-gel side gate (no additional conductor is introduced into the reflection system)

s-Polarization R in Quartz/Gr

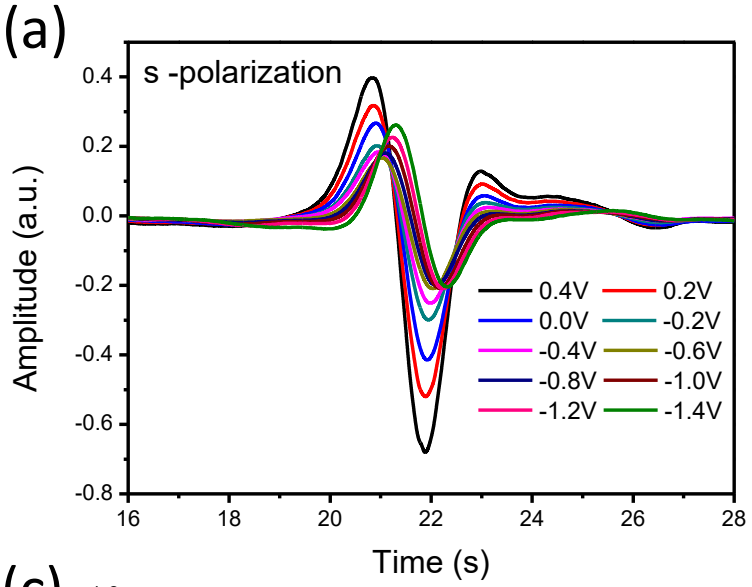

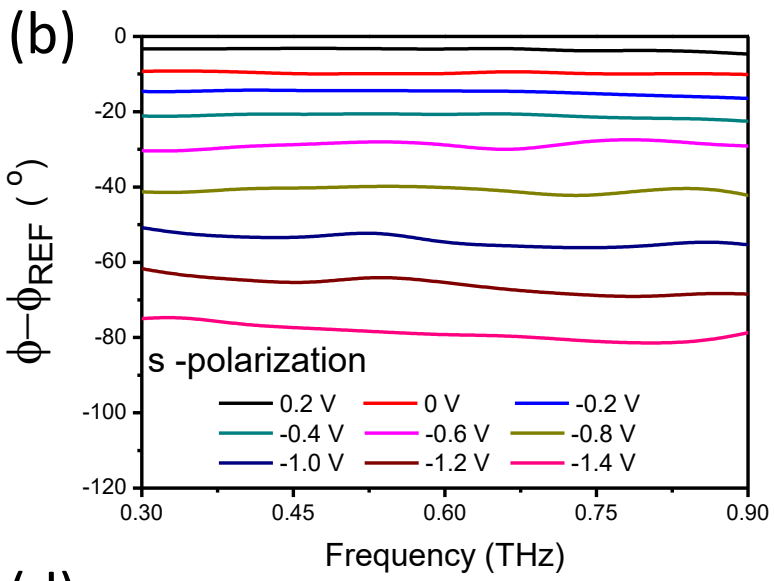

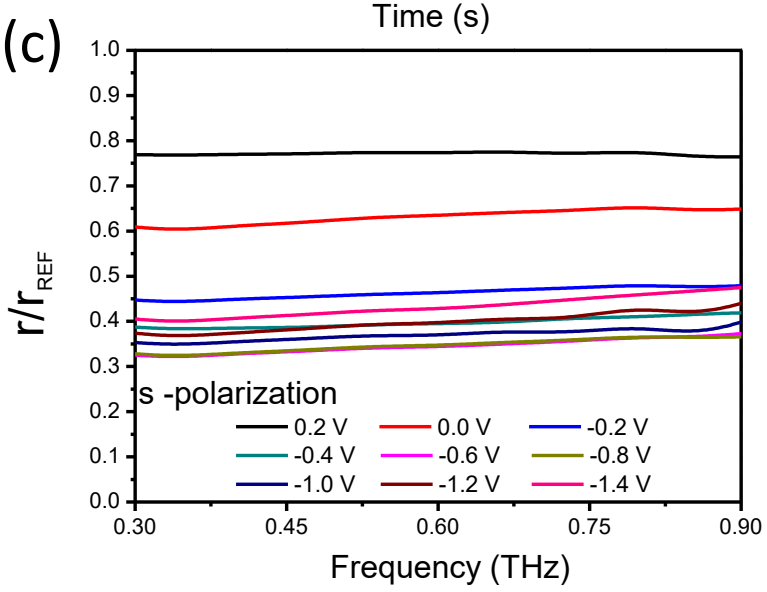

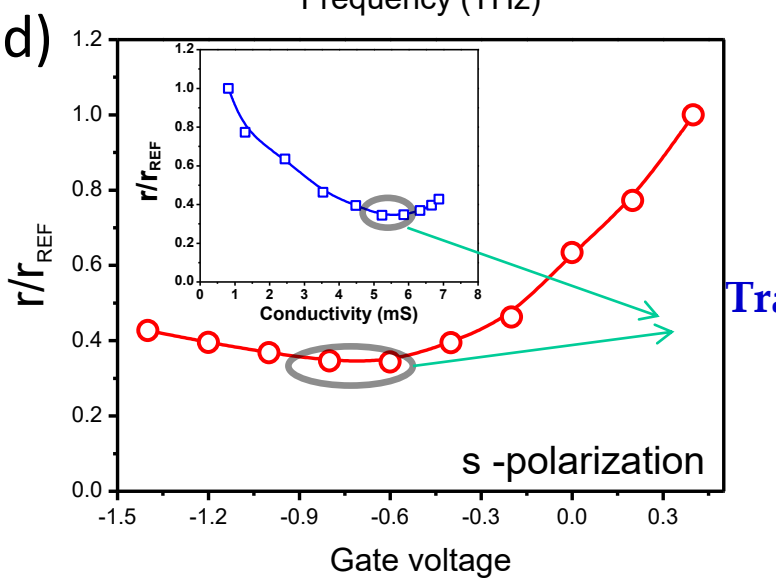

Phase can be tuned about 80^0 in the frequency region of 0.3 THz to 0.9 THz

Transition point

p-Polarization R in Quartz/Gr

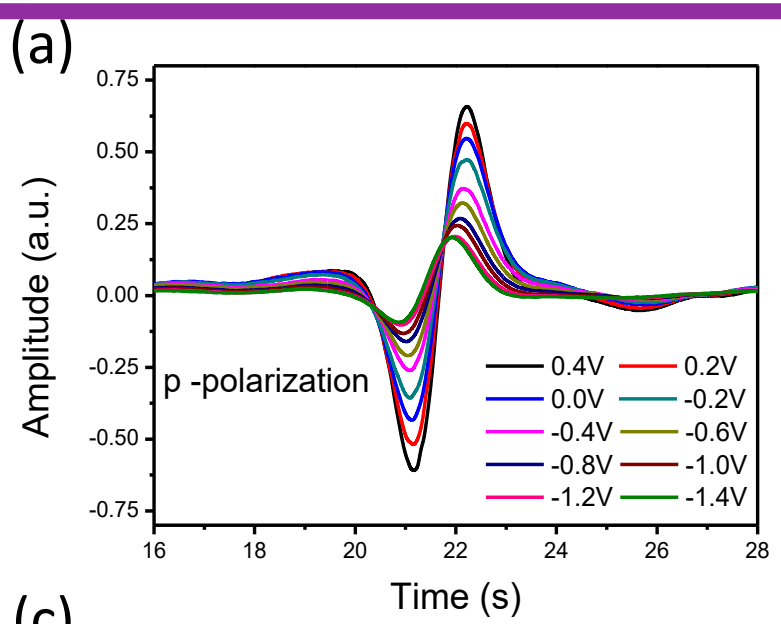

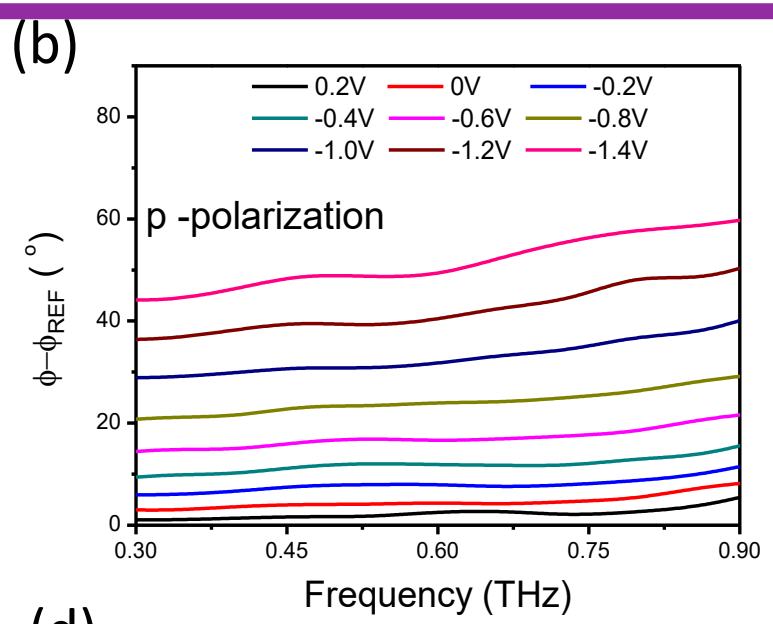

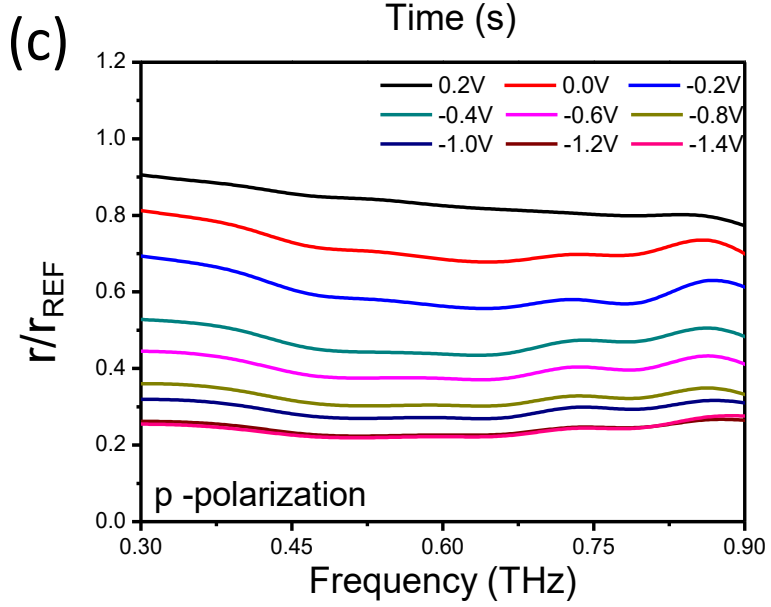

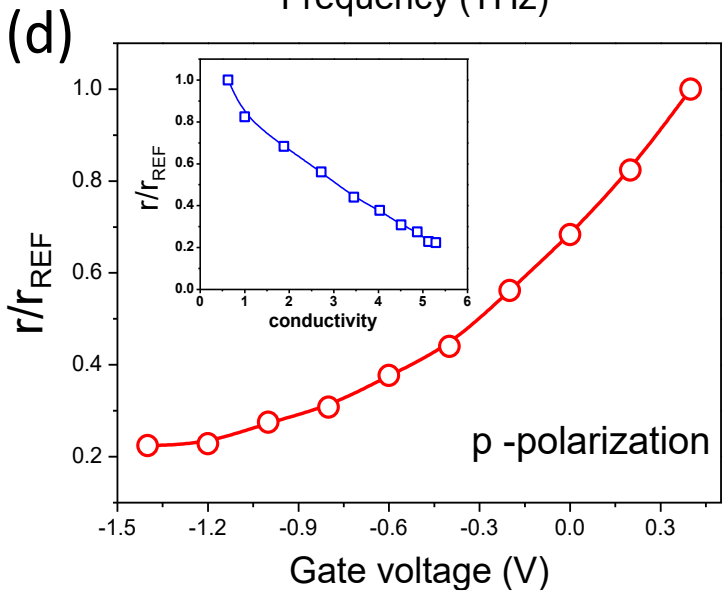

Phase can be tuned about 50° in the frequency region of 0.3 THz to 0.9 THz

Modulation under Brewster R

Physical Model

$$r_p = \frac{n\cos\theta_i - n_0\cos\Phi - Z_0\sigma_s\cos\theta_i\cos\Phi}{n\cos\Phi + n_0\cos\theta_i + Z_0\sigma_s\cos\theta_i\cos\Phi}$$

(a)

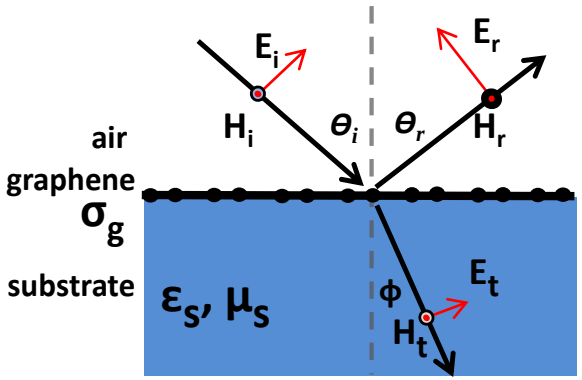

(b)

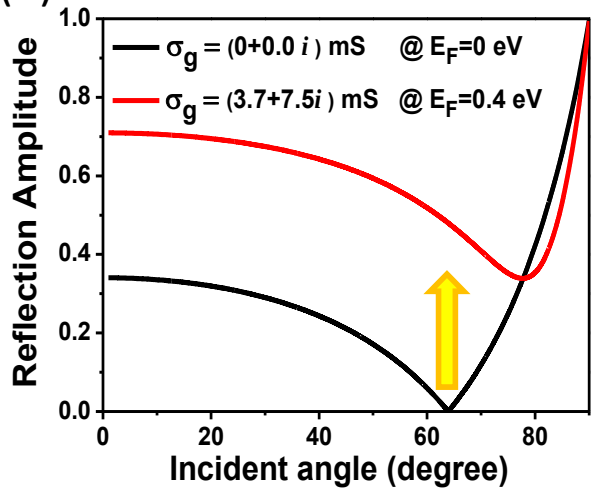

(c)

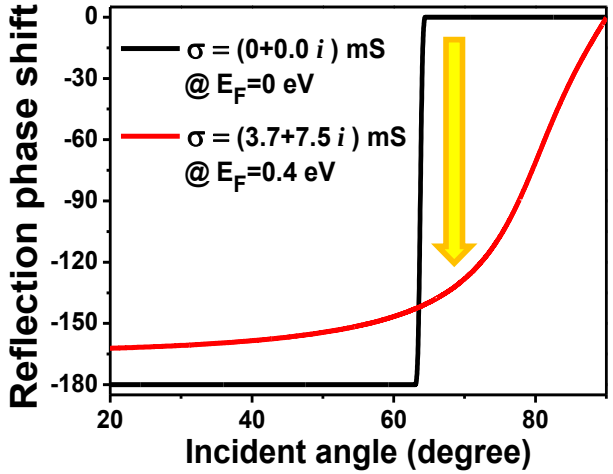

(d)

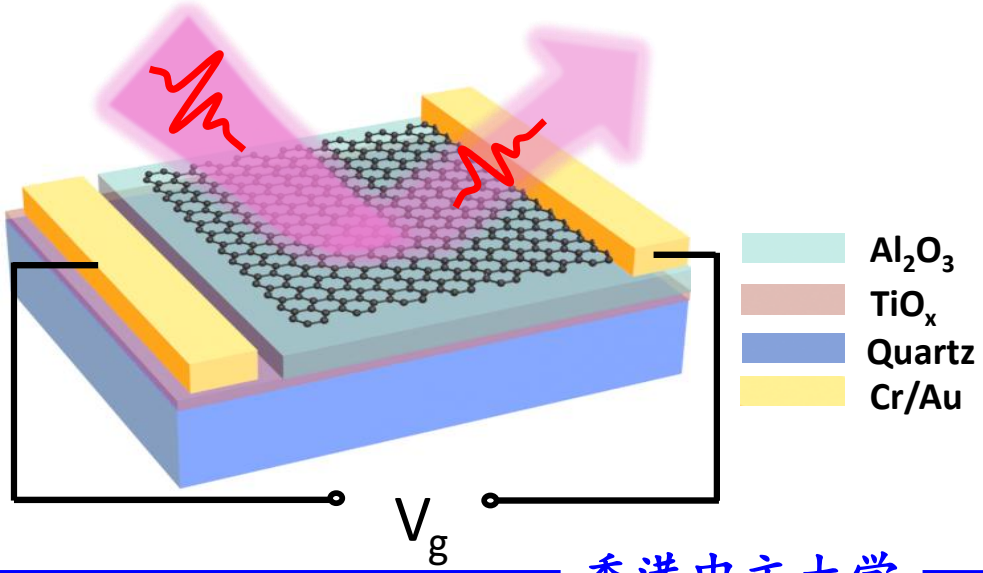

(e)

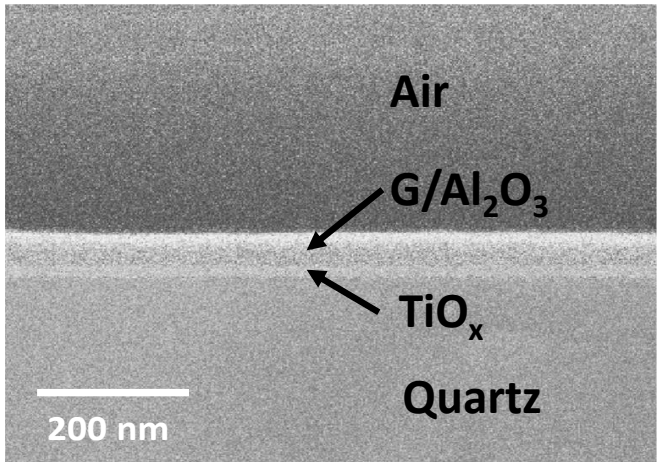

Z. F. Chen, JBX, et al., Nat. Comm. 2018

Modulation under Brewster R

Tunable conductivity of graphene verified by THz transmission spectrum

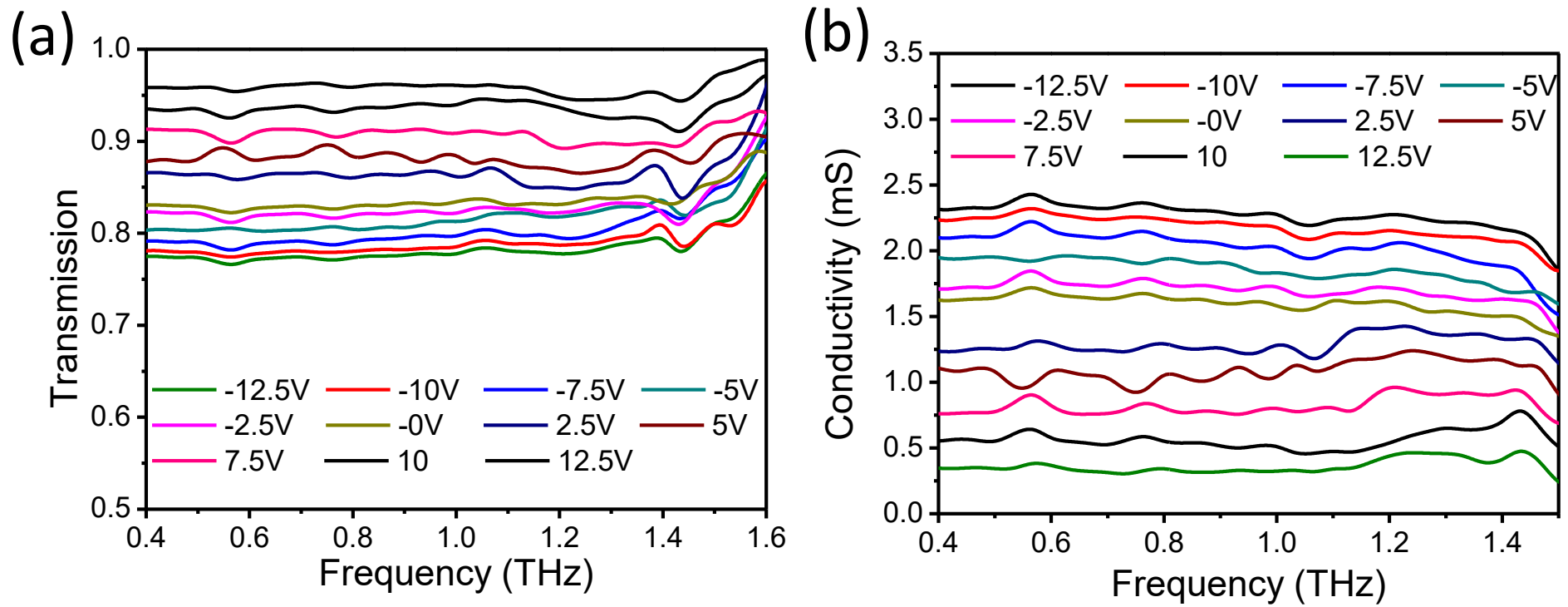

(a) and (b) transmission spectra and conductivity of graphene under different gate voltages

Z. F. Chen, JBX, et al., Nat. Comm. 2018

Angle Dependent Brewster R

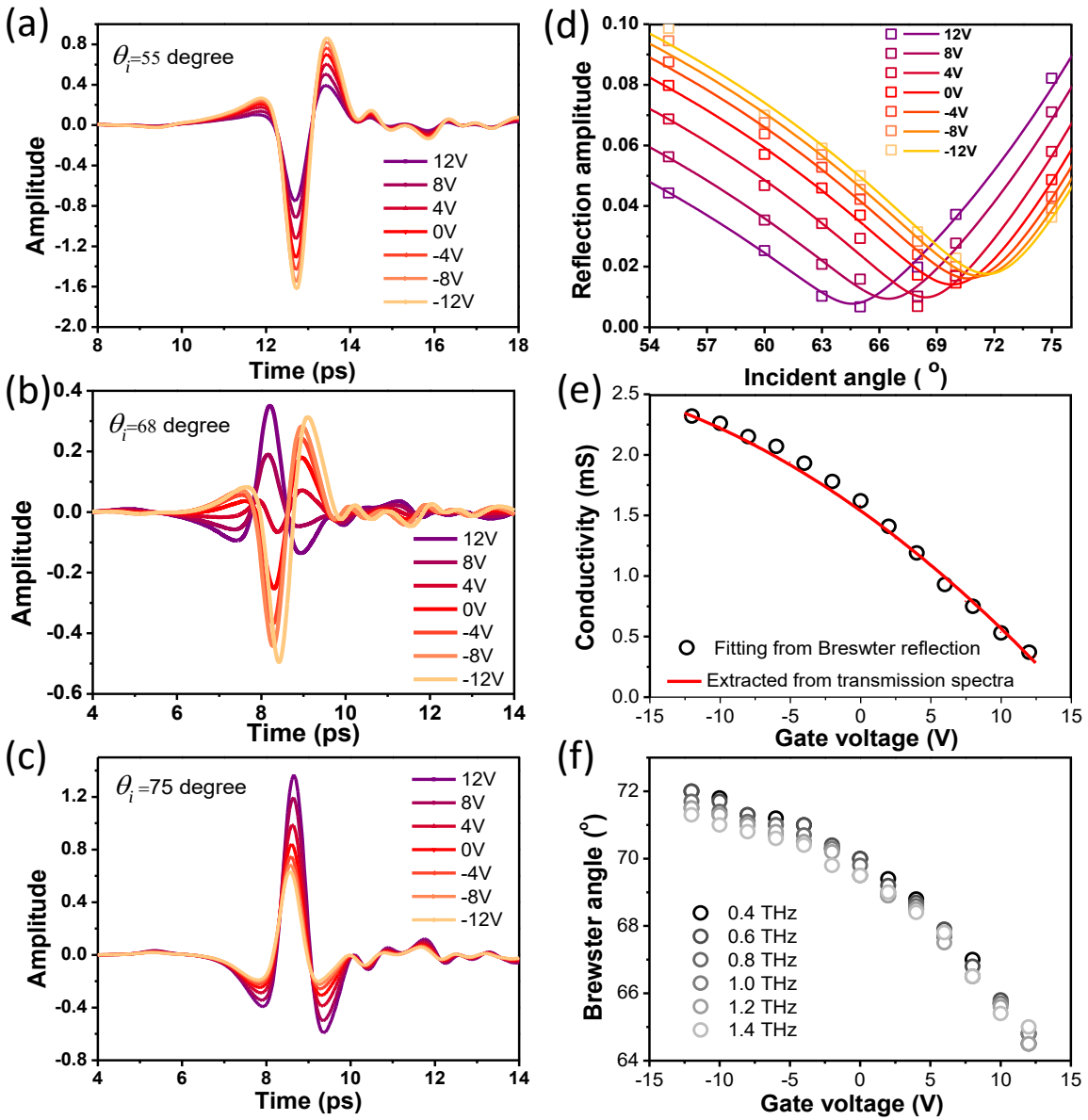

- θ_i =55º, pulse shape asymmetric 'M' (figure a)
- θ_i =68º, pulse shape asymmetric 'M' to 'W' (figure b)
- θ_i =75º, pulse shape asymmetric 'W' (figure c)

- Using the reflection result of 0.8 THz to fit Brewster angle model (figure d)
- The conductivity fitted from Brewster model is matched with that from transmission spectrum (figure e)
- Brewster angle between 65º to 73º (figure f)

Z. F. Chen, JBX, et al., Nat. Comm. 2018

THz Circular Dichroism

enabled by kirigami polarization modulators

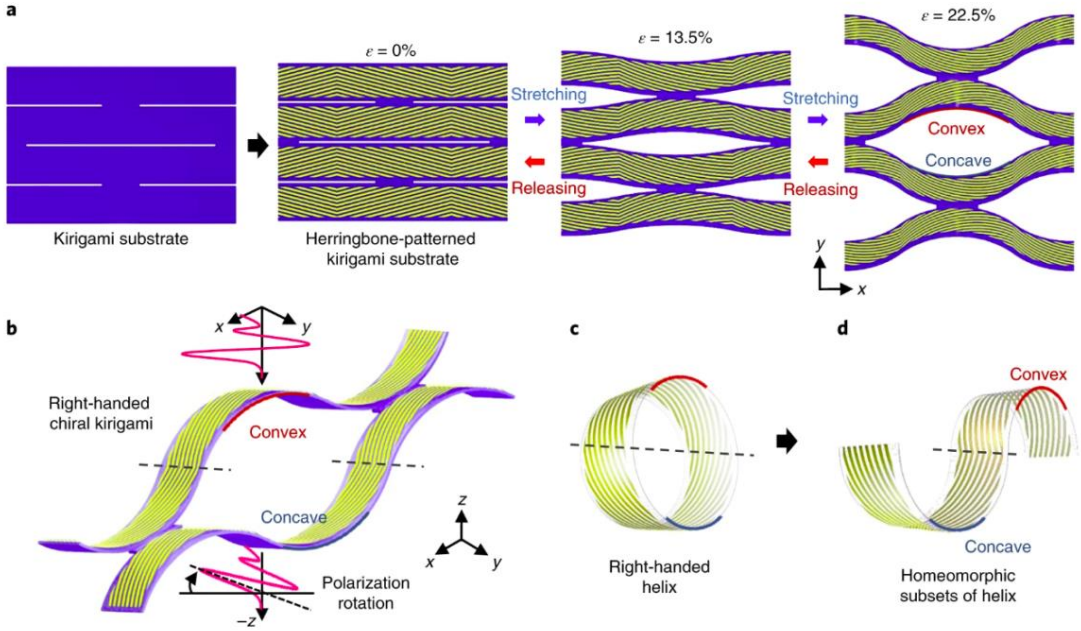

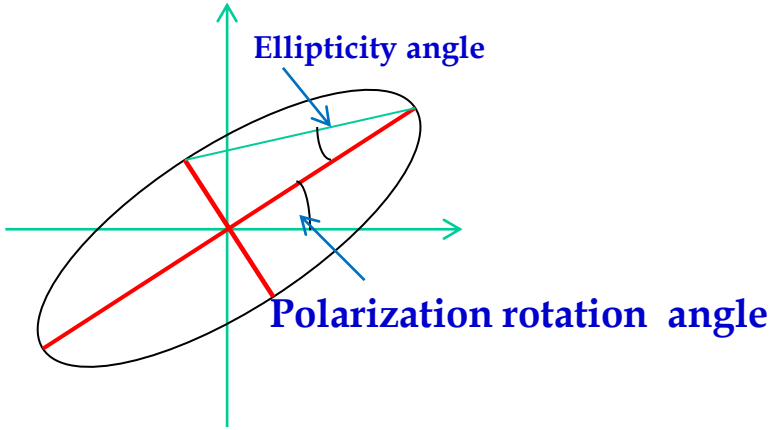

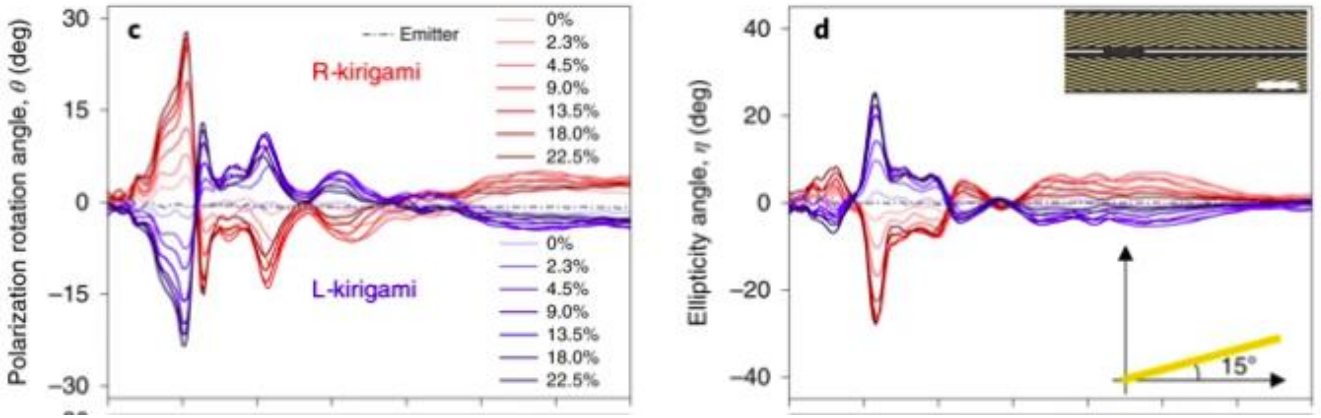

Won Jin Choi, Nature Material, https://doi.org/10.1038/s41563-019-0404-6

Polarization Modulation by Meta

Photo-induced handedness switching in terahertz chiral metamolecules

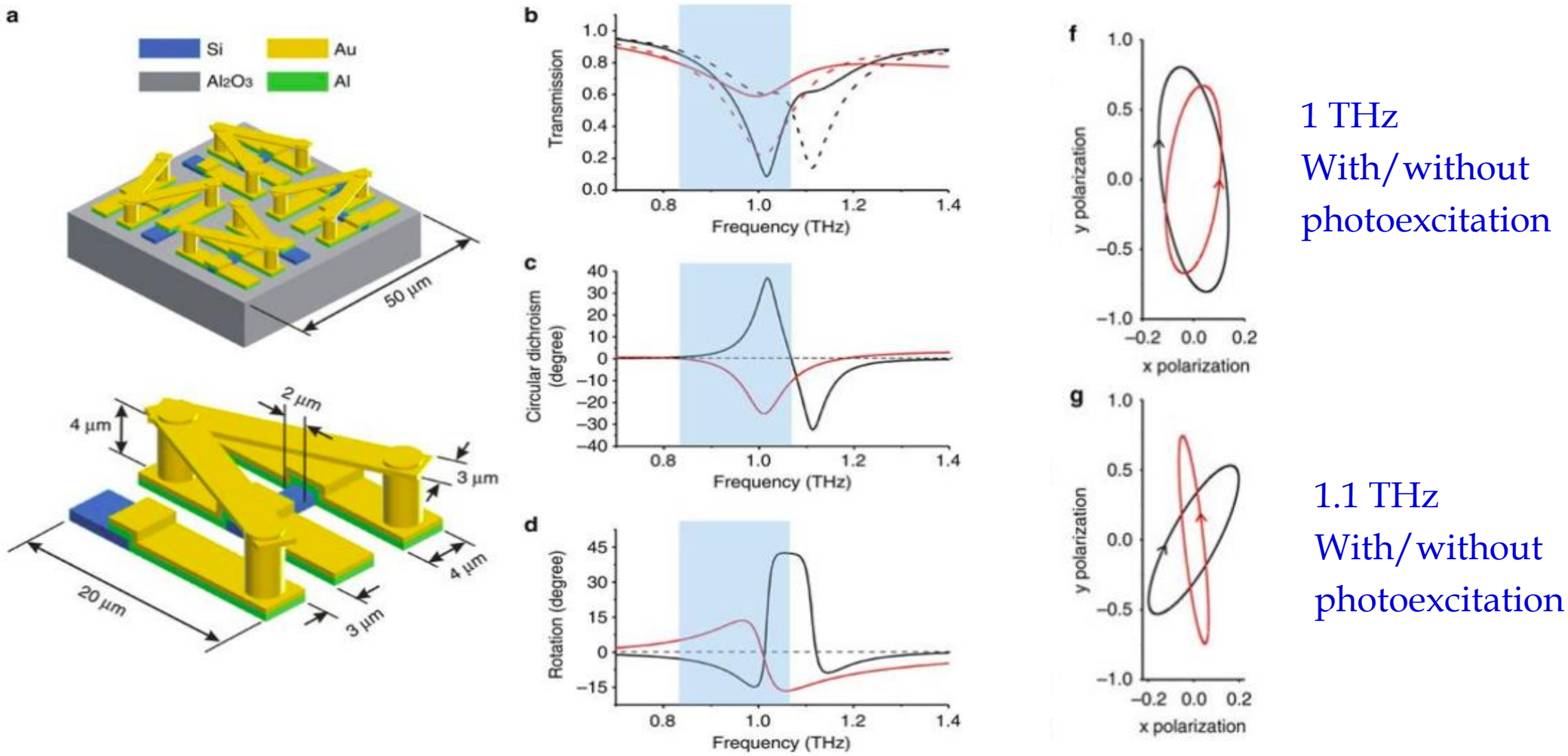

1 THz
With/without
photoexcitation

1.1 THz
With/without
photoexcitation

Shuang Zhang, et al Nature Communications volume3, Article number: 942 (2012)

s-Polarization THz Wave

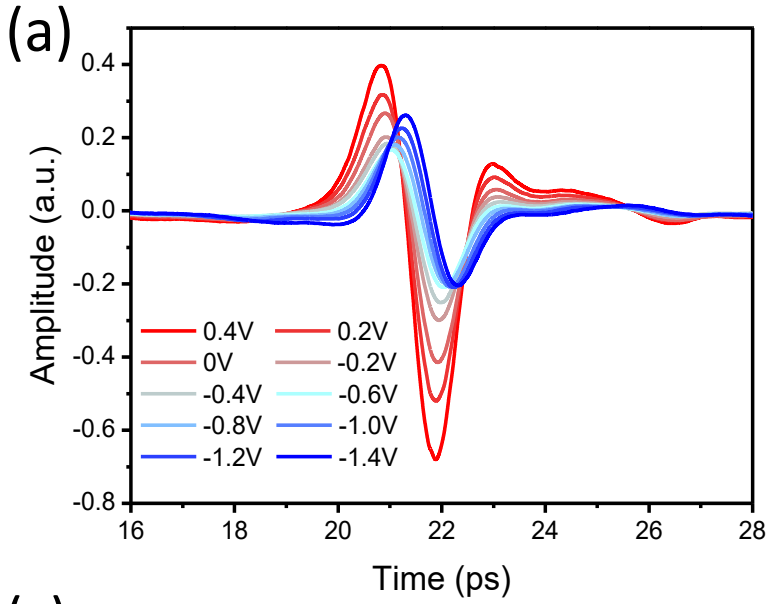

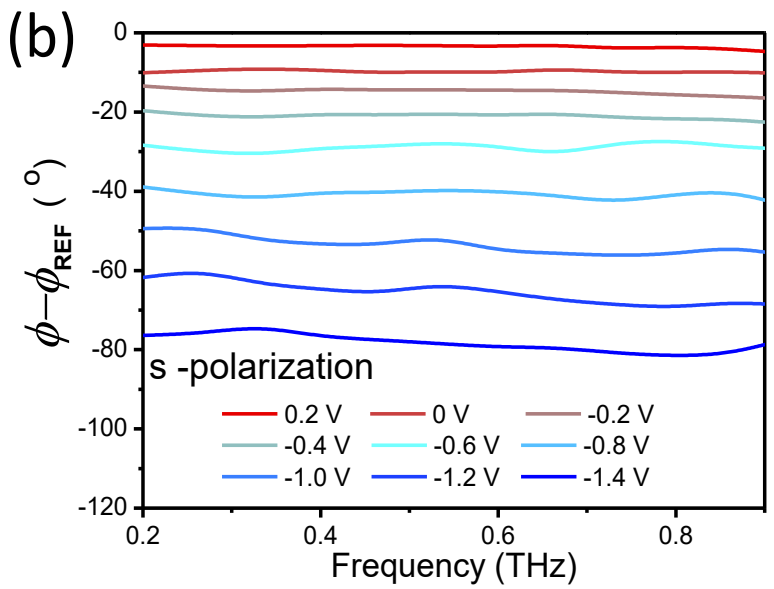

Phase modulation about 80°, broadband & spectrum flat

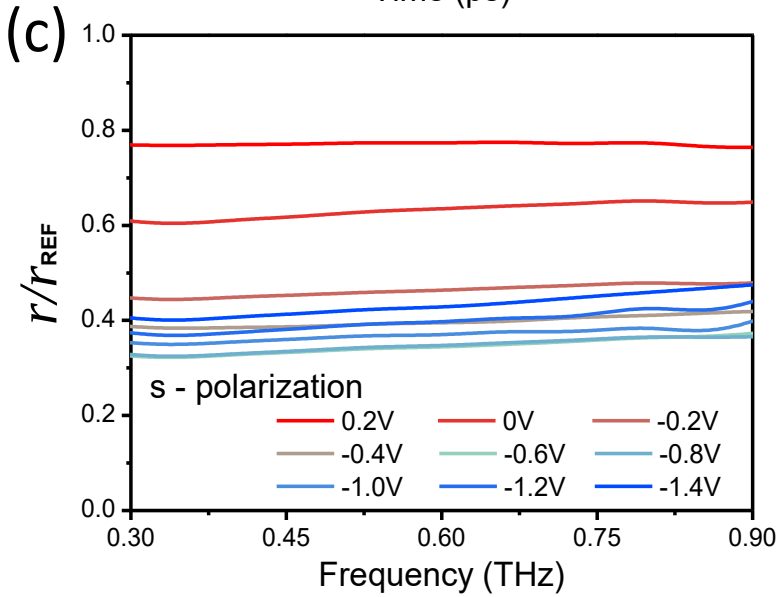

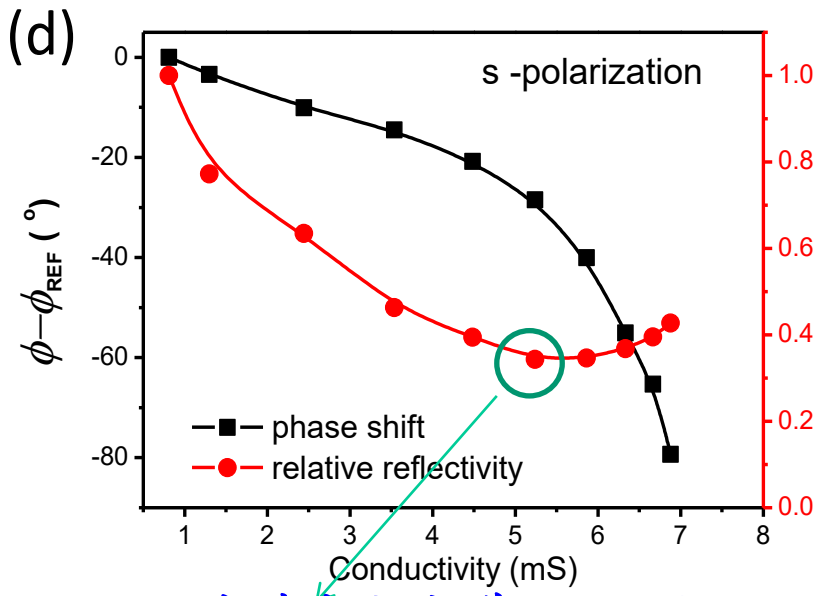

Transition point: from ITR to MMR

p-Polarization THz Wave

Phase modulation around 50°

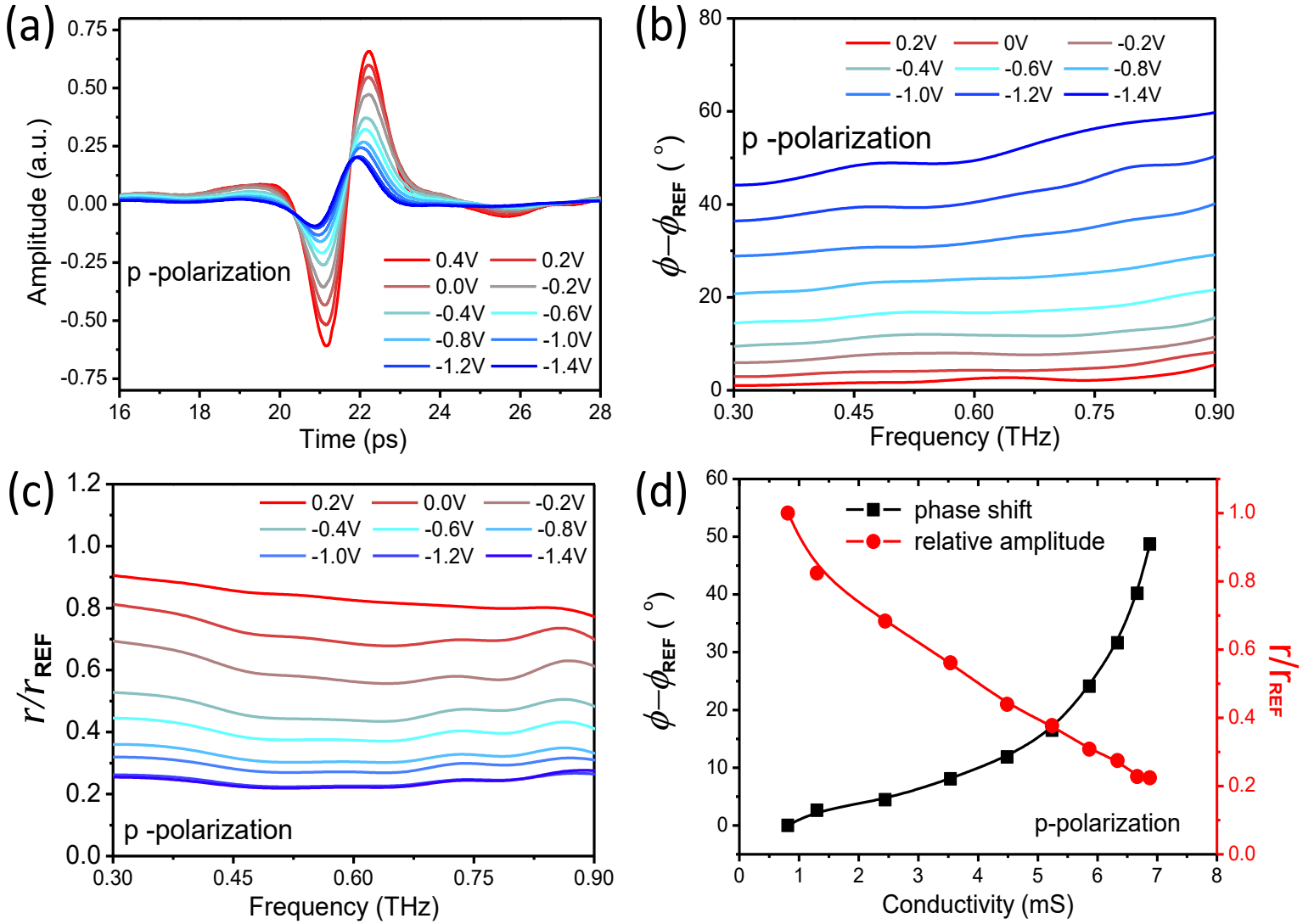

Polarization Modulation

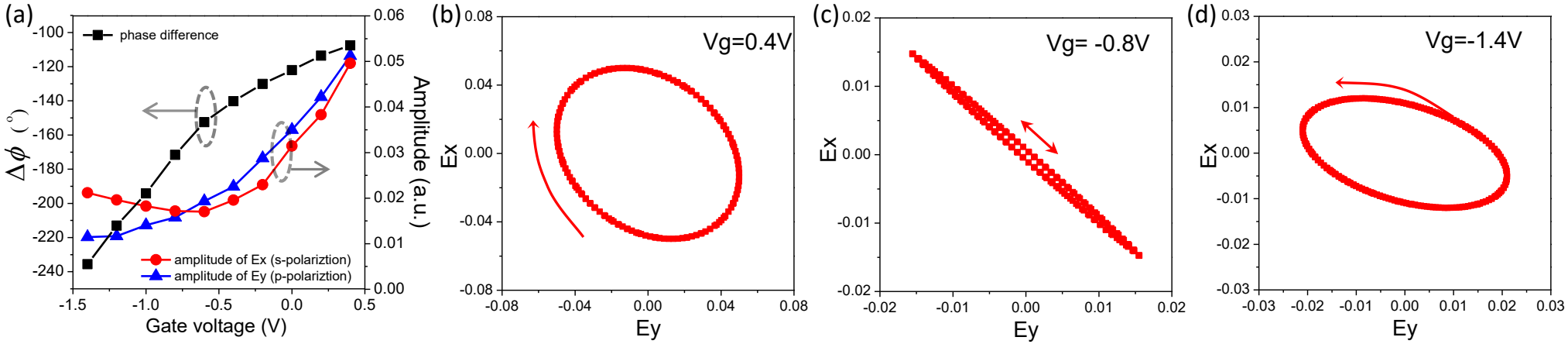

$$E(r,t) = \begin{bmatrix} E_x \\ E_y \end{bmatrix} = \begin{bmatrix} A_x e^{i(\omega t+\phi_x)} \\ A_y e^{i(\omega t+\phi_y)} \end{bmatrix}$$

$$\left(\frac{E_x}{A_x}\right)^2 + \left(\frac{E_y}{A_y}\right)^2 - 2cos\Delta\phi \frac{E_x E_y}{A_x A_y} = sin^2\Delta\phi \,.$$

Figure (a) the phase difference $\Delta\phi$ and amplitude of *s-/p-* polarization at the frequency of 0.6 THz as function of gate voltage. (b), (c) and (d) the electric-field trajectory at the gate voltage of 0.4V, -0.8V and -1.4V, respectively.

Z. F. Chen, JBX*, et al., ACS Photonics 9, 3633–3641 (2022)

XD Liu, DS Yu, DS; YW Sun, JBX*, et al., ACS Photonics 11, 2595-2603 (2024)

Waveform Shaping in *t* Domain

0.4 V

-0.8 V

-1.4 V

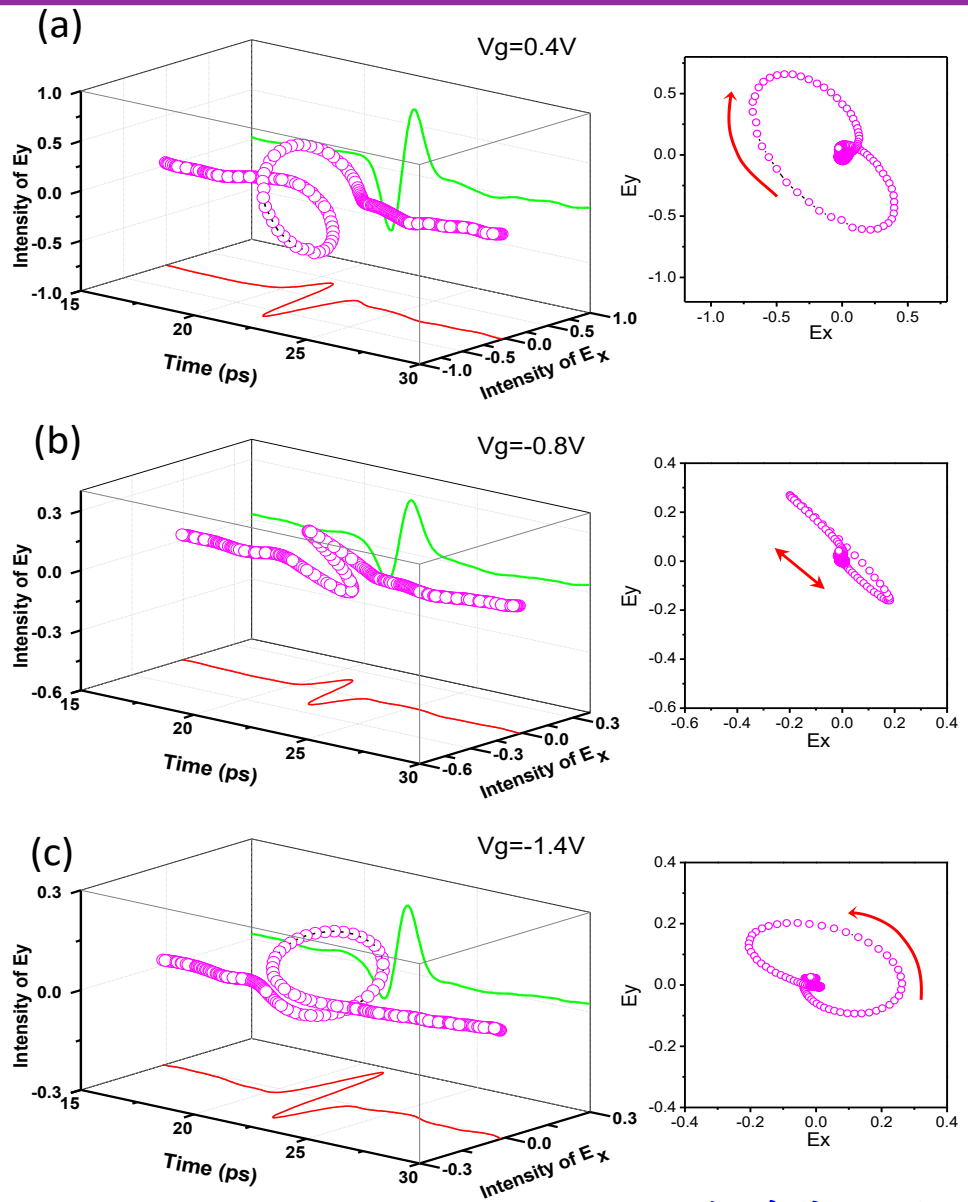

Experimentally obtained electric-field trajectories of the terahertz polarization-shaped waveform (left) and the projections on the E_x-E_y plane (right) under gate voltages of (a), 0.4 V, (b) -0.8V and (c) -1.4V.

Z. F. Chen, JBX*, et al., ACS Photonics 9, 3633–3641 (2022)

Optoelectronic Applications

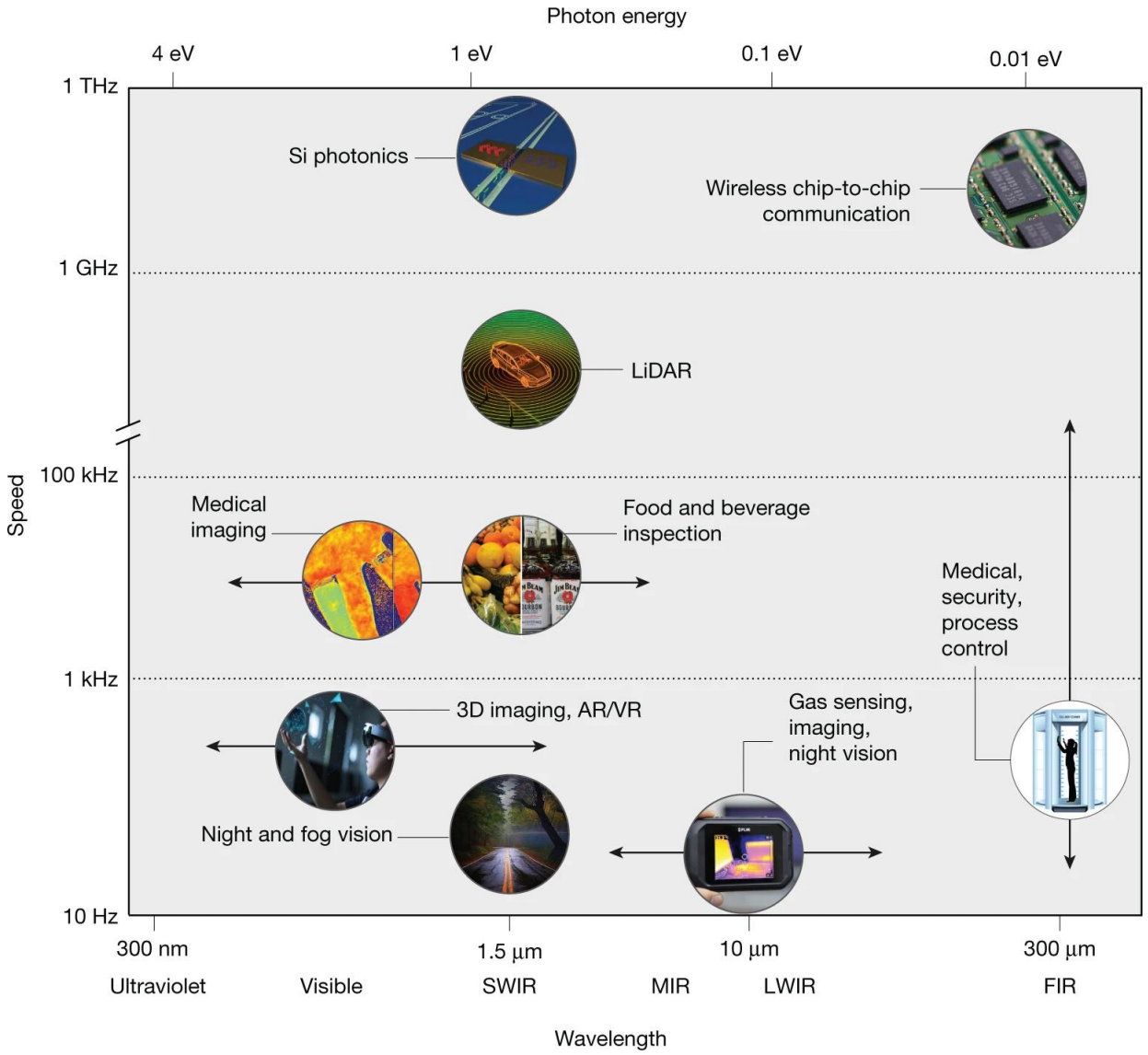

Technology areas of 2DM-based integrated opto-electronics, mapped in terms of required speed and operational wavelength range (lower x axis; the upper x axis gives the corresponding photon energy).

Deji Akinwande, & Frank H. L. Koppens, et al., Nature **573,** 507–518 (2019)

Integrated Gr & 2DPhotodevices

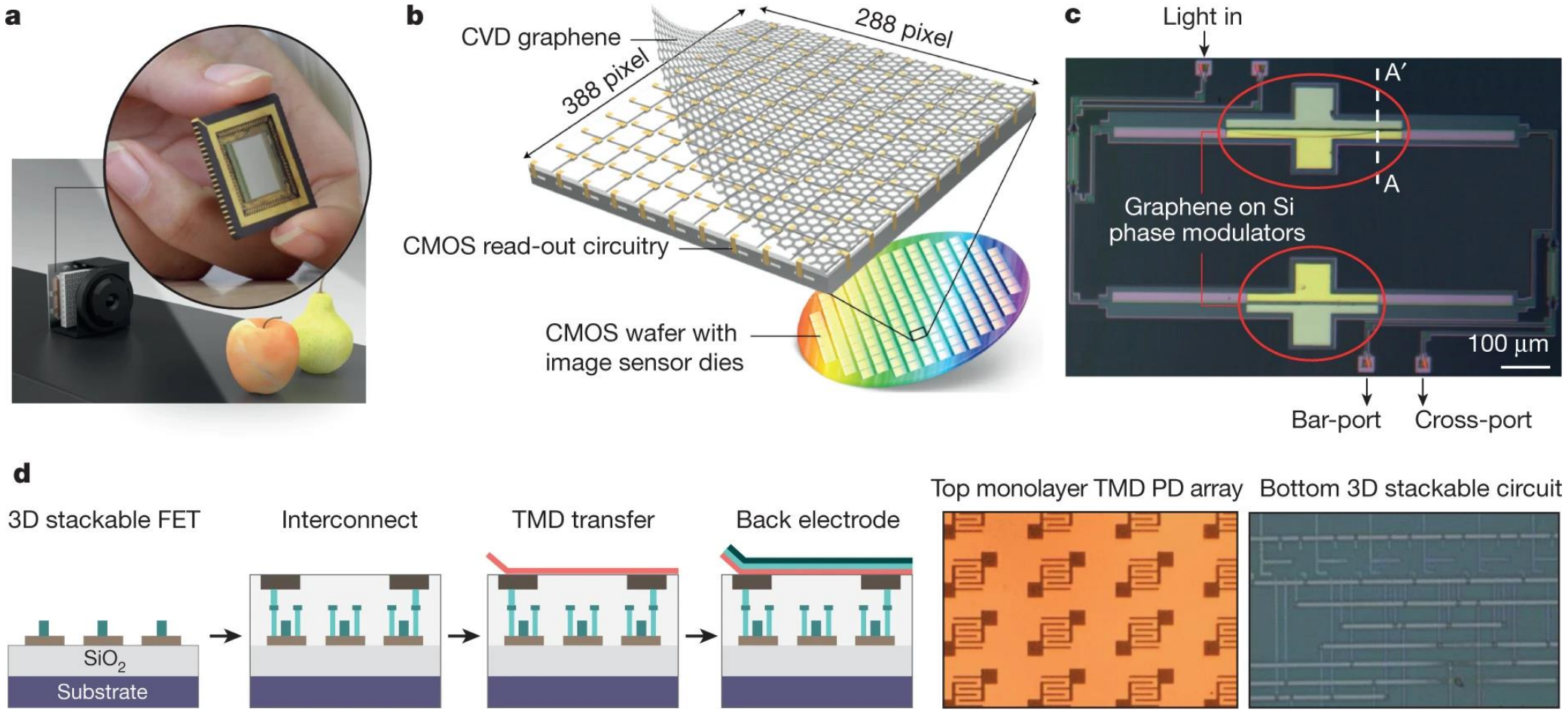

A broadband camera setup based on CMOS-integrated graphene–quantum dot photodetectors.

Deji Akinwande, Cedric Huyghebaert, Ching-Hua Wang, Martha I. Serna, Stijn Goossens, Lain-Jong Li, H.-S. Philip Wong & Frank H. L. Koppens, Nature **573,** 507–518 (2019)

Ultrafast Machine Vision with 2DM Neural Network Image Sensors

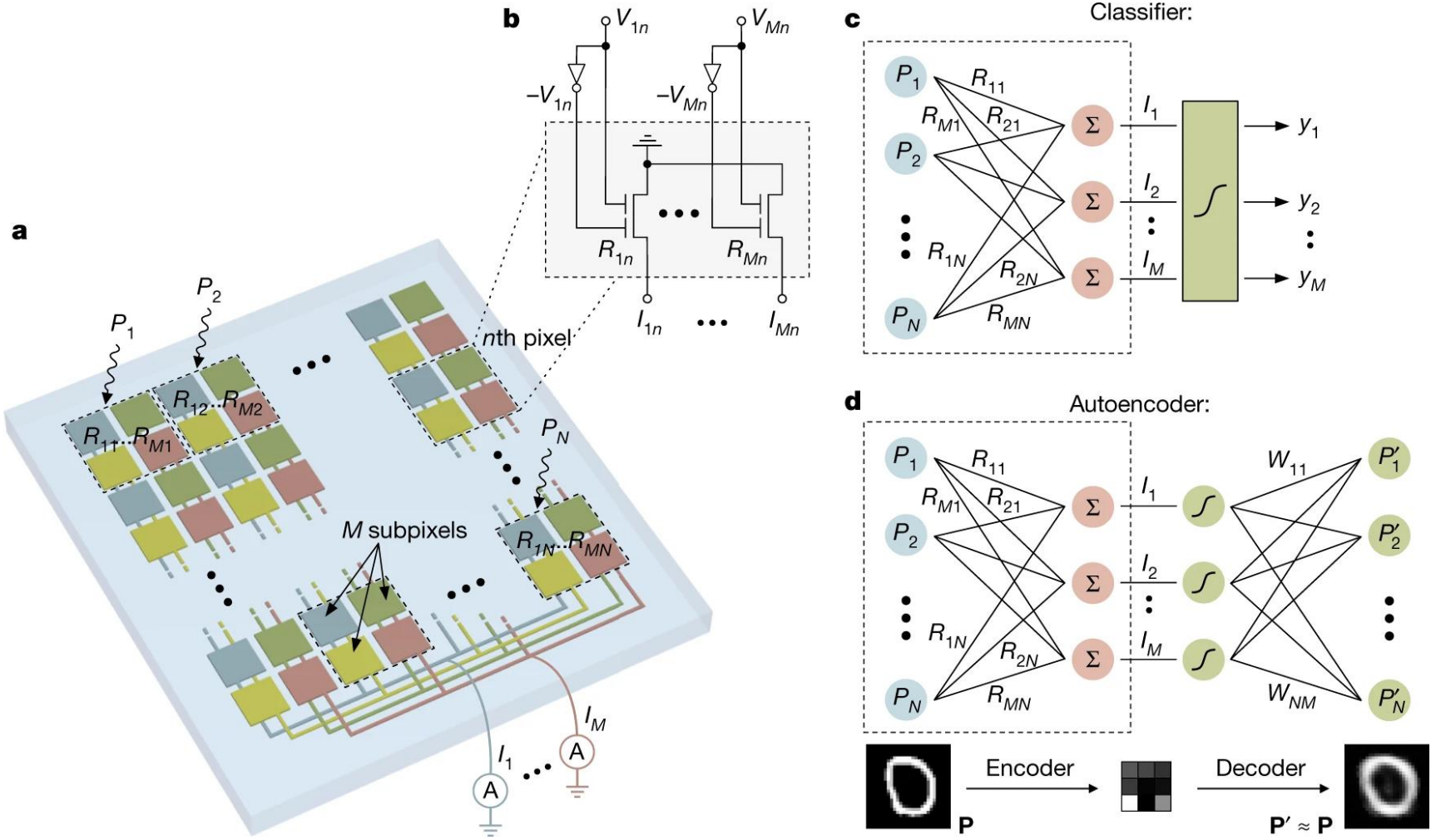

Imaging ANN Photodiode Array

Lukas Mennel, & Thomas Mueller, et al., Nature 579, 62–66 (2020)

Schematic Visualization of Tech. Roadmap for 2DMs in CMOS

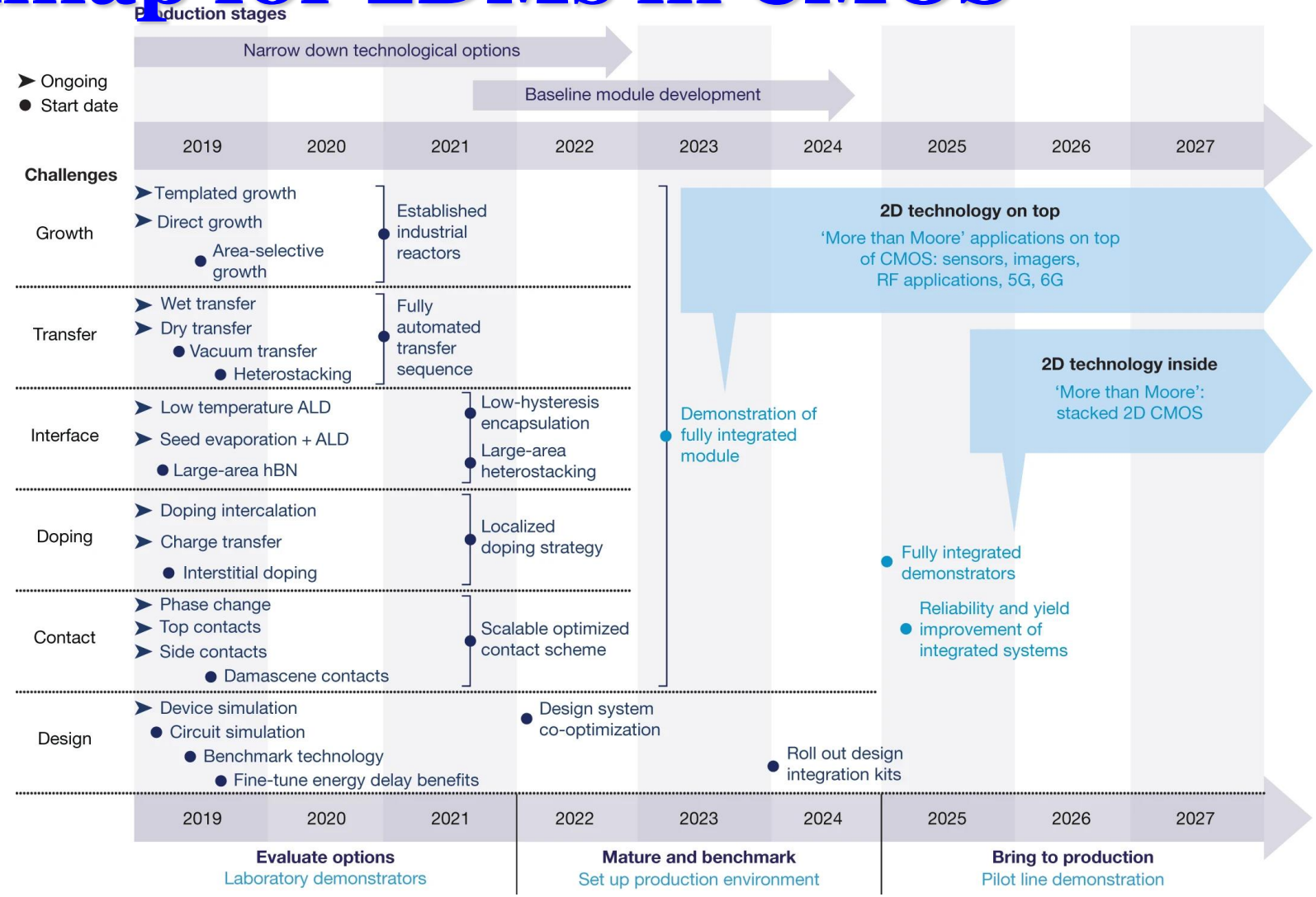

Deji Akinwande, & Frank H. L. Koppens, et al., Nature **573,** 507–518 (2019)

Applications of 2D materials in flexible electronics

including functionalized molecular MoS_2 ...

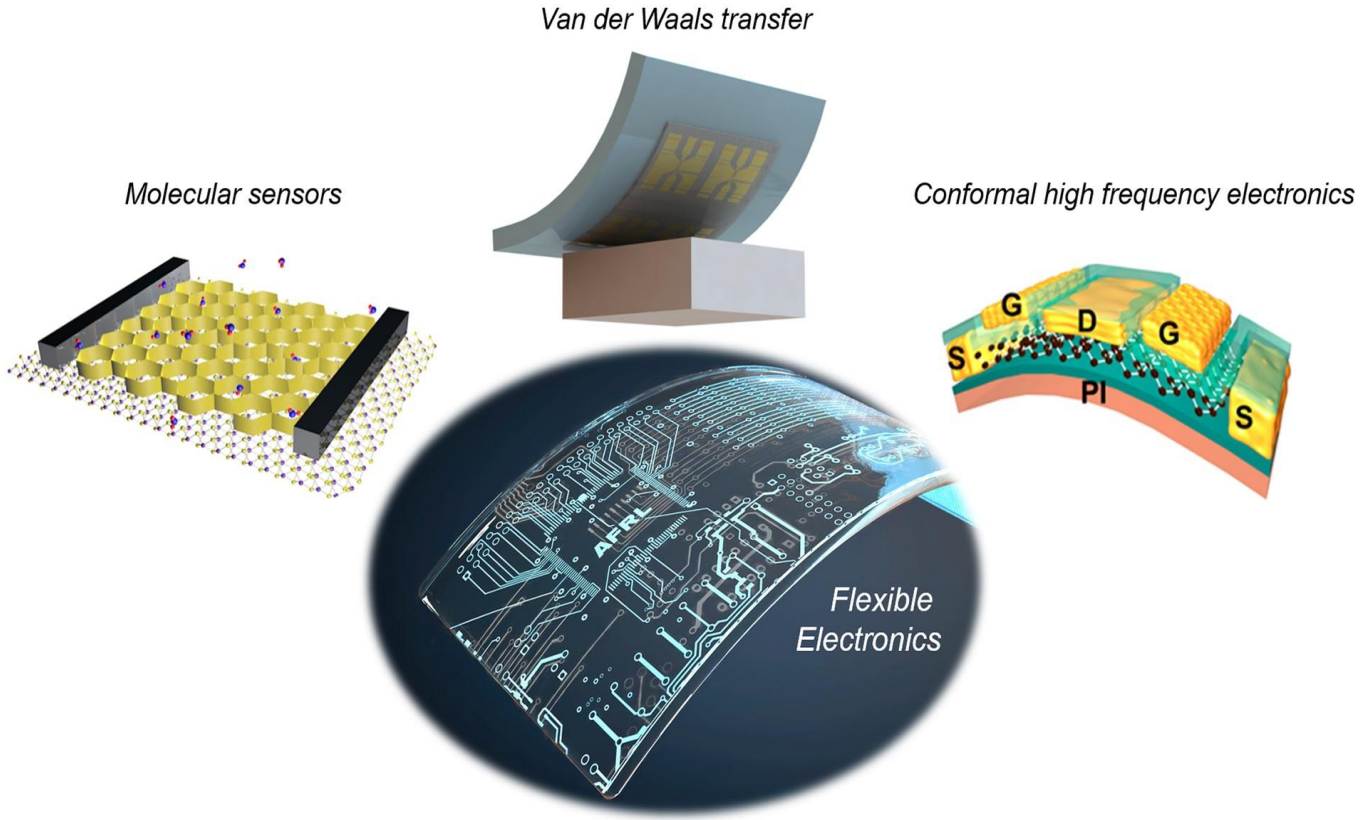

N. R. Glavin, Ch. Muratore, Michael Snure, *Open Mater Sci*, 1(1), 2021, itaa002, https://doi.org/10.1093/oxfmat/itaa002

Infrared APDs from Bulk to 2D Materials

Infrared avalanche photodiodes from bulk to 2D materials

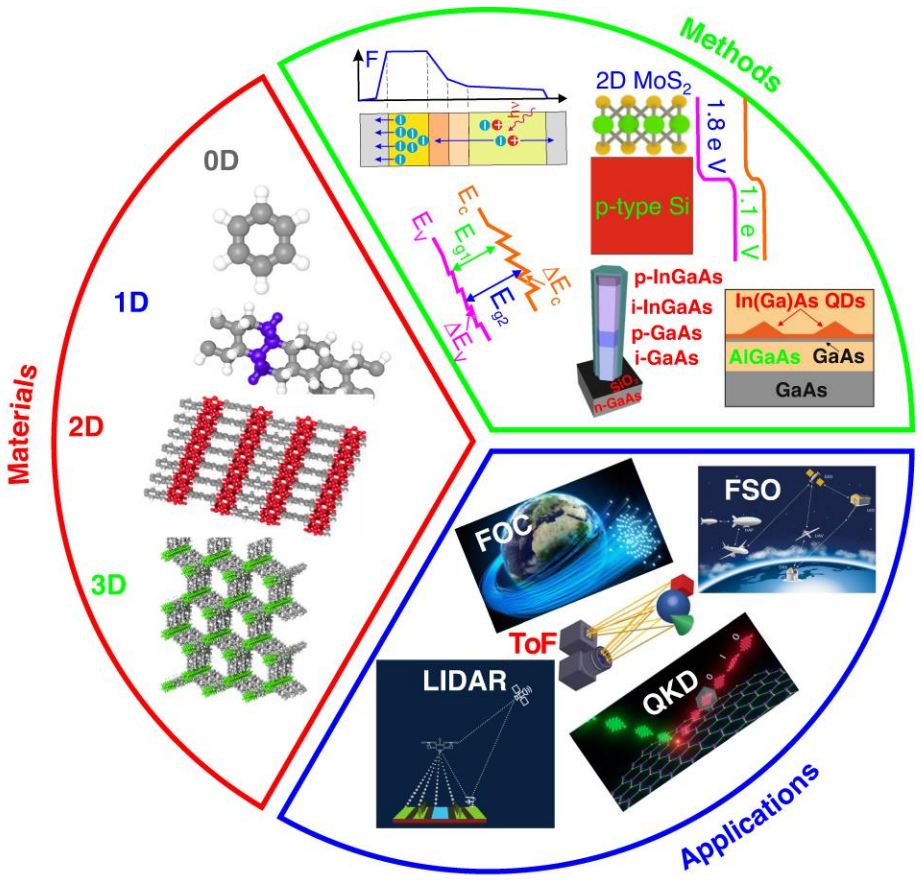

Methods, technologies, and applications roadmap for avalanche photon-sensing technologies starting from bulk to low-dimensional materials

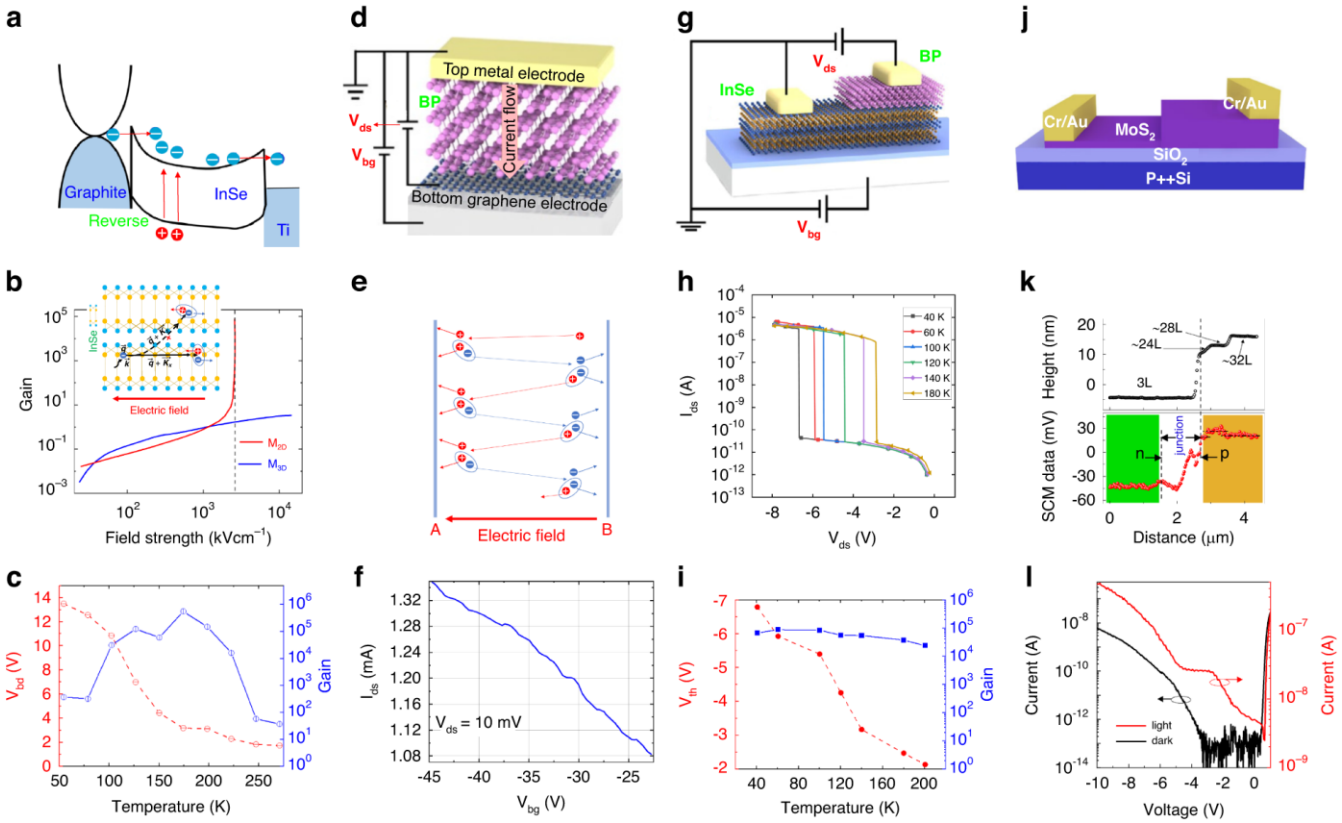

a graphite/InSe Schottky avalanche detector, b e-ph scattering dimensionality reduction affects electron acceleration process and gain versus electric field in 2D (red line) and 3D (blue line), c breakdown voltage (V_{bd}) and gain as a function of temperature—nano InSe/BP heterostructures ballistic APD: d schematic of the graphene/BP/metal avalanche device, e ballistic avalanche photodetector operating principle, f quasi-periodic current oscillations, g schematic of graphene InSe/BP, h I_{ds}–V_{ds} characteristics for selected temperatures (40 − 180 K), i avalanche breakdown V_{th} and gain versus temperature—showing a negative temperature coefficient. Pristine PN junction avalanche photodetector: j device structure, k as the number of layers increases, a positive/negative signal of SCM denotes hole/electron carries, l APD's low temperature (~100 K) dark and photocurrent I–V curves

Piotr Martyniuk, et al., Light: Science & Applications volume 12, Article number: 212 (2023)
https://www.nature.com/articles/s41377-023-01259-3

Conclusions

- 2D materials placed on silicon & silicon nitride photonic integrated circuits can significantly modify their linear, nonlinear and optoelectronic properties
- Graphene on silicon, silicon nitride & BIC waveguides offers useful additional properties that may be used for devices such as waveguide photodetectors
- Built-in field between graphene and substrate can be capitalized on for high-performance photodetectors
- Broad spectral response of graphene enables useful for devices at spectral regions where there are not so alternative technologies, e.g. room temperature mid-IR photodetector
- Graphene based THz modulators can be realized
- Elliptic THz wave is realized
- 2D Materials and Devices have great future ahead

Hong Kong PhD Fellowship Scheme

Established by the Research Grants Council (RGC) in 2009, the **Hong Kong PhD Fellowship Scheme (HKPFS)** aims at attracting the best and brightest students in the world to pursue their PhD programmes in Hong Kong's universities.

Website

www.gs.cuhk.edu.hk/hkpfs

CUHK Vice-Chancellor's HKPFS Scholarship

Tuition Fee Waiver
for the whole normative study period

Stipend
Up to HK$1.32 Million*
(approx. US$169,840)

Lodging Award
Up to HK$100,000*#
(approx. US$12,800)

Conference and Research-related Travel Allowance
Up to HK$85,200*
(approx. US$10,923)

1st Year Hostel Fee Waiver
and Guaranteed On-campus Accommodation*^

Totalling

up to HK$ 1.8 Million (~US$221,000)
financial assistance during the normative study period

* During the student's normative study period.
^ HKPFS awardees who submit hall applications and complete registration procedures in a timely manner.
# An award of HK$40,000 for lodging in the first year of study and HK$20,000 in subsequent years during the normative study period.

Hong Kong PhD Fellowship Scheme

Eligibility

Candidates who are seeking admission as new full-time PhD students in Hong Kong universities funded by the University Grants Committee (UGC), irrespective of their country of origin, prior work experience and ethnic background, are eligible to apply.

Timeline

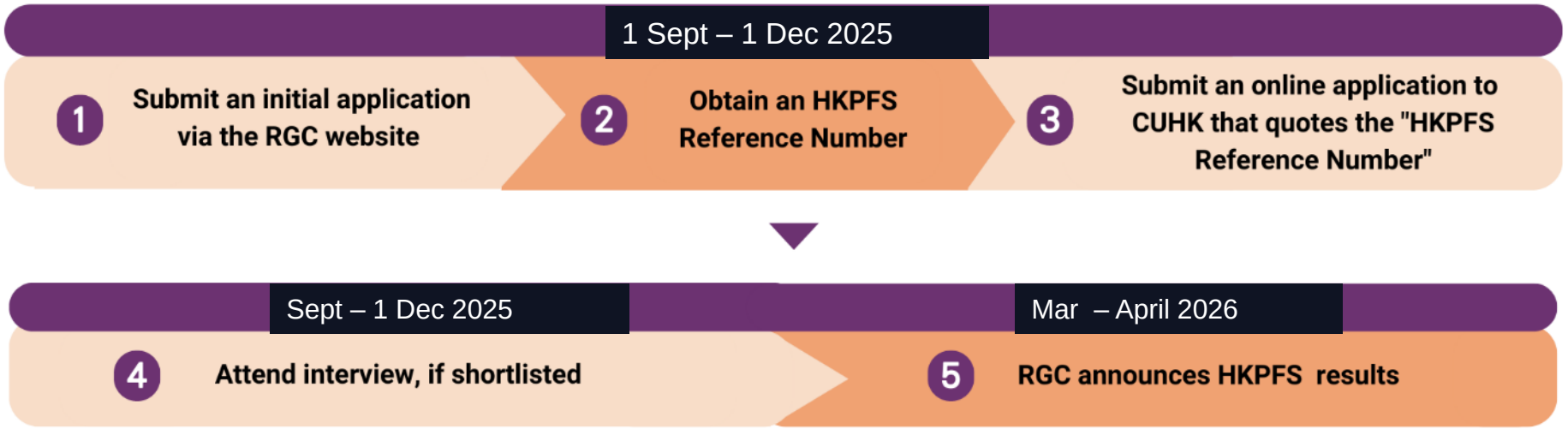

Chinese University of Hong Kong

香港中文大學

Chinese University of Hong Kong
香港中文大學

Research Assistant Professor, Postdoctoral & PhD positions available

www.cuhk.edu.hk/greencampus

綠山城 Green Campus